
DF40: Toward Next-Generation Deepfake Detection

Zhiyuan Yan¹, Taiping Yao², Shen Chen², Yandan Zhao², Xinghe Fu², Junwei Zhu²,
Donghao Luo², Li Yuan¹, Chengjie Wang², Shouhong Ding², Yunsheng Wu²

¹Peking University

²Tencent Youtu Lab

Abstract

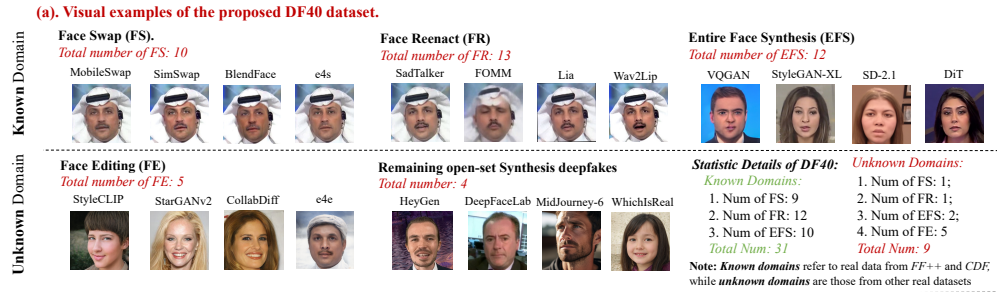
We propose a new comprehensive benchmark to revolutionize the current deepfake detection field to the next generation. Predominantly, existing works identify top-notch detection algorithms and models by adhering to the common practice: training detectors on one specific dataset (*e.g.*, FF++ [67]) and testing them on other prevalent deepfake datasets. This protocol is often regarded as a "golden compass" for navigating SoTA detectors. But can these stand-out "winners" be truly applied to tackle the myriad of realistic and diverse deepfakes lurking in the real world? If not, what underlying factors contribute to this gap? In this work, we found the **dataset** (both train and test) can be the "primary culprit" due to the following: (1) *forgery diversity*: Deepfake techniques are commonly referred to as both face forgery (face-swapping and face-reenactment) and entire image synthesis (AIGC, especially face). Most existing datasets only contain partial types of them, with limited forgery methods implemented (*e.g.*, 2 swapping and 2 reenactment methods in FF++); (2) *forgery realism*: The dominated training dataset, FF++, contains out-of-date forgery techniques from the past five years. "Honing skills" on these forgeries makes it difficult to guarantee effective detection generalization toward nowadays' SoTA deepfakes; (3) *evaluation protocol*: Most detection works perform evaluations on one type, *e.g.*, train and test on face-swapping types only, which hinders the development of universal deepfake detectors. To address this dilemma, we construct a highly diverse and large-scale deepfake detection dataset called *DF40*, which comprises **40** distinct deepfake techniques (10 times larger than FF++). We then conduct comprehensive evaluations using **4** standard evaluation protocols and **7** representative detection methods, resulting in over **2,000** evaluations. Through these evaluations, we provide an extensive analysis from various perspectives, leading to **12** new insightful findings contributing to the field. We also open up **5** valuable yet previously underexplored research questions to inspire future works.

Note: We will release the *DF40* dataset with easy-to-use instructions, a unified codebase for train and test, and pre-trained weights of all models on [GitHub](#). For a quick overview of our conclusions, please refer to the *takeaways* in Sec 9.

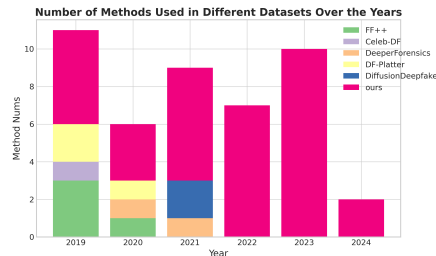
1 Introduction

We are currently in 2024, an explosive era of Artificial Intelligence Generated Content (AIGC), a world where you can effortlessly make anyone say anything at any time, a realm where reality and fiction blend seamlessly, creating a mesmerizing tapestry of digital artistry and potential deception. Amidst this AIGC revolution, the ease of generating *deepfakes*¹ has become a "double-edged sword." Unfortunately, deepfake is often misused for manipulating one person's identity (face-swapping) or controlling facial expressions and movements in a portrait (face-reenactment). It can be particularly

¹Deepfake is a term derived from "deep" (the use of deep nets) and "fake" (does not exist in the real world).



(b). Statistic comparison of forgery number used in different datasets



(c). Comparison with other dataset in diversity and scale.

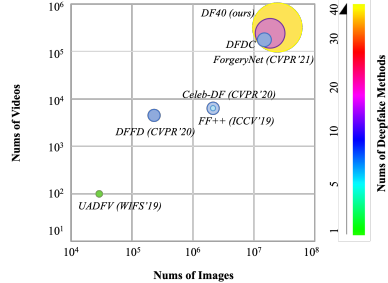


Figure 1: Overview of our DF40 dataset. DF40 shows advantages in data diversity, synthesis quality, and deepfake realism. Note *all* the above figures are deepfake, which does not exist in the real world.

harmful as it may lead to severe digital crimes and undermine social trust. Therefore, there is an urgent need to develop a reliable system for detecting deepfakes. In a narrow sense, deepfake refers to *face forgery*, generally including face-swapping and face-reenactment [94]. In a broader sense, it also includes entire image synthesis (not limited to face), widely called *AIGCs* [81]. Naturally, deepfake detection methods can be broadly classified into two sub-fields: face forgery detection and AIGC detection. Previous works often treat these sub-fields as separate issues, as it is widely believed that they may have distinct fake artifacts: face forgery can be local, with only the facial region manipulated, while AIGC artifacts can be global, involving the entire synthesized image content. For this reason, most detection methods can only be applied to solve one type of these issues.

To illustrate, in face forgery detection, blending-based detectors [11; 46; 70; 45; 95] have achieved SoTA results on existing datasets (*e.g.*, CDF [47]), which involve image blending to create pseudo-fake training fakes. All these methods are based on an assumption that existing face-swapping should share a blending step². However, actually, recent advancements in face-swapping (*e.g.*, Simswap [13], FaceDancer [66]) directly generate all content (including the background) without blending. Regrettably, this crucial observation may not be well-known in the field, as most existing datasets typically belong to "DF-family"³ (*e.g.*, CDF [47]). As a result, blending-based detection methods (*e.g.*, [100; 70]) can achieve remarkable generalization results on the existing deepfake datasets (*e.g.*, CDF [47]) due to the presence of blending artifacts but fail to generalize well outside the DF-family datasets (forgeries *wo* blending). As evidenced in [92], [70] achieves 85% AUC on the CDF dataset (from DF-family), but only 47% in testing SD [64] generated images (outside DF-family). In Sec. 4, we comprehensively re-evaluate it on 31 distinct deepfakes (some are nowadays' SoTA), showing that the generalization capability of current blending-based methods is still limited. Similar examples can be observed in the AIGC detection field. Recent work [87] proposed detecting diffusion-generated images by measuring the error between an input real image and its reconstruction counterpart using a pre-trained diffusion model. However, this detector is still "diffusion-heavy," meaning it only learns the diffusion-specific feature.

Hence, although many previous efforts have pursued detection generalization, they often remain limited in addressing only a subset of deepfake types (*e.g.*, only face-swapping belongs to the "DF-family") and cannot truly non-trivially be applied to generalize all deepfake types. In a real-world scenario with unpredictability and complexity, creating such a "unified" detector is essential. We

²Blending the altered face into an existing background image, as initially proposed by [45].

³The term "DF-family" refers to face forgery techniques that involve creating a mask around the facial region and blending the generated deepfake face back into the background image using that mask.

Table 1: Comparison of existing/previous deepfake datasets. DF40 surpasses any other dataset in diversity, scale, and modeling. Deepfake data in DF40 is created by **40** deepfake techniques, including **10** FS methods, **13** FR methods, **12** EFS methods, and **5** FE methods.

| Dataset | Publication | Latest Fake | Methods | FS | FR | EFS | FE | Fake Videos | Fake Images | Pretraining |
|--------------------------|-------------|------------------------------|-----------|-----------|-----------|-----------|----------|--------------|-------------|-------------|
| DF-TIMIT [41] | ArXiv'18 | faceswap-GAN [69] (2018) | 2 | 2 | - | - | - | 640 | - | - |
| UADFV [96] | ICASSP'19 | Unknown | 1 | 1 | - | - | - | 49 | 252 | - |
| FaceForensics++ [67] | ICCV'19 | NeuralTextures [76] | 4 | 2 | 2 | - | - | 4K | - | - |
| DeepFakeDetection [21] | None | Unknown | 5 | 5 | - | - | - | 3068 | - | - |
| CDF [47] | CVPR'20 | Unknown | 1 | 1 | - | - | - | 5,639 | - | - |
| DFFD [17] | CVPR'20 | StyleGAN [38] (2018) | 7 | 7 | - | - | - | 3000 | 0.2M+ | - |
| DeeperForensics-1.0 [35] | CVPR'20 | DF-VAE [35] (2020) | 1 | 1 | - | - | - | 10K | - | - |
| DFDC [22] | ArXiv'20 | StyleGAN [38] (2018) | 8 | 5 | 1 | 2 | - | 0.1M+ | - | - |
| ForgeryNet [27] | CVPR'21 | StarGANv2 [15] (2020) | 15 | 6 | 4 | 2 | 3 | 0.1M+ | 1M+ | ✓ |
| FakeAVCeleb [40] | NeurIPS'21 | Wav2Lip [60] (2021) | 4 | 2 | 2 | - | - | 9.5K | - | - |
| KoDF [42] | ICCV'21 | Wav2Lip [60] (2021) | 6 | 3 | 3 | - | - | 0.1M+ | - | - |
| FFIW [101] | CVPR'21 | FSGAN [57] (2019) | 3 | 3 | - | - | - | 10K | - | - |
| DF3 [36] | TMM'22 | StyleGAN3 [37] (2021) | 6 | - | - | 6 | - | 15k+ | - | - |
| DeepFakeFace [74] | ArXiv'23 | Stable-Diffusion [83] (2021) | 3 | 1 | - | 2 | - | - | 90K | - |
| DF-Platter [55] | CVPR'23 | FaceShifter [44] (2020) | 3 | 3 | - | - | - | 0.1M+ | - | - |
| DiffusionDeepfake [6] | ArXiv'24 | Stable-Diffusion [83] (2021) | 2 | - | - | 2 | - | - | 0.1M+ | - |
| DF40 (Ours) | - | PixArt- α [10] (2024) | 40 | 10 | 13 | 12 | 5 | 0.1M+ | 1M+ | ✓ |

i) **Latest Fake**: The year when the *latest* deepfake method was added to the dataset, *e.g.*, the latest method in ours is PixArt- α [10] (2024).

ii) **Methods**: The number of different deepfake methods used to generate fakes in the dataset. The methods are generally classified into: face-swapping (FS), face-reenactment (FR), entire face synthesis (EFS), and face editing (FE).

iii) **Fake Videos and Fake Images**: The number of *fake* videos and images involved in the dataset.

iv) **Pretraining**: Indicates if pretraining was conducted and pretraining weights were released in the dataset.

discovered previous work [82] attempted to detect all CNN-generated images within one unified model, but its scope is still limited to the entire image synthesis, not including recent popular diffusion models and other deepfake types (*e.g.*, face-swapping). Hence, this issue has persistently been challenging, as most existing datasets either contain limited types (see Tab. 1) or are specific to a single type (*e.g.*, DF-family only).

Therefore, we realize that a *diverse* and *comprehensive* dataset is the true key to "unlock" the potential of ideal deepfake detection. To this end, we "jump" from the previous protocol settings (*e.g.*, train and test solely on DF-family) and propose a new comprehensive dataset called *DF40*. Our main contribution can be generally summarized as three folds: **(1)** Our DF40 implements **40** different deepfake techniques, including face-swapping, face-reenactment, entire face synthesis, and face editing. We even include the just-released DiT [59], PixArt- α [10], and highly popular software DeepFaceLab [18] and HeyGen [28] to simulate real-world deepfakes; **(2)** We introduce 4 standard protocols for evaluations and show 8 insightful findings to the field. We also open up new research questions and topics to inspire future research toward next-generation deepfake detection. **(3)** We release all pre-trained weights from our evaluations, allowing other researchers can directly leverage them to develop their algorithms for improved detection. For example, we release the pre-trained model for CLIP-large (a vanilla binary classifier trained on the proposed DF40 dataset), which achieves an AUC of 98% on DeepForensics [35], 95% on FaceShifter [44], 90% on CDF-v2 [47], and 85% on DFDC [20] at the **frame level**. This performance outperforms almost all other existing SoTA detectors without relying on previously considered beneficial techniques such as blending methods and other complex constraints.

Furthermore, it is important to note that, without our DF40 dataset, we might only see "the tip of the iceberg" and assume that blending might be "all you need" to solve most deepfake problems. However, our work reveals that the generalization capabilities of blending-based detection methods are limited, and there is still much room for improvement in the deepfake detection domain. It is crucial to develop more robust detection methods that can effectively handle diverse deepfake techniques and data sources, going beyond blending artifacts to address the deepfake problem comprehensively. So in this work, we re-evaluate existing deepfake detectors thoroughly and open up several valuable yet previously underexplored research questions to inspire future works. For now, we believe we have entered the next generation of deepfake detection.

2 Background

This section *briefly* introduces the background and its related works, structured around three focal points. **First**, we briefly introduce deepfake generation techniques, including face-swapping (FS), face-reenactment (FR), entire face synthesis (EFS), and face editing (FE). We consider both academic works and popular software online. **Second**, we delve into deepfake detection, including face

forgery detection and AIGC detection. **Last**, we review existing deepfake datasets and benchmarks, underscoring the need for diverse and comprehensive datasets for next-generation deepfake detection.

2.1 Deepfake Generation.

Based on previous survey [54], deepfake techniques can be typically classified into four types: face-swapping (*FS*), face-reenactment (*FR*), entire face synthesis (*EFS*), and face editing (*FE*). **(1) Face-swapping:** This paper classifies the face-swapping technique into two domains: *DF-family* and *FS-family*. *(i) DF-family* involves creating a mask around the facial region (some even include the neck [50]) and blending the generated deepfake face back into the background image using that mask. Most existing and famous face forgery datasets, such as FF-DF [67], Celeb-DF [47] and DFDC [20], belong to this line. *(ii) FS-family* methods represent another significant category in face-swapping deepfake generation. These methods typically involve the use of an identity-background encoder. It disentangles a face image’s identity and background information during encoding. Notably, these methods directly generate all content, even the background. Much recent face-swapping research works [90; 13] and popular software (*e.g.*, Roop [65]) are within this line. **(2) Face-reenactment:** Generally, this technique can be used to modify source faces, imitating the actions or expressions of another face. Differing from face-swapping, face-reenactment techniques are *rarely* considered in existing datasets. Two commonly used reenactment-based forgeries are Face2Face [77] and NeuralTextures [76]. These two forgeries are implemented in the FF++ dataset. Face2Face employs pairs of original and target faces, using key facial points to generate varied expressions, while NeuralTexture uses rendered images from a 3D face model to migrate expressions. Although these forgeries achieve more realistic visual synthetic results compared to their face-swapping counterparts in FF++, Due to the amazingly rapid development of the AIGC technologies (*e.g.*, Digital Human), these relatively old-fashioned methods cannot represent the modern’ SoTA reenactment methods. Our DF40 implements 13 face-reenactment methods in total, including the classical animation [72; 73], SoTA’s audio-based driven methods [97; 60], image-based driven methods [86; 31; 7]. We also include the well-known best face generation technique, HeyGen [28], in our dataset for evaluation. **(3) Entire Face Synthesis:** This technique can be generally treated as "Face AIGC." With the rapid development of AIGCs, this technique has achieved remarkably notable improvement. The two widely used technologies to generate synthesis faces are GAN (*e.g.*, StarGAN [14]) and Diffusion models (*e.g.*, StableDiffusion [64]). **(4) Face Editing:** This technique aims to modify the facial attributes (*e.g.*, age and gender) of the given face images. Most of these works utilize the latent code of StyleGAN [39] to perform editing during GAN inversion. In our DF40 dataset, we also consider the diffusion-based face editing method [32].

2.2 Deepfake Detection

Since deepfake detection can be broadly classified into face forgery detection and (general) AIGC detection (not limited to face), we will briefly introduce the typical works of each sub-field. **(1) Face Forgery Detection.** Earlier deepfake detection techniques primarily relied on traditional digital image processing methods. These approaches utilized natural video characteristics such as phoneme-viseme mismatches [4], depth of field [34], color components [43], and head poses [96]. However, with the advent of deep learning, the focus has now shifted towards learning-based detectors due to their superior feature extraction capabilities. Following the *recent* deepfake benchmark [94], Most existing deepfake detectors can be broadly divided into naive, spatial, and frequency. *(i)* The naive detector employs CNNs to perform binary classification that distinguishes deepfake content from authentic data. Numerous CNN-based binary classifiers have been proposed, *e.g.*, MesoNet [2] and Xception [67]; *(ii)* Spatial detector delves deeper into specific representation such as forgery region location [56], disentanglement learning [93], image reconstruction [8], erasing technology [79], image blending [70; 45; 11], *etc*; *(iii)* The frequency detector addresses this limitation by focusing on the frequency domain for forgery detection. SPSP [48] and SRM [52] utilize phase spectrum analysis and high-frequency noises, respectively. F3Net [61] proposes using learnable filters for adaptive mining of frequency forgery clues using frequency-aware image decomposition. In our work, we further make another new type: blending-based detectors due to the distinct training paradigm. These methods specifically focus on the detection of blending artifacts [46; 45; 11], generating forged images during training in a self-supervised manner to boost detector generalization. These techniques aim to extract more comprehensive and discriminative features by leveraging various aspects of the input data. **(2) AIGC Detection.** As generative models produce increasingly realistic images, the

Table 2: Involved/Implemented deepfake methods of the proposed DF40 dataset. We use the following 40 distinct methods to create deepfake videos and images for evaluation.

| Type | ID-Number | Method | Sub-Types | Venue | Real Data Source | Data Format | Data Used | Data Scale | Code Link |
|-----------------------------|------------------|-----------------------|---------------------|---------------|------------------|-------------|--------------|----------------------------|----------------------------|
| Face-swapping (FS) | 1 | FSGAN [57] | Parsing mask | ArXiv 2019 | FF++ & CDF | Video | Train & Test | 1500+ | Hyper-link |
| | 2 | FaceSwap [11] | Graphic based | None | FF++ & CDF | Video | Train & Test | 1500+ | Hyper-link |
| | 3 | SimSwap [13] | Disentangle | ICCV 2019 | FF++ & CDF | Video | Train & Test | 1500+ | Hyper-link |
| | 4 | InSwapper [33] | Used in Reop [65] | None | FF++ & CDF | Video | Train & Test | 1500+ | Hyper-link |
| | 5 | BlendFace [71] | Disentangle | ICCV 2023 | FF++ & CDF | Video | Train & Test | 1500+ | Hyper-link |
| | 6 | UniFace [90] | Disentangle | ECCV 2022 | FF++ & CDF | Video | Train & Test | 1500+ | Hyper-link |
| | 7 | MobileSwap [91] | Lightweight | AAAI 2022 | FF++ & CDF | Video | Train & Test | 1500+ | Hyper-link |
| | 8 | e4s [50] | Disentangle | CVPR 2023 | FF++ & CDF | Video | Train & Test | 1500+ | Hyper-link |
| | 9 | FaceDancer [66] | Disentangle | WACV 2023 | FF++ & CDF | Video | Train & Test | 1500+ | Hyper-link |
| | 10 | DeepFaceLab [18] | High quality | PR 2023 | UADFV [96] | Video | Test Only | 100 | Hyper-link |
| Face-reenactment (FR) | 11 | FOMM [72] | Image Driven | NeurIPS 2019 | FF++ & CDF | Video | Train & Test | 1,500+ | Hyper-link |
| | 12 | FS_vid2vid [84] | Landmark Driven | ArXiv 2019 | FF++ & CDF | Video | Train & Test | 1,500+ | Hyper-link |
| | 13 | Wav2Lip [60] | Audio Driven | MM 2020 | FF++ & CDF | Video | Train & Test | 1,500+ | Hyper-link |
| | 14 | MRAA [73] | Image Driven | CVPR 2021 | FF++ & CDF | Video | Train & Test | 1,500+ | Hyper-link |
| | 15 | OneShot [85] | Image Driven | CVPR 2021 | FF++ & CDF | Video | Train & Test | 1,500+ | Hyper-link |
| | 16 | PIRender [63] | Image Driven | ICCV 2021 | FF++ & CDF | Video | Train & Test | 1,500+ | Hyper-link |
| | 17 | TPSMM [99] | Image Driven | CVPR 2022 | FF++ & CDF | Video | Train & Test | 1,500+ | Hyper-link |
| | 18 | LIA [86] | Image Driven | ICLR 2022 | FF++ & CDF | Video | Train & Test | 1,500+ | Hyper-link |
| | 19 | DaGAN [31] | Image Driven | CVPR 2022 | FF++ & CDF | Video | Train & Test | 1,500+ | Hyper-link |
| | 20 | SadTalker [97] | Audio Driven | CVPR 2023 | FF++ & CDF | Video | Train & Test | 1,500+ | Hyper-link |
| | 21 | MCNet [30] | Image Driven | ICCV 2023 | FF++ & CDF | Video | Train & Test | 1,500+ | Hyper-link |
| | 22 | HyperReenact [7] | Image Driven | ICCV 2023 | FF++ & CDF | Video | Train & Test | 1,500+ | Hyper-link |
| | 23 | HeyGen [28] | Text Driven | None | VFHQ [89] | Video | Test Only | 50 | Hyper-link |
| Entire Face Synthesis (EFS) | 24 | VQGAN [24] | GAN based | CVPR 2021 | FF++ & CDF | Image | Train & Test | 48,000+ | Hyper-link |
| | 25 | StyleGAN2 [39] | GAN based | ArXiv 2019 | FF++ & CDF | Image | Train & Test | 48,000+ | Hyper-link |
| | 26 | StyleGAN3 [37] | GAN based | NeurIPS 2021 | FF++ & CDF | Image | Train & Test | 48,000+ | Hyper-link |
| | 27 | StyleGAN-XL [68] | GAN based | SIGGRAPH 2022 | FF++ & CDF | Image | Train & Test | 48,000+ | Hyper-link |
| | 28 | SD-2.1 [64] | GAN based | CVPR 2022 | FF++ & CDF | Image | Train & Test | 48,000+ | Hyper-link |
| | 29 | DDPM [29] | Latent Diffusion | NeurIPS 2020 | FF++ & CDF | Image | Train & Test | 48,000+ | Hyper-link |
| | 30 | RDDM [49] | Latent Diffusion | ArXiv 2023 | FF++ & CDF | Image | Train & Test | 48,000+ | Hyper-link |
| | 31 | PixArt- α [10] | Latent Diffusion | ICLR 2024 | FF++ & CDF | Image | Train & Test | 48,000+ | Hyper-link |
| | 32 | DIT-XL/2 [59] | Latent Diffusion | ICCV 2023 | FF++ & CDF | Image | Train & Test | 48,000+ | Hyper-link |
| | 33 | SIF-XL/2 [51] | Latent Diffusion | ArXiv 2024 | FF++ & CDF | Image | Train & Test | 48,000+ | Hyper-link |
| | 34 | MidJourney v6 [53] | Popular Application | None | FFHQ [38] | Image | Test Only | 1,000 | Hyper-link |
| 35 | WhichisReal [88] | GAN based | None | FFHQ [38] | Image | Test Only | 1,000 | Hyper-link | |
| Face Editing (FE) | 36 | CollabDiff [32] | Diffusion based | CVPR 2023 | FF++ & CDF | Image | Test Only | 48,000+ | Hyper-link |
| | 37 | e4e [78] | StyleGAN based | SIGGRAPH 2021 | FF++ & CDF | Image | Test Only | 48,000+ | Hyper-link |
| | 38 | StarGAN [14] | StarGAN based | CVPR 2018 | CelebA [51] | Image | Test Only | 2,000 | Hyper-link |
| | 39 | StarGANv2 [15] | StarGAN based | CVPR 2020 | CelebA [51] | Image | Test Only | 2,000 | Hyper-link |
| 40 | StyleCLIP [58] | StyleGAN based | ICCV 2021 | CelebA [51] | Image | Test Only | 2,000 | Hyper-link | |

i) **Note-1:** The nine "test only" data is utilized as the **unknown** domain data, simulating the domain shift of real people distributions.

ii) **Note-2:** For HeyGen and DeepFaceLab, these two SoTA deepfakes are widely used and highly realistic. However, since they belong to *one-to-one* type [54], their implementation requires significantly more time and resources. Thus, we only create 50 and 100 for each.

importance of AIGC detection has grown. In earlier studies, AutoGAN [98] revealed the presence of unique artifacts in GAN-generated images, which can be observed periodically in the images' frequency spectrum. Wang et al. [82] suggested that a classifier trained on one CNN generator, with suitable training data and data augmentation, can generalize effectively to other unseen generators. However, these approaches have exhibited limited generalization capabilities when applied to images generated by diffusion models. Recently, DIRE [87] employed the error between an input image and its reconstruction using a pre-trained diffusion model to detect fake images. Nonetheless, this method is specifically designed for diffusion models and cannot be directly applied to detecting GAN-based models.

2.3 Existing Deepfake Datasets.

Most earlier public deepfake datasets published before 2021 [41; 96; 21; 47; 67; 17] generate deepfakes using only the face-swapping technique within "DF-family." Also, these datasets contain only single or no more than 4 specific manipulation approaches. Notably, DFDC [20] implements 7 deepfake approaches (most are DF-family face-swapping) and extends the data scale to the million-level. After that, ForgeryNet [27] applies 15 methods to create forgery data with a million-level data scale. However, with the advent of both AIGCs and diffusion-based generators, producing realistic content has become increasingly popular and widely seen on social media. Consequently, it is uncertain whether a detector trained on older forgery methods can generalize to today's SoTA deepfakes, *e.g.*, diffusion-generated content. In response, many recent works [36; 74] have begun to focus on current generative models. A very recent study, DiffusionDeepfake [6], proposes a diffusion-specific dataset containing two mainstream state-of-the-art diffusion generators: Stable-Diffusion [64] and MidJourney [53]. Furthermore, to detect these AIGC-generated images (not limited to face), GenImage [102] introduces a million-scale dataset created by 8 different generative models (including both GAN and Diffusion). However, it is crucial to note that [6] and [102] are still within only the AIGC scope and may not guarantee successful detection of other deepfakes, *e.g.*, face-swapping. A more comprehensive comparison of existing datasets can be referred to Tab. 1.

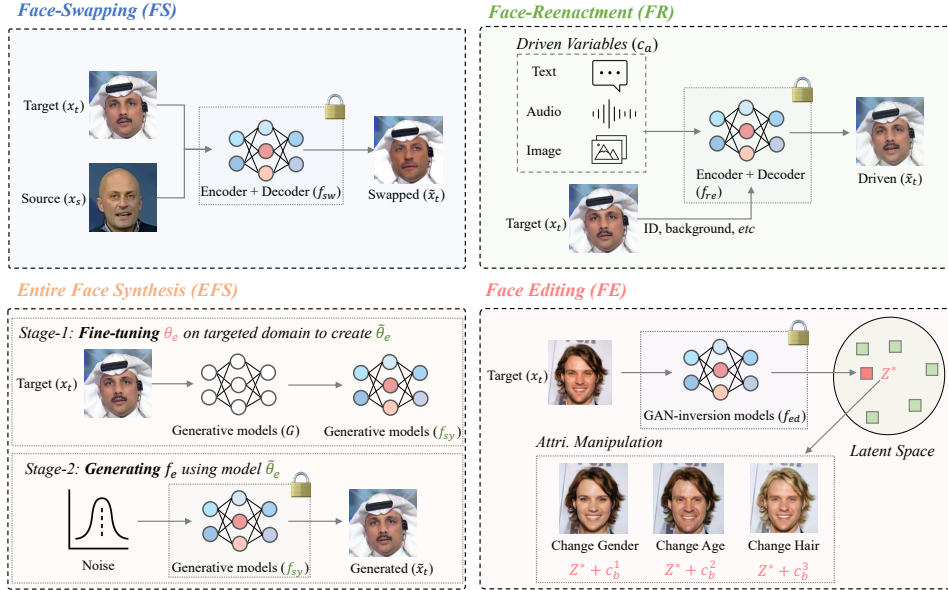


Figure 2: The general fake data generation pipeline of the proposed DF40 dataset.

3 DF40 Benchmark

3.1 Research Scope and Summary of DF40.

In this work, our scope specifically focuses on *face* deepfake detection, including face-swapping (FS), face-reenactment (FR), entire face synthesis (EFS), and face editing (FE). Natural image synthesis (such as art) is not within our scope, but we show the potential of using model training on face deepfake to detect these (non-face) AIGC-generated images. DF40 dataset provides 40 deepfake approaches with 4 different types: FS, FR, EFS, and FE. For FS and FR, we provide video format data (over 0.1M video clips in total), and image format for EFS and FE (over 1M+ images in total). We also introduce several latest/popular generation techniques (*e.g.*, PixArt- α [10] in 2024) and widely used software (*e.g.*, HeyGen [28], DeepFaceLab [18]). Furthermore, some classical and representative methods are also included, *e.g.*, FOMM [72]. Our dataset shows the advantages in both data diversity and scale (see Tab. 1).

3.2 Original Data Collection and Deepfake Data Generation.

Real Data: We consider two mainstream and popular face datasets specifically used in the deepfake detection field: FF++ [67] (c23 version) and CDF [47] as our original data. There are two main reasons why we chose these two data domains as the original data for creating fakes: **(1)** Consistency with previous work: By using these datasets for training and evaluation, we can align with prior studies and assess whether their conclusions and methods are still valid in the context of our new dataset. For instance, many previous works [45; 26] follow the "cross-manipulation" evaluation protocol to test the generalization ability when the forgery method differs while the data domain remains the same (FF++). Therefore, creating fakes of DF40 using FF++ allows us to extend their results from evaluating solely on four limited and outdated forgery methods to more than 30 distinct and latest deepfakes. **(2)** Impact study of domain and forgery: Prior studies have not considered the scenario where only the data domain changes while the forgery method remains the same. This omission hinders the analysis of the sole impact of the data domain on model generalization. In our DF40 dataset, we use both FF++ and CDF domains to facilitate the research on the influence of both data domain and forgery method, as detailed in our **Finding-6**. In essence, the choice of these two data domains enables us to build upon previous work and to conduct a more comprehensive analysis of the factors influencing the performance of deepfake detection models. We also provide real data from other existing datasets (*e.g.*, CelebA [51]) to facilitate the unknown domain evaluations (see Tab. 2 for details). We show more details of these original face datasets in the supplementary.

Table 3: Same data domain, different forgery types (**Protocol-1**): Cross-manipulation evaluation of different models on FF domain. Within-forgery evaluations are in gray. FS (FF) denotes all FS data within FF domain, with FR (FF), FS (CDF), *etc.*, being similar.

| Training Set | Model | Testing Set (FF) | | | |
|--------------|---------------|------------------|---------|----------|-----------|
| | | FS (FF) | FR (FF) | EFS (FF) | Avg. (FF) |
| FS (FF) | Xception [16] | 0.991 | 0.892 | 0.810 | 0.898 |
| | CLIP [62] | 0.996 | 0.908 | 0.837 | 0.914 |
| | SRM [52] | 0.988 | 0.867 | 0.703 | 0.853 |
| | SPSL [48] | 0.987 | 0.849 | 0.735 | 0.857 |
| | RECCE [8] | 0.991 | 0.855 | 0.758 | 0.868 |
| | RFM [80] | 0.992 | 0.884 | 0.821 | 0.899 |
| FR (FF) | Xception [16] | 0.838 | 0.996 | 0.670 | 0.835 |
| | CLIP [62] | 0.932 | 0.999 | 0.798 | 0.910 |
| | SRM [52] | 0.893 | 0.998 | 0.698 | 0.863 |
| | SPSL [48] | 0.901 | 0.998 | 0.695 | 0.865 |
| | RECCE [8] | 0.865 | 0.997 | 0.716 | 0.859 |
| | RFM [80] | 0.892 | 0.999 | 0.776 | 0.889 |
| EFS (FF) | Xception [16] | 0.665 | 0.807 | 0.999 | 0.824 |
| | CLIP [62] | 0.688 | 0.889 | 0.999 | 0.859 |
| | SRM [52] | 0.596 | 0.776 | 0.999 | 0.790 |
| | SPSL [48] | 0.659 | 0.811 | 0.999 | 0.823 |
| | RECCE [8] | 0.691 | 0.801 | 0.999 | 0.830 |
| | RFM [80] | 0.653 | 0.795 | 0.999 | 0.816 |
| BI (FF) | SBI [70] | 0.810 | 0.714 | 0.678 | 0.734 |

Table 4: Same forgery types, different data domains (**Protocol-2**): Cross-domain evaluation of different models on CDF domain. Within-forgery evaluations are in gray. FS (FF) denotes all FS data within the FF domain, with FR (FF), FS (CDF), *etc.*, having similar meanings.

| Training Set | Model | Testing Set (CDF) | | | |
|--------------|---------------|-------------------|----------|-----------|------------|
| | | FS (CDF) | FR (CDF) | EFS (CDF) | Avg. (CDF) |
| FS (FF) | Xception [16] | 0.922 | 0.657 | 0.642 | 0.740 |
| | CLIP [62] | 0.967 | 0.744 | 0.730 | 0.814 |
| | SRM [52] | 0.919 | 0.621 | 0.603 | 0.714 |
| | SPSL [48] | 0.938 | 0.656 | 0.648 | 0.747 |
| | RECCE [8] | 0.926 | 0.632 | 0.610 | 0.723 |
| | RFM [80] | 0.939 | 0.637 | 0.628 | 0.735 |
| FR (FF) | Xception [16] | 0.481 | 0.857 | 0.369 | 0.569 |
| | CLIP [62] | 0.638 | 0.933 | 0.209 | 0.593 |
| | SRM [52] | 0.454 | 0.869 | 0.326 | 0.550 |
| | SPSL [48] | 0.479 | 0.852 | 0.256 | 0.529 |
| | RECCE [8] | 0.452 | 0.881 | 0.332 | 0.555 |
| | RFM [80] | 0.492 | 0.882 | 0.359 | 0.578 |
| EFS (FF) | Xception [16] | 0.586 | 0.594 | 0.983 | 0.721 |
| | CLIP [62] | 0.617 | 0.735 | 0.988 | 0.780 |
| | SRM [52] | 0.589 | 0.620 | 0.964 | 0.724 |
| | SPSL [48] | 0.635 | 0.651 | 0.975 | 0.754 |
| | RECCE [8] | 0.623 | 0.603 | 0.984 | 0.737 |
| | RFM [80] | 0.644 | 0.666 | 0.981 | 0.764 |
| BI (FF) | SBI [70] | 0.679 | 0.609 | 0.723 | 0.670 |

Fake Data: To guarantee the *diversity* of deepfake approaches in the proposed DF40, we introduce and implement **40** distinct deepfake techniques, which are listed in Tab. 2. A detailed description of each deepfake method is provided in the supplementary. They are selected according to perspectives of modeling types, conditional sources, forgery effects, and functions. Formally, we denote $x_t(i_t, a_t, b_t)$ as the *target* subject to be manipulated, which possesses attributes (i : person identity, a : identity-agnostic content, b : external attributes) that can uniquely determine itself, while the *source* $x_s(i_s, a_s, b_s)$ is regarded as the *conditional media* (c), driving the *target* to change either identity or attributes or even both. We use $f_{sw}, f_{re}, f_{sy}, f_{ed}$ to represent four types of deepfakes in our work: *FS*, *FR*, *EFS*, and *FE*, respectively. Fig. 1 provides some visual examples for each category in DF40, and Fig. 16 generally illustrates them from the method perspective. (i) *FS Approach*: From Fig. 16(a), FS aims to replace the content of x_t with that of x_s preserving the identity i_s . Formally, $\tilde{x}_t(i_s, a_t, b_t)$ only swaps identity i from the source x_s to the target x_t , and the identity-agnostic content a are preserved. The swapping process can be expressed as:

$$f_{sw}(x_t(i_t, a_t, b_t), x_s(i_s, a_s, b_s)|\text{swap}) = \tilde{x}_t(i_s, a_t, b_t) \quad (1)$$

(ii) *FR Approach*: From Fig. 16(b), FR on $x_t(i_t, a_t, b_t)$ preserves its identity i_t but has its *intrinsic* attributes a_t , *e.g.*, pose, mouth and expression manipulated by a driven variable c_a and forms $\tilde{x}_t(i_t, \tilde{a}_s, b_t)$. Mathematically, we can drive the following equation:

$$f_{re}(x_t(i_t, a_t, b_t)|c_a) = \tilde{x}_t(i_t, \tilde{a}_s, b_t). \quad (2)$$

(iii) *EFS Approach*: EFS generates a completely synthesis face $\tilde{x}_t(\tilde{i}_t, \tilde{a}_t, \tilde{b}_t)$. In order to bridge the personal identity gap between generative models and other deepfake methods, we fine-tune the generative model G with the same real data as other forgery methods (*e.g.*, e4s [50]) and obtain a face-synthesis model f_{sy} . After that, we can synthesize new synthesis faces from noise n as follows:

$$f_{sy}(n) = \tilde{x}_t(\tilde{i}_t, \tilde{a}_t, \tilde{b}_t). \quad (3)$$

The general generation process can be seen in Fig. 16(c). (iv) *FE Approach*: From Fig. 16(d), FE on $x_t(i_t, a_t, b_t)$ has its *external* attributes b_t altered, such as facial hair, age, gender, and ethnicity, controlled by conditional source c_b , to obtain $\tilde{x}_t(i_t, a_t, \tilde{b}_s)$. We also include multiple attribute manipulation with two editing approaches, *e.g.*, both hair and eyebrows are manipulated. We can formulate the transformation as follows:

$$f_{ed}(x_t(i_t, a_t, b_t)|c_b) = \tilde{x}_t(i_t, a_t, \tilde{b}_s), \quad (4)$$

where $\tilde{\cdot}$ means that the element is manipulated by forgery algorithms.

4 Evaluations and Analysis

4.1 Experimental Setup

All pre-processing and training codebases in this work adhere to *DeepfakeBench* [94] to align the *standardized* settings. By following these *standardized* procedures, we aim to provide reliable and

Table 5: Different forgery types, different data domains (**Protocol-3**): toward real-world open-set evaluation of different models on the unknown domain. FS (FF) denotes all FS data within the FF domain, with FR (FF) and EFS (FF) being similar. BI donates using "BlendFake" only to train. Here, we use ① to mark the FS method, ② for the FR, ③ for the EFS, and ④ for the FE.

| Training Set | Model | Testing Set | | | | | | | | | |
|--------------|---------------|-----------------|------------|------------------|-----------------|-------------|--------------|---------------|---------|----------------|-------|
| | | DeepFaceLab (①) | HeyGen (②) | MidJourney-6 (③) | Whichisreal (④) | StarGAN (⑤) | StarGAN2 (⑥) | StyleCLIP (⑦) | e4c (⑧) | CollabDiff (⑨) | Avg. |
| FS (FF) | Xception [16] | 0.882 | 0.394 | 0.384 | 0.535 | 0.577 | 0.616 | 0.426 | 0.553 | 0.546 | 0.546 |
| | CLIP [62] | 0.930 | 0.539 | 0.540 | 0.439 | 0.896 | 0.746 | 0.730 | 0.738 | 0.674 | 0.692 |
| | SRM [52] | 0.866 | 0.473 | 0.298 | 0.538 | 0.606 | 0.617 | 0.572 | 0.410 | 0.699 | 0.564 |
| | SPSL [48] | 0.930 | 0.370 | 0.414 | 0.557 | 0.559 | 0.590 | 0.536 | 0.574 | 0.584 | 0.565 |
| | RECCE [8] | 0.899 | 0.537 | 0.293 | 0.509 | 0.580 | 0.599 | 0.399 | 0.520 | 0.492 | 0.536 |
| | RFM [80] | 0.918 | 0.719 | 0.286 | 0.496 | 0.652 | 0.570 | 0.705 | 0.689 | 0.798 | 0.648 |
| FR (FF) | Xception [16] | 0.705 | 0.473 | 0.459 | 0.323 | 0.492 | 0.456 | 0.006 | 0.175 | 0.050 | 0.349 |
| | CLIP [62] | 0.845 | 0.614 | 0.632 | 0.466 | 0.762 | 0.436 | 0.298 | 0.631 | 0.611 | 0.588 |
| | SRM [52] | 0.786 | 0.604 | 0.510 | 0.357 | 0.473 | 0.434 | 0.044 | 0.428 | 0.080 | 0.413 |
| | SPSL [48] | 0.704 | 0.543 | 0.446 | 0.272 | 0.348 | 0.423 | 0.002 | 0.585 | 0.060 | 0.376 |
| | RECCE [8] | 0.724 | 0.576 | 0.314 | 0.278 | 0.529 | 0.374 | 0.005 | 0.177 | 0.060 | 0.337 |
| | RFM [80] | 0.739 | 0.588 | 0.511 | 0.325 | 0.407 | 0.423 | 0.009 | 0.201 | 0.030 | 0.360 |
| EFS (FF) | Xception [16] | 0.497 | 0.325 | 0.472 | 0.772 | 0.777 | 0.677 | 0.984 | 0.611 | 0.997 | 0.679 |
| | CLIP [62] | 0.745 | 0.506 | 0.534 | 0.828 | 0.946 | 0.823 | 0.929 | 0.923 | 0.983 | 0.802 |
| | SRM [52] | 0.527 | 0.358 | 0.338 | 0.794 | 0.769 | 0.703 | 0.982 | 0.509 | 0.997 | 0.664 |
| | SPSL [48] | 0.641 | 0.383 | 0.427 | 0.694 | 0.699 | 0.723 | 0.922 | 0.602 | 0.967 | 0.673 |
| | RECCE [8] | 0.583 | 0.505 | 0.442 | 0.753 | 0.769 | 0.724 | 0.964 | 0.643 | 0.979 | 0.707 |
| | RFM [80] | 0.619 | 0.349 | 0.551 | 0.623 | 0.730 | 0.636 | 0.966 | 0.665 | 0.979 | 0.680 |
| BI (FF) | SBI [70] | 0.764 | 0.402 | 0.342 | 0.426 | 0.591 | 0.586 | 0.564 | 0.379 | 0.570 | 0.514 |

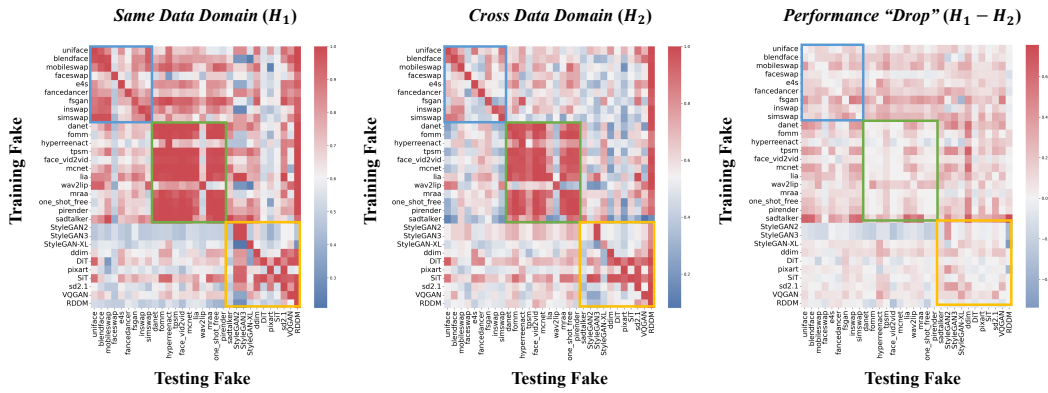


Figure 3: Heatmaps of One-Verse-All (OvA) evaluation (**Protocol-4**): Training the baseline (*i.e.*, Xception) on one fake and testing it on other remaining fakes. We show the within-domain evaluation (FF++ domain) and cross-domain evaluation (CDF domain). We also show the performance "drop" from the FF++ to the CDF. Blue donates all FS methods, Green for FR, and Yellow for EFS.

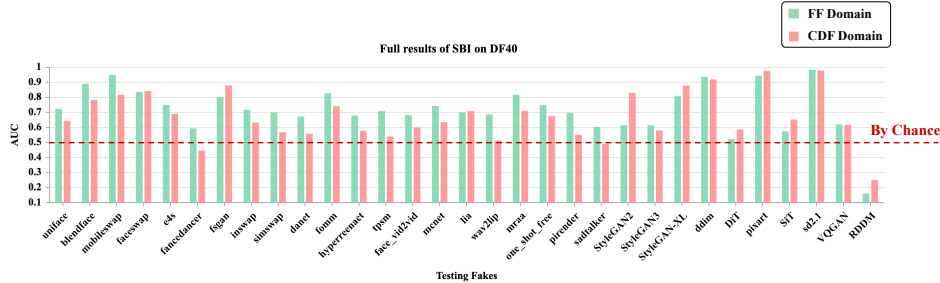


Figure 4: Full results of SBI [70] on the proposed DF40 dataset for both the FF (within) and CDF domain (cross). Discussion and analysis for the figure can be seen in Sec. 5.1. We evaluate other detectors, including Xception [67] and SPSL [48]) on our DF40 (CDF) in Fig. 9.

reproducible results for evaluations. The details of dataset configuration, algorithm implementation, and full training can be seen in the supplementary. Regarding evaluation, we compute the frame-level Area Under the Curve (AUC) as our primary evaluation metric. For detection selection, we choose the classical baseline Xception [16] with four SoTA detectors (SRM [52], SPSL [48], RECCE [8], RFM [80]) that use Xception as the backbone and implement a new algorithm for improved detection. In this manner, we aim to revisit the extra improvement over the baseline under our setting. We also include one SoTA blending-based method SBI [70]. Note that the original SBI paper only uses "BlendFake" (BI) for training, so here we do not train it with DF40 in evaluations.

4.2 Evaluations

In this work, we conduct main evaluations using four types of protocols: Cross-forgery evaluation (**Protocol-1**), Cross-domain evaluation (**Protocol-2**), Toward unknown forgery and domain evaluation (**Protocol-3**), and One-Verse-All (OvA) evaluation (**Protocol-4**). Our findings are highlighted in **blue**. We show the observations and use t-SNE, logit distributions, and the causal graph for analysis.

Protocol-1: Cross-forgery evaluation. This evaluation aims to evaluate the model’s performance within the same data domain but across different forgery methods. The results are presented in Tab. 3, and the observations are as follows: **Finding-1: Asymmetric performance drop among different forgery types.** Notably, the performance drop between FS and FR is moderate but more significant between these two and EFS. Specifically, model training on FS yields higher results (around 0.8) on EFS, while training on EFS only achieves about 0.6 on FS. **Finding-2: Existing well-designed (SoTA) detectors may not have obvious advantages over the baseline.** In our experiments, SRM, SPSL, RECCE, and RFM, all state-of-the-art deepfake detectors using Xception as their backbone, achieve results similar to the simple baseline Xception. This implies that these SoTA models might only learn sub-optimal forgery features and lack clear advantages over the baseline, although these SoTAs show higher results on previous datasets, *e.g.*, DFDC. **Finding-3: CLIP excels in deepfake detection than other baselines.** Outperforming other SoTA detectors and the Xception baseline across all scenarios, CLIP demonstrates the power of pre-training in deepfake detection. This raises the question: can we perform pre-training in the specific deepfake domain instead of the general CV domain? We will explore pre-training with CLIP in Sec. 5.2. **Finding-4: Blending is not all you need to detect deepfakes, even for face-swapping.** As observed, the SoTA blend-based detector SBI only achieves an average AUC result of 0.734, although it has demonstrated significant generalization performance on previous deepfake datasets. Previous research [45; 70; 12] has shown that models trained on blending data can achieve significantly higher results than those trained on deepfake data, suggesting that using blending for training is a necessary condition to achieve SoTA results. However, our results indicate that blending is *not* all you need. We conduct further analysis by testing SBI on individual forgery types of our DF40 to determine which type of forgery SBI can successfully simulate (see Sec. 5.1).

Protocol-2: Cross-domain evaluation. Cross-domain evaluation assesses the model’s performance across different data domains but with the same forgery methods. The results are presented in Tab. 4, and the observations are as follows: **Finding-5: Relatively minor performance drop when solely crossing data domains or forgery methods.** As we can see, the performance drop between FS and EFS is relatively small (0.9+) compared to FR (0.8+). Also, we found that the discriminative forgery artifacts of EFS do not have solid casual with data domain a very minor performance drop (only about 1%). **Finding-6: Forgery methods and data domains together contribute to discriminative forgery artifacts.** A significant performance drop is observed when both forgeries and domains change. For example, Xception training on FS (FF) achieves only 0.657 and 0.642 on FR (CDF) and EFS (CDF), respectively. These results are significantly lower (nearly a 20% drop) compared to results on FS (CDF) and FR (FF), which involve crossing only one of the domains or forgeries. This suggests that both factors together contribute to discriminative forgery artifacts for distinguishing real and fake.

We conduct further casual analysis below for better clarification. To intuitively convey our conclusions, we draw a **causal graph** to illustrate the causal relationship of how domain (D) and forgery method (F) influence the model’s generalization (R). The causal graph is presented in Fig. 5. In this graph, D represents the data domain, and F represents the forgery method. We hypothesize that these two factors influence three intermediate variables, X_1 , X_2 , and X_3 , which in turn affect the result R . The relationships are described as follows: X_1 represents the effect of the domain (D) on the result (R) independently; X_3 represents the effect of the forgery method (F) on the result (R) independently; and X_2 represents the combined effect of both the domain (D) and the forgery method (F) on the result (R). Mathematically, the model’s generalization result R can be expressed as a function of these intermediate variables: $R = f(X_1, X_2, X_3)$, where $X_1 = g(D)$ represents the domain-specific influence, $X_3 = h(F)$ represents the forgery method-specific influence, and $X_2 = k(D, F)$ represents the combined influence of both domain and forgery method. Each of these variables

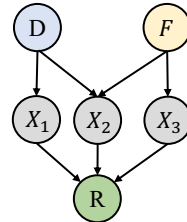


Figure 5: Causal graph for analyzing the influence of domain (D) and forgery (F).

Table 6: Comparison of different models/baselines used for pre-training. FS (CDF) denotes all FS data within the CDF domain. DF40 (FF) is the combination of FS (FF), FR (FF), and EFS (FF).

| Training Set | Model | Testing Set | | | | | | | | | | | | |
|--------------|------------|--------------|--------------|--------------|--------------|--------------|--------------|--------------|--------------|--------------|--------------|--------------|--------------|--------------|
| | | FS (CDF) | FR (CDF) | EFS (CDF) | DeepFaceLab | HeyGen | MidJourney-6 | Whichisreal | StarGAN | StarGAN2 | StyleCLIP | CollabDiff | e4e | Avg. |
| DF40 (FF) | Xception | 0.752 | 0.831 | 0.681 | 0.851 | 0.704 | 0.269 | 0.632 | 0.721 | 0.569 | 0.495 | 0.675 | 0.542 | 0.644 |
| | CLIP-base | 0.915 | 0.926 | 0.843 | 0.907 | 0.671 | 0.548 | 0.684 | 0.913 | 0.782 | 0.813 | 0.948 | 0.823 | 0.814 |
| | CLIP-large | 0.942 | 0.896 | 0.858 | 0.948 | 0.784 | 0.746 | 0.849 | 0.974 | 0.909 | 0.929 | 0.977 | 0.967 | 0.898 |

Table 7: Similar to Tab. 6, we evaluate on GenImage [102] (**non-face domain**), pure AIGCs.

| Training Set | Model | Testing Set | | | | | | | | |
|--------------|------------|-------------|--------|-------|------------|-------|-------|-------|--------|-------|
| | | ADM | BigGAN | GLide | MidJourney | SD-v4 | SD-v5 | Vqdm | Wukong | Avg. |
| DF40 (FF) | Xception | 0.723 | 0.529 | 0.514 | 0.558 | 0.490 | 0.494 | 0.469 | 0.505 | 0.535 |
| | CLIP-base | 0.940 | 0.850 | 0.666 | 0.447 | 0.494 | 0.494 | 0.682 | 0.542 | 0.639 |
| | CLIP-large | 0.911 | 0.967 | 0.736 | 0.571 | 0.630 | 0.614 | 0.882 | 0.660 | 0.746 |

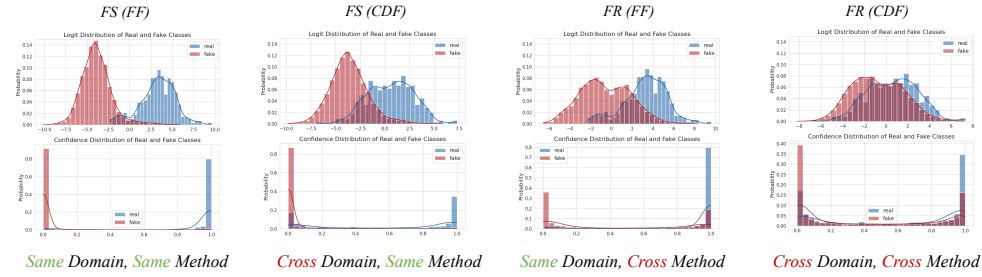
X_1 , X_2 , and X_3 captures different aspects of how D and F interact to impact the overall performance R . The functions g , h , and k are mappings that quantify the respective influences: $X_1 = g(D)$, $X_3 = h(F)$, and $X_2 = k(D, F)$. Finally, the result R is determined by integrating these influences: $R = f(g(D), k(D, F), h(F))$. This formalization helps us understand and analyze the separate and combined effects of the data domain and forgery method on the model’s generalization capability.

The logits and confidence analysis (shown in Fig. 6) further supports this point, showing the increased overlap between real and fake logits as domains and methods change incrementally. Also, crossing domains can result in "wrong confidence" for real predictions and vice versa. More specifically, we can observe from Fig. 6, as follows: **(1) For Xception:** (i) *Same Domain and Method:* Real and fake class distributions have small variance and high mean, with minimal ambiguity in confidence and less overlap between the real and fake logits. (ii) *Cross Method, Same Domain:* Fake class distribution has increased variance and lower mean, while real class remains relatively unchanged. (iii) *Cross Domain, Same Method:* Real class distribution has increased variance and lower mean, while fake class remains relatively unchanged, causing a slight performance decrease. (iv) *Cross Method and Domain:* Both real and fake class distributions have significantly increased variance and lower means, decreasing overall performance. Furthermore, in this case, the overlap between the real and fake distributions becomes obviously larger than the case(i), where both the domain and method are the same. **(2) For SBI:** It shows a different behavior than Xception. The real class distribution consistently has a small variance and high mean, while the fake class distribution has a larger variance and lower mean. This might suggest that SBI can learn a more robust distribution for real classes than the baseline (*wo* using blending), generalizing well in the FF domain using the FS method (0.81 AUC). However, when the real class distribution changes (*e.g.*, in the CDF domain), performance drops significantly (to 0.679 AUC). We will give a further discussion of SBI in Sec. 5.1.

Protocol-3: Unknown forgery and domain evaluation. This protocol tests model performance across different data domains and forgery methods, incorporating SoTA and popular software like DeepFaceLab [18], MidJourney-6 [53], and HeyGen [28] to simulate real-world scenarios. From the whole results in Tab. 5, we can see that: **(i)** Forgery artifacts can vary significantly across different forgeries (especially for FR and EFS), and artifacts of EFS can be similar to that of FE (see the results of StarGAN2 and CollabDiff); **(ii)** Models trained on FR display limited generalization ability, even falling below chance levels (0.5 AUC). Notably, Xception achieves only a 0.006 AUC on StyleCLIP. We provide further analysis of this phenomenon with both logit distribution and t-SNE visualization in Sec. 5.9. **(ii)** HeyGen and MidJourney-6 seem to pose significant challenges for detecting unknown forgeries, as most detectors only achieve unexpected results (AUC below 0.5). A possible reason for this is that both testing datasets exhibit highly realistic forgery quality. Consequently, it is essential to develop more robust detection methods in the future that can effectively identify forgeries with not only high-quality fakes but also high-resolution images.

Protocol-4: One-Verse-All (OvA) evaluation. The OvA evaluation trains a model on a specific forgery and tests it on all other forgeries. The results, presented in Fig. 3, reflect 31×31 evaluations for the heatmap (excluding 9 unknown domain forgeries). **Finding-7: FR forgeries may share transferable patterns for detecting other FR instances.** Most FR forgery methods demonstrate high AUC within the heatmap, even across data domains. However, Wav2Lip, an audio-driven reenactment forgery that only modifies the mouth region, is an exception. Its artifacts are more localized compared to other FRs that generate all content, making it different.

Xception



SBI

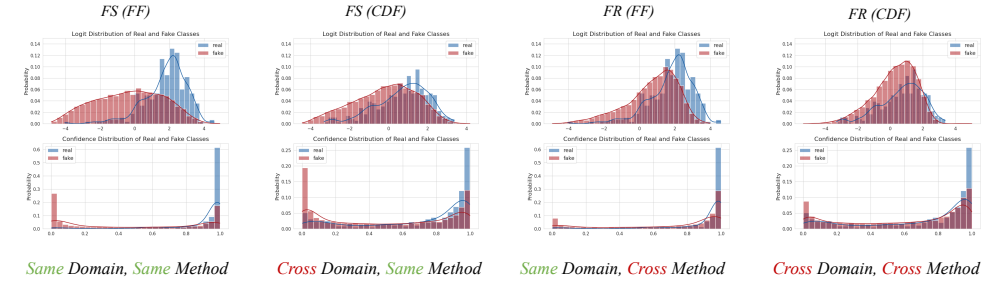


Figure 6: Logits and confidence distribution analysis. We visualize the logits distribution (before SoftMax) and confidence distribution (after SoftMax) for both real and fake classes. The overlap in the logits distribution represents the portion of "wrong classifications." We analyze two models: Xception [67] and SBI [70]. More discussion and analysis can be referred to Sec. 5.

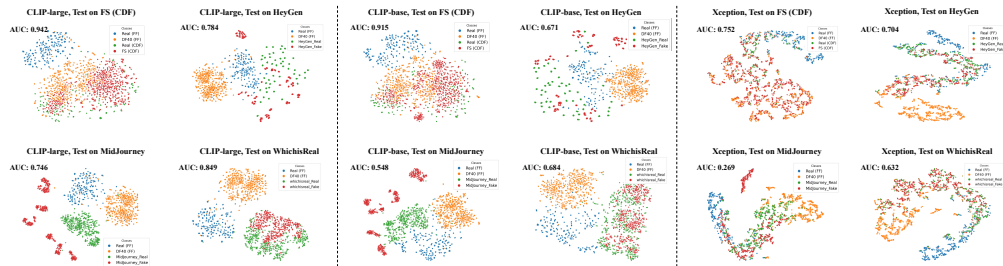


Figure 7: t-SNE Visualizations for three models: CLIP-large, CLIP-base, and Xception (from left to right). These models are trained on FS (FF). We conduct visualizations on FS (CDF), HeyGen [28], MidJourney [53], and WhichisReal [53]. More discussion and analysis can be referred to Sec. 5.

5 Analysis

In this subsection, we will dive deeper to provide insightful analysis based on previous observations and offer several new findings to the detection field to inspire future research.

5.1 Is Blending All You Need for Deepfake Detection?

Blending-based detectors have been considered highly effective for generalizable deepfake detection. Many SoTA detectors [70; 45; 11] use blending-generated pseudo-fake data and exclude actual deepfake data for training. However, our evaluations empirically show that **blending might not all you need**, as models trained with blending generally *underperform* compared to those trained on actual deepfake data (Tab. 3, Tab. 4, Tab. 5). This is likely because blending simulates fake artifacts similar to the "DF-family" of Face Swapping (FS) and may struggle to generalize forgeries that do not involve blending, such as the "FS-family" of FS and AI-generated content (EFS). Also, we evaluate SBI on 31 known forgeries across FF++ and CDF domains (see Fig. 4) and find that SBI performs well on some FS forgeries but also achieves near-perfect results on non-blending methods, *e.g.*, SD-2.1. However, it performs poorly on RDDM (FF), far below chance levels. Thus, an interesting

and meaningful question (**Question-1**) arises: *Which types of forgeries can be addressed by blending? And how to effectively combine blending fakes with actual deepfakes for training?* Moreover, we also found that: **Finding-8: SBI could be viewed as an "anomaly detection" model.** SBI can be considered an "anomaly detection" model, which might utilize the real features for classifying fakes. Results in Fig. 6 show that when forgery samples appear significantly different from real samples, SBI classifies them as anomalies (forgery samples), likely because the pseudo-fake samples generated by SBI closely resemble their original real counterparts.

5.2 Desirable Baselines/Backbones in Deepfake Detection for Pre-training.

Xception is often used as a baseline for deepfake detection, but is it the most suitable backbone? In this work, we re-evaluate Xception and compare it with the "stand-out" model CLIP (see **Finding-3**). We also include the large version of CLIP (CLIP-large), attempting to assess the "scaling law." As seen in Tab. 6, CLIP-large *significantly* outperforms CLIP-base (+8.4%) and Xception (+20.54%) on average. We also evaluate **non-face domain data** to determine if models trained on face-domain data can transfer to non-face-domain detection. In Tab. 7, surprisingly, CLIP-large achieves a 0.746 AUC on previously unseen non-face AIGCs, while Xception only reaches a 0.535 AUC, near chance levels. This leads to **Finding-9: CLIP-large is the most powerful baseline, significantly outperforming Xception** and **Finding-10: CLIP-large can even generalize to some non-face AIGCs when trained only on face data.** However, why can CLIP-large outperform the base by a notable margin? We analyze this point in the following paragraph from the view of real face distribution.

5.3 Analysis of the Real Face Distribution.

The results in Tab. 6 raise the question: why does CLIP-large significantly outperform Xception and its base version? We investigate further by analyzing the learned features of the three models, as visualized in Fig. 7. **(1)** We see that both versions of CLIP learn more informative features that can gather some real samples into several different "groups" (see HeyGen and MidJourney), while the real features of Xception mix all of them together. Leveraging large-scale pre-training, CLIP can capture more informative facial features (*e.g.*, ID) about real faces and thus "know" that these features are *unrelated* to deepfakes, while Xception could be overfitted to ID, as evidenced by [23]. **(2)** Between the large and base versions, CLIP-large's real samples are closer to each other (see WhichisReal), suggesting it learns more comprehensive features of real faces. We also see that **Finding-11: CLIP-large can implicitly "separate and align" different forgeries and data domains** ("orthogonal" in WhichisReal), with no need for explicit constraints as [75]. This point is further discussed and confirmed through t-SNE and logit distribution analysis in Sec. 5.4 below.

5.4 Comparative Analysis of CLIP-base and CLIP-large for Deepfake Detection

t-SNE visualization: Through t-SNE visualizations, we observe that the distribution of real images (blue points) for CLIP-large is significantly more compact than CLIP-base, where the points are more loosely scattered. This tight clustering among the blue points for CLIP-large indicates that it can more effectively capture the finer details and specific characteristics of different real images. Additionally, CLIP-large demonstrates a superior ability to learn the distinct features of various datasets. When performing dataset classification, we notice that the decision boundaries between different real domains and between real and fake domains can be orthogonal. This orthogonality is achieved without the need for explicitly adding a loss to align these boundaries, as suggested in the literature [75]. This implies that CLIP-large inherently distinguishes between domain-specific and domain-agnostic features, potentially due to insufficient real data, which makes it challenging to learn truly common features. Instead of attempting to decouple these features explicitly, CLIP-large identifies which features are domain-independent more efficiently.

Logits Distribution Analysis: The logits distributions provide further insights into the superior performance of CLIP-large. The logits for real images learned by CLIP-large are more concentrated and "tall and narrow," whereas those for CLIP-base are more "short and wide." This indicates that CLIP-large has a better grasp of the characteristics of real images, which enhances its ability to detect fakes. As evidenced by the reduced overlap between the real and fake logits distributions, CLIP-large's deep understanding of real images translates into a clearer differentiation between real

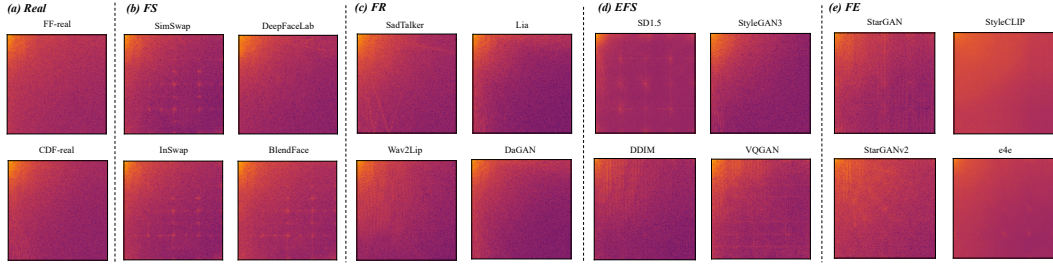


Figure 8: Frequency analysis on selected datasets of DF40. We compute the average frequency spectra of high-pass filtered images, following [82]. Although the deepfake types differ, they can show similar patterns/artifacts in the average spectra. For instance, methods from FS (*i.e.*, SimSwap [13], BlendFace [71], InSwap) show similar "checkboard" patterns that can also be observed in EFS (*i.e.*, SD1.5 [64], VQGAN [24]) and FE (*i.e.*, e4e [78]).

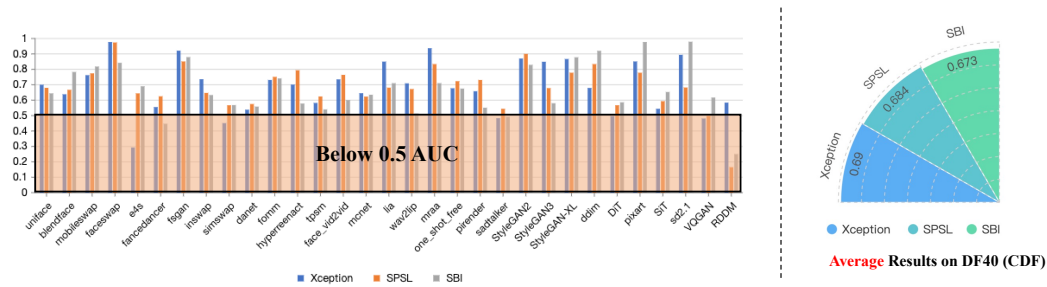


Figure 9: Results of evaluating three (previous) SoTA models (trained on FF++), *i.e.*, Xception [67], SPSL [48], and SBI [70]), on our DF40 (CDF). We show that, in most cases, these SoTAs fail to generalize well in our proposed forgeries, highlighting the importance of developing a comprehensive and diverse dataset.

and fake, improving detection accuracy. This suggests that better comprehending real images directly contributes to an improved understanding and detection of fake images.

Overall, the analysis highlights that CLIP-large outperforms CLIP-base in generalization for deepfake detection due to its superior feature learning capabilities. The compact clustering in t-SNE visuals and the focused logits distributions underscore its ability to distinguish between real and fake images more effectively. This enhanced understanding allows it to define more precise and orthogonal decision boundaries, leading to improved performance in detecting deepfakes across diverse datasets.

5.5 Generalization to Non-face Domain AIGCs

We also evaluate **non-face domain data** to determine if models trained on face-domain data can transfer to non-face-domain detection. From Tab. 8, we can observe the following: **(1)** The model trained on EFS (FF) demonstrates the highest average AUC value (0.815) when tested on non-face domain GenImage deepfakes. This suggests that the model, when trained on EFS, learns features related to forgery traces rather than features specific to face content. This ability to generalize from

Table 8: Evaluation of training CLIP-large on different variants of the proposed DF40 (face domain) to detect GenImage [102] (**non-face domain**), pure AIGCs.

| Model | Training Set | Testing Set | | | | | | | | |
|------------|--------------|-------------|--------|-------|------------|-------|-------|-------|--------|-------|
| | | ADM | BigGAN | GLide | MidJourney | SD-v4 | SD-v5 | Vqdm | Wukong | Avg. |
| CLIP-large | FS (FF) | 0.589 | 0.679 | 0.407 | 0.447 | 0.513 | 0.494 | 0.806 | 0.574 | 0.564 |
| | FR (FF) | 0.695 | 0.595 | 0.230 | 0.505 | 0.437 | 0.417 | 0.549 | 0.519 | 0.493 |
| | EFS (FF) | 0.912 | 0.992 | 0.906 | 0.591 | 0.729 | 0.72 | 0.956 | 0.713 | 0.815 |
| | DF40 (FF) | 0.911 | 0.967 | 0.736 | 0.571 | 0.630 | 0.614 | 0.882 | 0.660 | 0.746 |

Table 9: Results of evaluating three models (*i.e.*, I3D, CLIP-base, and CLIP-large) trained on different variants of the proposed DF40 on other *previous* deepfake datasets. Note that only FF-F2F [77] and FF-NT [76] are FR methods, while other testing data all belong to FS.

| Model | Training Set | Testing Set | | | | | | |
|-----------------------|-------------------|-------------|------------|-------------|------------|------------|------------------|------------|
| | | CDF-v2 [47] | FF-DF [19] | FF-F2F [77] | FF-FS [25] | FF-NT [76] | FaceShifter [44] | DF1.0 [35] |
| I3D (video-level AUC) | FS (FF) | 0.863 | 0.980 | 0.939 | 0.999 | 0.879 | 0.979 | 0.875 |
| | FR (FF) | 0.684 | 0.917 | 0.846 | 0.374 | 0.895 | 0.876 | 0.807 |
| | FS (FF) + FR (FF) | 0.764 | 0.970 | 0.926 | 0.994 | 0.928 | 0.953 | 0.929 |
| CLIP-base | FS (FF) | 0.823 | 0.965 | 0.678 | 0.985 | 0.585 | 0.932 | 0.945 |
| | FR (FF) | 0.649 | 0.669 | 0.572 | 0.457 | 0.682 | 0.625 | 0.947 |
| | EFS (FF) | 0.553 | 0.618 | 0.604 | 0.634 | 0.539 | 0.653 | 0.590 |
| | DF40 (FF) | 0.799 | 0.932 | 0.698 | 0.973 | 0.683 | 0.889 | 0.937 |
| CLIP-large | FS (FF) | 0.905 | 0.989 | 0.777 | 0.991 | 0.608 | 0.963 | 0.965 |
| | FR (FF) | 0.698 | 0.756 | 0.614 | 0.487 | 0.738 | 0.626 | 0.983 |
| | EFS (FF) | 0.616 | 0.733 | 0.634 | 0.730 | 0.571 | 0.772 | 0.739 |
| | DF40 (FF) | 0.891 | 0.978 | 0.753 | 0.973 | 0.717 | 0.927 | 0.986 |

face AIGCs to non-face AIGCs indicates the robustness of the model and its potential to detect deepfakes across different domains.

(2) The models trained on FS (FF) and FR (FF) show lower average AUC values (0.564 and 0.493, respectively) when tested on non-face domain GenImage deepfakes. This suggests that these models may be learning features more specific to face content or the particular manipulation techniques (face swap or drive) used in their training sets, limiting their ability to generalize to non-face AIGCs.

(3) The model trained on DF40 (FF), which includes a combination of different deepfake techniques, shows a relatively high average AUC value (0.746). While this is lower than the model trained on EFS (FF), it still indicates some level of generalization to non-face AIGCs. This suggests that training on a diverse set of deepfake techniques can help the model learn more general forgery-related features.

In summary, these results emphasize the importance of the training set in deepfake detection. Models trained on EFS (FF) appear to learn more general forgery-related features, enabling them to perform better on non-face AIGCs. Models trained on FS (FF) and FR (FF), on the other hand, maybe learning more technique-specific or face-specific features, limiting their performance on non-face AIGCs. This highlights the need for more research into training methods to help models generalize better across different deepfake techniques and domains.

5.6 Artifacts of Deepfake Forgeries in Frequency

Brief Introduction: Inspired by [82], we adopt a similar approach to visualize the average frequency spectra of each dataset. The purpose is to examine the artifacts generated by deepfake forgeries. Our methodology involves computing various statistics for image datasets, either in grayscale or across each color channel separately, and visualizing these statistics using heatmaps. We use two metrics to evaluate the results: *mean* and *std*. (1) The mean represents the average value of the DCT coefficients across the images in the dataset. A higher mean value means that, on average, the images are brighter or have more detailed features. For deepfake images, this might indicate that the synthetic process adds extra brightness or emphasizes certain facial details. On the other hand, a lower mean value suggests that the images are generally darker or smoother, possibly missing some fine details. By comparing the mean values of deepfake images to those of real images, we can see how well the fake images replicate the overall brightness and texture of real human faces. (2) The standard deviation (*std*) measures the spread or variability of the DCT coefficients around the mean. A higher standard deviation means more variation in the textures and details within the images. For deepfakes, this could point to inconsistencies or artifacts from the generation process, making the images easier to spot as fake. Conversely, a lower standard deviation indicates that the images are more similar, which might suggest a more uniform generation process but could also mean the images lack the natural diversity seen in real faces. We can assess how consistent and realistic the deepfake images are compared to real human faces by looking at the standard deviation.

Mean Analysis: **Finding-12: We observe that many GAN-generated images, such as those from StyleGAN, often exhibit a checkerboard or grid-like pattern of bright spots on the mean heatmap** This phenomenon occurs because of the upsampling methods used in the GAN architecture, which can introduce such artifacts during the image generation process. These patterns are typically a result of the transposed convolution operations, which can cause uneven overlaps and thus create these visible grid artifacts. Moreover, it appears that different forgery methods can share similar patterns.

For instance, face-swapping techniques like SimSwap also exhibit these GAN-like checkerboard artifacts. This similarity indicates that these methods generate the entire image using AI without a blending process. This contrasts with other Deepfake methods, such as those used in Celeb-DF, which involve blending and thus do not produce the same checkerboard artifacts.

Std Analysis: The standard deviation heatmaps reveal additional artifacts. For example, methods like DDPM and StarGAN also display checkerboard artifacts in the standard deviation maps. Interestingly, while StyleGAN exhibits these checkerboard patterns in the mean heatmaps, it does not show similar artifacts in the standard deviation maps. This discrepancy suggests that while the upsampling process affects StyleGAN’s mean values, the overall variability or consistency across multiple generated images is not influenced similarly. This could imply that StyleGAN maintains a certain level of uniformity regarding pixel variance, even though the generation process distorts the mean values. Additionally, we observe radial artifacts in the standard deviation heat maps through methods such as HeyGen, DeepFaceLab, and DaGAN. These radial patterns indicate a different type of artifact, possibly resulting from how these methods handle image transformations and blending processes. The presence of these radial artifacts in the standard deviation maps suggests inconsistencies in the generation process, where certain regions of the images exhibit more variability than others.

5.7 Generalization to External/Previous Deepfake Datasets

We also evaluate the model trained on DF40 to detect previous deepfake datasets. Results in Tab. 9 show that **(1)** For the I3D detection method, training on FS (FF) and FR (FF) combined (FS (FF) + FR (FF)) results in better performance across most testing sets compared to training on FS (FF) or FR (FF) individually. This suggests that combining face-swapping and face-reenactment datasets for training improves the generalization capabilities of the I3D method. **(2)** Among the CLIP-base detection methods, training on DF40 (FF) leads to better performance across most testing sets compared to training on FS (FF), FR (FF), or EFS (FF) individually. This indicates that incorporating diverse deepfake techniques in the training set improves the generalization capabilities of the CLIP-base method. **(3)** The same trend is observed for the CLIP-large detection methods, where training on DF40 (FF) results in better performance across most testing sets compared to training on FS (FF), FR (FF), or EFS (FF) individually. This further supports the importance of training on diverse deepfake techniques to enhance the generalization capabilities of the detection methods. **(4)** The CLIP-large detection method generally outperforms the CLIP-base method across most testing sets when trained on the same training sets. This suggests that the larger model size of CLIP-large contributes to better deepfake detection performance (similar to **Finding-9**).

5.8 Detection Results of Previous Detectors on the Proposed DF40 dataset

To evaluate the generalization capabilities of various deepfake detection models, we tested three pre-trained (on FF++) models: Xception (baseline), SPSL (frequency-based model), and SBI (blending-based model) on our DF40 (CDF) dataset, which includes 31 known deepfake methods. These models were initially trained on the FF++ dataset. The results in Fig. 9 indicate that all three models struggle to generalize effectively to the DF40 dataset, with an average AUC of only around 0.6. This performance is significantly below the ideal detection threshold, underscoring the limitations of current models in handling a diverse range of deepfake techniques. This finding highlights the critical need for developing larger and more comprehensive datasets to train robust deepfake detection systems. By expanding the diversity and volume of the training data, we can improve the models’ ability to detect and generalize across various deepfake methods, enhancing their real-world applicability and effectiveness.

5.9 Analysis of "Anomalous Values" in Experiments

In our previous experimental results summarized in Tab. 5 (protocol-3), we observed an anomalous outcome where the Xception model, trained on FF (FR), achieved an AUC of less than 0.2 on the StyleCLIP dataset. Given that an AUC of 0.5 indicates performance by chance, this result is particularly perplexing. To investigate further, we conducted a t-SNE analysis on the feature distributions of different classes, as well as examined the logits and confidence distributions for different prediction results.

Xception, Train on FR (FF), Test on StyleCLIP

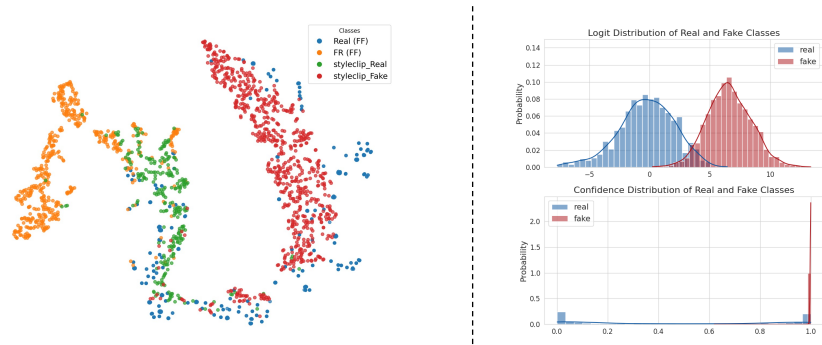
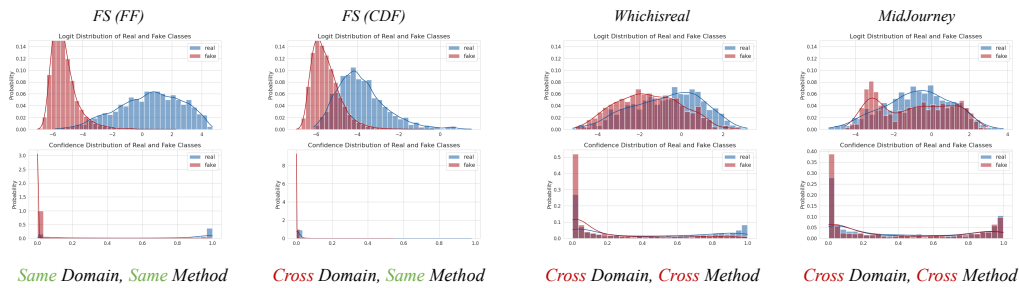


Figure 10: t-SNE visualization and logits analysis for analyzing the model, which is trained on FR (FF) and tested on StyleCLIP, achieving only about 0.05 AUC in Tab. 5 (Protocol-3). See the text in Sec. 5.9 for our analysis and more details.

CLIP-base



CLIP-large

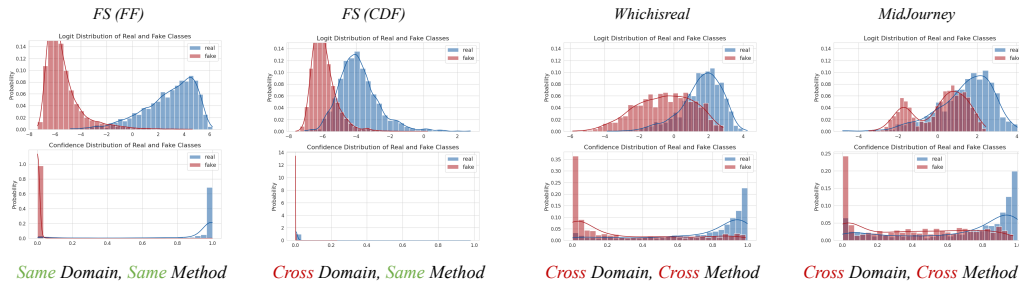


Figure 11: Logits and confidence analysis for comparing CLIP-base and CLIP-large models.

The t-SNE analysis 10 revealed that the features learned during training for real and fake images were inversely mapped during testing. Specifically, the features for the training real images overlapped with the testing fake images, indicating that the model might not have effectively learned robust real features. This inversion suggests that the model’s naive discriminative learning approach failed to adequately differentiate between real and fake images, leading to a complete misclassification in the new testing set.

The logits distribution 10 further supports this observation. The confidence curves for real and fake predictions were flipped, reinforcing the notion that the model was predicting the opposite of what it should. This inversion implies that the Xception model, in this context, was not only failing to generalize but was actively misclassifying due to its inability to learn stable and transferable features.

This analysis highlights a critical limitation of simple discriminative learning approaches in deepfake detection. It underscores the need for more sophisticated training strategies that can better capture the intrinsic characteristics of real and fake images, ensuring more robust performance across

varied datasets. This could involve incorporating more diverse training data, using advanced feature extraction techniques, or employing generative adversarial networks to improve feature robustness and generalization.

6 Open Questions and Potential Topics for Future Research

Here, we will give further discussion on interesting research questions to inspire future research toward next-generation deepfake detection.

(1) **Question-1** in Sec. 5.1 highlights the role of blending data in training deepfake detectors. Instead of using "BlendFake" only for training, how can we effectively mine the true potential and position of BlendFake? For instance, how can we combine Deepfake and BlendFake together for improved training (creating "1+1>2" results)? And what kinds of forgeries can BlendFake address?

(2) Also, as the diversity of deepfake data increasingly goes up, **Question-2** raise: *how to design an incremental learning framework to effectively learn (many) different forgeries incrementally?* In the implementation of this incremental learning framework, how can we deal with the real data?

(3) Previous research [93; 92] classified deepfake types at the instance level. For example, if four deepfakes are applied for training, they will be regarded as four *distinct* deepfakes. However, there are so many forgery techniques available that it is hard to elaborate on them all. **Question-3:** *can we classify deepfakes based on FS, FR, EFS, and FE?* It is still questionable since different forgeries can share similar forgery patterns, *e.g.*, generative artifacts (see Fig. 8). So, it would be possible to define a "metric" to classify different forgeries into different classes, aiming to learn effectively specific forgery features and common features jointly (following the framework of UCF [93]).

(4) In our research, it can be seen that CLIP-large can achieve obvious advantages over other models (including CLIP-base). We perform t-SNE (Fig. 7) and logit distribution (Fig. 6) for deeper analysis. We found that CLIP-large can learn a more robust distribution for the real face than CLIP-base. So, **Question-4:** *can we further "inflate" this CLIP-large model into a video model for detecting deepfake videos?* Or similarly, **Question-5:** *can we leverage the power of the current SoTA multi-modality technique to develop a better real face representation for deepfake detection?*

7 Conclusions, Board Impacts, Limitations, and Dataset Usage

(1) **Conclusions:** We have developed *DF40*, a highly diverse and groundbreaking benchmark, comprising 40 distinct deepfake techniques to support the detection. Leveraging *DF40*, we conducted over 2,000+ evaluations using 7 representative detectors under 4 standard evaluation protocols, creating 12 new findings and 5 open questions for future works. We hope the proposed *DF40* could revolutionize the whole field for the next generation.

(2) **Board Impacts:** *DF40* offers high-quality and realistic deepfake techniques, facilitating the detection of today's real-world deepfakes. Also, our benchmark assists in safeguarding societal trust and promoting the responsible use of such technology.

(3) **Limitations:** One limitation is the lack of comprehensive analysis for *video-level detectors*. Actually, we provide evaluations using video models, *e.g.*, I3D [9] in the supplementary. However, we have not delved deeply into discussing and analyzing certain issues, *e.g.*, assessing and visualizing whether video models can effectively capture both temporal and spatial artifacts. In future work, we plan to broaden our benchmark's scope and address these concerns in detail.

(4) **Dataset Usage:** The proposed *DF40* dataset can be incorporated seamlessly into the codebase of DeepfakeBench [94], where the user can use the existing more than 30 detection methods to train or test on our *DF40*, making it convenient to use. We will release the dataset on [GitHub](#).

8 Content Structure in Supplementary

We have organized additional important content in the supplementary due to the limited space. We present a brief outline of the content structure of the supplementary to facilitate readers to find the corresponding content, as follows:

- **Section A.1: Dataset Generation Methods & Original Data:**
 - Section A.1.1: Brief Introduction of Generation Methods;
 - Section A.1.2: Details of 40 Implemented Synthesis Methods;
 - Section A.1.3: Formulation of Manipulation Methods;
 - Section A.1.4: Details of Original Datasets;
- **Section A.2: Introduction of the Used Detection Methods:**
- **Section A.3: Experimental Setup & Full Results:**
 - Section A.3.1: Experimental Setup and Details;
 - Section A.3.2: Full Experimental Results and Further Discussion;
- **Section A.4 Additional information on Dataset Publication:**
 - Section A.4.1: Descriptions of Links;
 - Section A.4.2: Descriptions of the Hosting Platform and Access to the Dataset;
 - Section A.4.3: Descriptions of licensing.

9 Takeaways

In this section, we very briefly outline several key takeaways to encapsulate our contributions and conclusions:

- (1) The dataset is pivotal in addressing the generalization problem in deepfake detection. To this end, we build a highly diverse deepfake dataset incorporating 40 distinct deepfake techniques, including the most recent ones. The visual example can be seen in Fig. 12 (FS), Fig. 13, Fig. 14 (EFS), and Fig. 15 (FE and other novel methods);
- (2) Data domain and forgery method collectively determine the final detection results (see the causal graph Fig. 5 for intuitive understanding);
- (3) Many recent face-swapping methods (*e.g.*, Inswapper [33], SimSwap [13]) do *not* involve a blending process but generate all content directly (including the background). See the artifacts between SimSwap (FS) and SD1.5 (EFS) in Fig. 8.
- (4) Blending is not all you need to detect deepfakes, even face-swapping forgeries (Sec. 5.1);
- (5) CLIP-large is the most powerful baseline model due to its notable ability to learn robust real-face distribution (see Sec. 5.3);
- (6) The model trained on the face domain (our dataset) can also be somehow applied to the non-face domain (pure AIGC) fakes (see Sec. 5.5);
- (7) There is an urgent need to develop an effective incremental learning framework aiming to produce improved results, creating "1+1>2" results when combining many different forgeries together for training (see Question-2).

Acknowledgments and Disclosure of Funding

We would like to express our profound gratitude to all the individuals (all collaborators) who have contributed to the successful completion of this work. Our heartfelt appreciation goes out to Yue Han and Chengming Xu from Tencent Youtu Lab, as well as Wentang Song from Shenzhen University, for their invaluable support in code implementation and reproduction.

Furthermore, we extend our gratitude to Ke Sun from Xiamen University, Mingli Zhu from the Chinese University of Hong Kong, Shenzhen (CUHK-Shenzhen), Shaokui Wei from CUHK-Shenzhen, Mingda Zhang from CUHK-Shenzhen, and Yuhao Luo from CUHK-Shenzhen for their insightful discussions and contributions to this work.

Our sincere thanks go to the code developers of DeepfakeBench for their easy-to-use codebase and unified training/testing framework. This includes Xinghang Yuan (previously in CUHK-Shenzhen), Yize Chen (CUHK-Shenzhen), Kangran Zhao (CUHK-Shenzhen), and Jikang Cheng (Wuhan University). Once again, we thank everyone involved for their dedication and efforts in making this big project successful.

References

- [1] Faceswap. <https://github.com/MarekKowalski/FaceSwap>. Accessed: 2020-05-10.
- [2] Darius Afchar, Vincent Nozick, Junichi Yamagishi, and Isao Echizen. Mesonet: a compact facial video forgery detection network. In *2018 IEEE International Workshop on Information Forensics and Security*, pages 1–7. IEEE, 2018.
- [3] Triantafyllos Afouras, Joon Son Chung, and Andrew Zisserman. Lrs3-ted: a large-scale dataset for visual speech recognition. *arXiv preprint arXiv:1809.00496*, 2018.
- [4] Shruti Agarwal, Hany Farid, Ohad Fried, and Maneesh Agrawala. Detecting deep-fake videos from phoneme-viseme mismatches. In *Proceedings of the IEEE/CVF Conference on Computer Vision and Pattern Recognition Workshops*, pages 660–661, 2020.
- [5] Sara Atito, Muhammad Awais, and Josef Kittler. Sit: Self-supervised vision transformer. *arXiv preprint arXiv:2104.03602*, 2021.
- [6] Chaitali Bhattacharyya, Hanxiao Wang, Feng Zhang, Sungho Kim, and Xiatian Zhu. Diffusion deepfake. *arXiv preprint arXiv:2404.01579*, 2024.
- [7] Stella Bounareli, Christos Tzelepis, Vasileios Argyriou, Ioannis Patras, and Georgios Tzimiropoulos. Hyperreenact: one-shot reenactment via jointly learning to refine and retarget faces. In *Proceedings of the IEEE/CVF International Conference on Computer Vision*, pages 7149–7159, 2023.
- [8] Junyi Cao, Chao Ma, Taiping Yao, Shen Chen, Shouhong Ding, and Xiaokang Yang. End-to-end reconstruction-classification learning for face forgery detection. In *Proceedings of the IEEE/CVF Conference on Computer Vision and Pattern Recognition*, pages 4113–4122, 2022.
- [9] Joao Carreira and Andrew Zisserman. Quo vadis, action recognition? a new model and the kinetics dataset. In *proceedings of the IEEE Conference on Computer Vision and Pattern Recognition*, pages 6299–6308, 2017.
- [10] Junsong Chen, Jincheng Yu, Chongjian Ge, Lewei Yao, Enze Xie, Yue Wu, Zhongdao Wang, James Kwok, Ping Luo, Huchuan Lu, et al. Pixart-alpha: Fast training of diffusion transformer for photorealistic text-to-image synthesis. *arXiv preprint arXiv:2310.00426*, 2023.
- [11] Liang Chen, Yong Zhang, Yibing Song, Lingqiao Liu, and Jue Wang. Self-supervised learning of adversarial example: Towards good generalizations for deepfake detection. In *Proceedings of the IEEE/CVF Conference on Computer Vision and Pattern Recognition*, pages 18710–18719, 2022.
- [12] Liang Chen, Yong Zhang, Yibing Song, Jue Wang, and Lingqiao Liu. Ost: Improving generalization of deepfake detection via one-shot test-time training. In *Nips*, 2022.
- [13] Renwang Chen, Xuanhong Chen, Bingbing Ni, and Yanhao Ge. Simswap: An efficient framework for high fidelity face swapping. In *Proceedings of the 28th ACM international conference on multimedia*, pages 2003–2011, 2020.
- [14] Yunjey Choi, Minje Choi, Munyoung Kim, Jung-Woo Ha, Sunghun Kim, and Jaegul Choo. Stargan: Unified generative adversarial networks for multi-domain image-to-image translation. In *Proceedings of the IEEE conference on computer vision and pattern recognition*, pages 8789–8797, 2018.
- [15] Yunjey Choi, Youngjung Uh, Jaejun Yoo, and Jung-Woo Ha. Stargan v2: Diverse image synthesis for multiple domains. In *Proceedings of the IEEE/CVF conference on computer vision and pattern recognition*, pages 8188–8197, 2020.
- [16] François Chollet. Xception: Deep learning with depthwise separable convolutions. In *Proceedings of the IEEE/CVF Conference on Computer Vision and Pattern Recognition*, pages 1251–1258, 2017.
- [17] Hao Dang, Feng Liu, Joel Stehouwer, Xiaoming Liu, and Anil K Jain. On the detection of digital face manipulation. In *Proceedings of the IEEE/CVF Conference on Computer Vision and Pattern Recognition*, 2020.
- [18] DeepFaceLab. <https://github.com/iperov/DeepFaceLab>.
- [19] DeepFakes. www.github.com/deepfakes/faceswap Accessed 2021-04-24.
- [20] Deepfake detection challenge. <https://www.kaggle.com/c/deepfake-detection-challenge> Accessed 2021-04-24.

- [21] DFD. <https://ai.googleblog.com/2019/09/contributing-data-to-deepfake-detection.html> Accessed 2021-04-24.
- [22] Brian Dolhansky, Joanna Bitton, Ben Pfau, Jikuo Lu, Russ Howes, Menglin Wang, and Cristian Canton Ferrer. The deepfake detection challenge dataset. *arXiv preprint arXiv:2006.07397*, 2020.
- [23] Shichao Dong, Jin Wang, Renhe Ji, Jiajun Liang, Haoqiang Fan, and Zheng Ge. Implicit identity leakage: The stumbling block to improving deepfake detection generalization. In *Proceedings of the IEEE/CVF Conference on Computer Vision and Pattern Recognition*, pages 3994–4004, 2023.
- [24] Patrick Esser, Robin Rombach, and Bjorn Ommer. Taming transformers for high-resolution image synthesis. In *Proceedings of the IEEE/CVF conference on computer vision and pattern recognition*, pages 12873–12883, 2021.
- [25] FaceSwap. www.github.com/MarekKowalski/FaceSwap Accessed 2021-04-24.
- [26] Alexandros Haliassos, Konstantinos Vougioukas, Stavros Petridis, and Maja Pantic. Lips don't lie: A generalisable and robust approach to face forgery detection. In *CVPR*, 2021.
- [27] Yanan He, Bei Gan, Siyu Chen, Yichun Zhou, Guojun Yin, Luchuan Song, Lu Sheng, Jing Shao, and Ziwei Liu. Forgerynet: A versatile benchmark for comprehensive forgery analysis. In *Proceedings of the IEEE/CVF conference on computer vision and pattern recognition*, pages 4360–4369, 2021.
- [28] HeyGen. <https://www.heygen.com>.
- [29] Jonathan Ho, Ajay Jain, and Pieter Abbeel. Denoising diffusion probabilistic models. *Advances in neural information processing systems*, 33:6840–6851, 2020.
- [30] Fa-Ting Hong and Dan Xu. Implicit identity representation conditioned memory compensation network for talking head video generation. In *Proceedings of the IEEE/CVF International Conference on Computer Vision*, pages 23062–23072, 2023.
- [31] Fa-Ting Hong, Longhao Zhang, Li Shen, and Dan Xu. Depth-aware generative adversarial network for talking head video generation. In *Proceedings of the IEEE/CVF conference on computer vision and pattern recognition*, pages 3397–3406, 2022.
- [32] Ziqi Huang, Kelvin CK Chan, Yuming Jiang, and Ziwei Liu. Collaborative diffusion for multi-modal face generation and editing. In *Proceedings of the IEEE/CVF Conference on Computer Vision and Pattern Recognition*, pages 6080–6090, 2023.
- [33] inswapper. <https://github.com/haofanwang/inswapper>.
- [34] Yonghyun Jeong, Jongwon Choi, Doyeon Kim, Sehyeon Park, Minki Hong, Changhyun Park, Seungjai Min, and Youngjune Gwon. Dofnet: Depth of field difference learning for detecting image forgery. In *Proceedings of the Asian Conference on Computer Vision*, 2020.
- [35] Liming Jiang, Ren Li, Wayne Wu, Chen Qian, and Chen Change Loy. Deepforensics-1.0: A large-scale dataset for real-world face forgery detection. In *Proceedings of the IEEE/CVF Conference on Computer Vision and Pattern Recognition*, 2020.
- [36] Yan Ju, Shan Jia, Jialing Cai, Haiying Guan, and Siwei Lyu. Gllf: Global and local feature fusion for ai-synthesized image detection. *IEEE Transactions on Multimedia*, 2023.
- [37] Tero Karras, Miika Aittala, Samuli Laine, Erik Härkönen, Janne Hellsten, Jaakko Lehtinen, and Timo Aila. Alias-free generative adversarial networks. *Advances in neural information processing systems*, 34:852–863, 2021.
- [38] Tero Karras, Samuli Laine, and Timo Aila. A style-based generator architecture for generative adversarial networks. In *Proceedings of the IEEE/CVF conference on computer vision and pattern recognition*, pages 4401–4410, 2019.
- [39] Tero Karras, Samuli Laine, Miika Aittala, Janne Hellsten, Jaakko Lehtinen, and Timo Aila. Analyzing and improving the image quality of stylegan. In *Proceedings of the IEEE/CVF conference on computer vision and pattern recognition*, pages 8110–8119, 2020.
- [40] Hasam Khalid, Shahroz Tariq, Minha Kim, and Simon S Woo. Fakeavceleb: A novel audio-video multimodal deepfake dataset. *arXiv preprint arXiv:2108.05080*, 2021.
- [41] Pavel Korshunov and Sébastien Marcel. Deepfakes: a new threat to face recognition? assessment and detection. *arXiv preprint arXiv:1812.08685*, 2018.

- [42] Patrick Kwon, Jaeseong You, Gyuhyeon Nam, Sungwoo Park, and Gyeongsu Chae. Kodf: A large-scale korean deepfake detection dataset. In *Proceedings of the IEEE/CVF International Conference on Computer Vision*, pages 10744–10753, 2021.
- [43] Haodong Li, Bin Li, Shunquan Tan, and Jiwu Huang. Identification of deep network generated images using disparities in color components. *Signal Processing*, 174:107616, 2020.
- [44] Lingzhi Li, Jianmin Bao, Hao Yang, Dong Chen, and Fang Wen. Advancing high fidelity identity swapping for forgery detection. In *Proceedings of the IEEE/CVF Conference on Computer Vision and Pattern Recognition*, pages 5074–5083, 2020.
- [45] Lingzhi Li, Jianmin Bao, Ting Zhang, Hao Yang, Dong Chen, Fang Wen, and Baining Guo. Face x-ray for more general face forgery detection. In *Proceedings of the IEEE/CVF Conference on Computer Vision and Pattern Recognition*, 2020.
- [46] Yuezun Li and Siwei Lyu. Exposing deepfake videos by detecting face warping artifacts. *arXiv preprint arXiv:1811.00656*, 2018.
- [47] Yuezun Li, Xin Yang, Pu Sun, Honggang Qi, and Siwei Lyu. Celeb-df: A new dataset for deepfake forensics. In *Proceedings of the IEEE/CVF Conference on Computer Vision and Pattern Recognition*, 2020.
- [48] Honggu Liu, Xiaodan Li, Wenbo Zhou, Yuefeng Chen, Yuan He, Hui Xue, Weiming Zhang, and Nenghai Yu. Spatial-phase shallow learning: rethinking face forgery detection in frequency domain. In *Proceedings of the IEEE/CVF Conference on Computer Vision and Pattern Recognition*, 2021.
- [49] Jiawei Liu, Qiang Wang, Huijie Fan, Yinong Wang, Yandong Tang, and Liangqiong Qu. Residual denoising diffusion models. *arXiv preprint arXiv:2308.13712*, 2023.
- [50] Zhian Liu, Maomao Li, Yong Zhang, Cairong Wang, Qi Zhang, Jue Wang, and Yongwei Nie. Fine-grained face swapping via regional gan inversion. In *Proceedings of the IEEE/CVF conference on computer vision and pattern recognition*, pages 8578–8587, 2023.
- [51] Ziwei Liu, Ping Luo, Xiaogang Wang, and Xiaoou Tang. Large-scale celebfaces attributes (celeba) dataset. Retrieved August, 15(2018):11, 2018.
- [52] Yuchen Luo, Yong Zhang, Junchi Yan, and Wei Liu. Generalizing face forgery detection with high-frequency features. In *Proceedings of the IEEE/CVF Conference on Computer Vision and Pattern Recognition*, 2021.
- [53] MidJourney. <https://www.midjourney.com/home>.
- [54] Yisroel Mirsky and Wenke Lee. The creation and detection of deepfakes: A survey. *ACM computing surveys (CSUR)*, 54(1):1–41, 2021.
- [55] Kartik Narayan, Harsh Agarwal, Kartik Thakral, Surbhi Mittal, Mayank Vatsa, and Richa Singh. Df-platter: multi-face heterogeneous deepfake dataset. In *Proceedings of the IEEE/CVF Conference on Computer Vision and Pattern Recognition*, pages 9739–9748, 2023.
- [56] Huy H Nguyen, Fuming Fang, Junichi Yamagishi, and Isao Echizen. Multi-task learning for detecting and segmenting manipulated facial images and videos. In *IEEE International Conference on Biometrics Theory, Applications and Systems*, pages 1–8. IEEE, 2019.
- [57] Yuval Nirkin, Yosi Keller, and Tal Hassner. Fsgan: Subject agnostic face swapping and reenactment. In *Proceedings of the IEEE/CVF international conference on computer vision*, pages 7184–7193, 2019.
- [58] Or Patashnik, Zongze Wu, Eli Shechtman, Daniel Cohen-Or, and Dani Lischinski. Styleclip: Text-driven manipulation of stylegan imagery. In *Proceedings of the IEEE/CVF international conference on computer vision*, pages 2085–2094, 2021.
- [59] William Peebles and Saining Xie. Scalable diffusion models with transformers. In *Proceedings of the IEEE/CVF International Conference on Computer Vision*, pages 4195–4205, 2023.
- [60] KR Prajwal, Rudrabha Mukhopadhyay, Vinay P Namboodiri, and CV Jawahar. A lip sync expert is all you need for speech to lip generation in the wild. In *Proceedings of the 28th ACM international conference on multimedia*, pages 484–492, 2020.
- [61] Yuyang Qian, Guojun Yin, Lu Sheng, Zixuan Chen, and Jing Shao. Thinking in frequency: Face forgery detection by mining frequency-aware clues. In *European Conference Computer Vision*, pages 86–103. Springer, 2020.

- [62] Alec Radford, Jong Wook Kim, Chris Hallacy, Aditya Ramesh, Gabriel Goh, Sandhini Agarwal, Girish Sastry, Amanda Askell, Pamela Mishkin, Jack Clark, et al. Learning transferable visual models from natural language supervision. In *International conference on machine learning*, pages 8748–8763. PMLR, 2021.
- [63] Yurui Ren, Ge Li, Yuanqi Chen, Thomas H Li, and Shan Liu. Pirenderer: Controllable portrait image generation via semantic neural rendering. In *Proceedings of the IEEE/CVF International Conference on Computer Vision*, pages 13759–13768, 2021.
- [64] Robin Rombach, Andreas Blattmann, Dominik Lorenz, Patrick Esser, and Björn Ommer. High-resolution image synthesis with latent diffusion models. In *Proceedings of the IEEE/CVF conference on computer vision and pattern recognition*, pages 10684–10695, 2022.
- [65] Roop. <https://github.com/s0md3v/roop>.
- [66] Felix Rosberg, Eren Erdal Aksoy, Fernando Alonso-Fernandez, and Cristofer Englund. Facedancer: Pose-and occlusion-aware high fidelity face swapping. In *Proceedings of the IEEE/CVF winter conference on applications of computer vision*, pages 3454–3463, 2023.
- [67] Andreas Rossler, Davide Cozzolino, Luisa Verdoliva, Christian Riess, Justus Thies, and Matthias Nießner. Faceforensics++: Learning to detect manipulated facial images. In *Proceedings of the IEEE/CVF Conference on International Conference on Computer Vision*, pages 1–11, 2019.
- [68] Axel Sauer, Katja Schwarz, and Andreas Geiger. Stylegan-xl: Scaling stylegan to large diverse datasets. In *ACM SIGGRAPH 2022 conference proceedings*, pages 1–10, 2022.
- [69] shaoanlu. <https://github.com/shaoanlu/faceswap-GAN>.
- [70] Kaede Shiohara and Toshihiko Yamasaki. Detecting deepfakes with self-blended images. In *Proceedings of the IEEE/CVF Conference on Computer Vision and Pattern Recognition*, pages 18720–18729, 2022.
- [71] Kaede Shiohara, Xingchao Yang, and Takafumi Taketomi. Blendface: Re-designing identity encoders for face-swapping. In *Proceedings of the IEEE/CVF International Conference on Computer Vision*, pages 7634–7644, 2023.
- [72] Aliaksandr Siarohin, Stéphane Lathuilière, Sergey Tulyakov, Elisa Ricci, and Nicu Sebe. First order motion model for image animation. *Advances in neural information processing systems*, 32, 2019.
- [73] Aliaksandr Siarohin, Oliver J Woodford, Jian Ren, Menglei Chai, and Sergey Tulyakov. Motion representations for articulated animation. In *Proceedings of the IEEE/CVF Conference on Computer Vision and Pattern Recognition*, pages 13653–13662, 2021.
- [74] Haixu Song, Shiyu Huang, Yinpeng Dong, and Wei-Wei Tu. Robustness and generalizability of deepfake detection: A study with diffusion models. *arXiv preprint arXiv:2309.02218*, 2023.
- [75] Yiyu Sun, Yaojie Liu, Xiaoming Liu, Yixuan Li, and Wen-Sheng Chu. Rethinking domain generalization for face anti-spoofing: Separability and alignment. In *Proceedings of the IEEE/CVF Conference on Computer Vision and Pattern Recognition*, pages 24563–24574, 2023.
- [76] Justus Thies, Michael Zollhöfer, and Matthias Nießner. Deferred neural rendering: Image synthesis using neural textures. *Transactions on Graphics*, 38(4):1–12, 2019.
- [77] Justus Thies, Michael Zollhofer, Marc Stamminger, Christian Theobalt, and Matthias Nießner. Face2face: Real-time face capture and reenactment of rgb videos. In *Proceedings of the IEEE/CVF Conference on Computer Vision and Pattern Recognition*, 2016.
- [78] Omer Tov, Yuval Alaluf, Yotam Nitzan, Or Patashnik, and Daniel Cohen-Or. Designing an encoder for stylegan image manipulation. *ACM Transactions on Graphics (TOG)*, 40(4):1–14, 2021.
- [79] Chengrui Wang and Weihong Deng. Representative forgery mining for fake face detection. In *Proceedings of the IEEE/CVF Conference on Computer Vision and Pattern Recognition*, 2021.
- [80] Chengrui Wang and Weihong Deng. Representative forgery mining for fake face detection. In *Proceedings of the IEEE/CVF conference on computer vision and pattern recognition*, pages 14923–14932, 2021.
- [81] Jian Wang, Shangqing Liu, Xiaofei Xie, and Yi Li. Evaluating aigc detectors on code content. *arXiv preprint arXiv:2304.05193*, 2023.

- [82] Sheng-Yu Wang, Oliver Wang, Richard Zhang, Andrew Owens, and Alexei A Efros. Cnn-generated images are surprisingly easy to spot... for now. In *Proceedings of the IEEE/CVF Conference on Computer Vision and Pattern Recognition*, pages 8695–8704, 2020.
- [83] Tengfei Wang, Yong Zhang, Yanbo Fan, Jue Wang, and Qifeng Chen. High-fidelity gan inversion for image attribute editing. *arXiv preprint arXiv:2109.06590*, 2021.
- [84] Ting-Chun Wang, Ming-Yu Liu, Andrew Tao, Guilin Liu, Jan Kautz, and Bryan Catanzaro. Few-shot video-to-video synthesis. *arXiv preprint arXiv:1910.12713*, 2019.
- [85] Ting-Chun Wang, Arun Mallya, and Ming-Yu Liu. One-shot free-view neural talking-head synthesis for video conferencing. In *Proceedings of the IEEE/CVF conference on computer vision and pattern recognition*, pages 10039–10049, 2021.
- [86] Yaohui Wang, Di Yang, Francois Bremond, and Antitza Dantcheva. Latent image animator: Learning to animate images via latent space navigation. *arXiv preprint arXiv:2203.09043*, 2022.
- [87] Zhendong Wang, Jianmin Bao, Wengang Zhou, Weilun Wang, Hezhen Hu, Hong Chen, and Houqiang Li. Dire for diffusion-generated image detection. In *Proceedings of the IEEE/CVF International Conference on Computer Vision*, pages 22445–22455, 2023.
- [88] WhichFaceisReal. <https://www.whichfaceisreal.com/>.
- [89] Liangbin Xie, Xintao Wang, Honglun Zhang, Chao Dong, and Ying Shan. Vfhq: A high-quality dataset and benchmark for video face super-resolution. In *Proceedings of the IEEE/CVF Conference on Computer Vision and Pattern Recognition*, pages 657–666, 2022.
- [90] Chao Xu, Jiangning Zhang, Yue Han, Guanzhong Tian, Xianfang Zeng, Ying Tai, Yabiao Wang, Chengjie Wang, and Yong Liu. Designing one unified framework for high-fidelity face reenactment and swapping. In *European conference on computer vision*, pages 54–71. Springer, 2022.
- [91] Zhiliang Xu, Zhibin Hong, Changxing Ding, Zhen Zhu, Junyu Han, Jingtuo Liu, and Errui Ding. Mobilefaceswap: A lightweight framework for video face swapping. In *Proceedings of the AAAI Conference on Artificial Intelligence*, volume 36, pages 2973–2981, 2022.
- [92] Zhiyuan Yan, Yuhao Luo, Siwei Lyu, Qingshan Liu, and Baoyuan Wu. Transcending forgery specificity with latent space augmentation for generalizable deepfake detection. In *Proceedings of the IEEE/CVF Conference on Computer Vision and Pattern Recognition*, 2024.
- [93] Zhiyuan Yan, Yong Zhang, Yanbo Fan, and Baoyuan Wu. Ucf: Uncovering common features for generalizable deepfake detection. *arXiv preprint arXiv:2304.13949*, 2023.
- [94] Zhiyuan Yan, Yong Zhang, Xinhang Yuan, Siwei Lyu, and Baoyuan Wu. Deepfakebench: A comprehensive benchmark of deepfake detection. In A. Oh, T. Neumann, A. Globerson, K. Saenko, M. Hardt, and S. Levine, editors, *Advances in Neural Information Processing Systems*, volume 36, pages 4534–4565. Curran Associates, Inc., 2023.
- [95] Tianyun Yang, Juan Cao, Qiang Sheng, Lei Li, Jiaqi Ji, Xirong Li, and Sheng Tang. Learning to disentangle gan fingerprint for fake image attribution. *arXiv preprint arXiv:2106.08749*, 2021.
- [96] Xin Yang, Yuezun Li, and Siwei Lyu. Exposing deep fakes using inconsistent head poses. In *IEEE International Conference on Acoustics, Speech and Signal Processing*, pages 8261–8265. IEEE, 2019.
- [97] Wenxuan Zhang, Xiaodong Cun, Xuan Wang, Yong Zhang, Xi Shen, Yu Guo, Ying Shan, and Fei Wang. Sadtalker: Learning realistic 3d motion coefficients for stylized audio-driven single image talking face animation. In *Proceedings of the IEEE/CVF Conference on Computer Vision and Pattern Recognition*, pages 8652–8661, 2023.
- [98] Xu Zhang, Svebor Karaman, and Shih-Fu Chang. Detecting and simulating artifacts in gan fake images. *arXiv preprint arXiv:1907.06515*, 2019.
- [99] Jian Zhao and Hui Zhang. Thin-plate spline motion model for image animation. In *Proceedings of the IEEE/CVF Conference on Computer Vision and Pattern Recognition*, pages 3657–3666, 2022.
- [100] Tianchen Zhao, Xiang Xu, Mingze Xu, Hui Ding, Yuanjun Xiong, and Wei Xia. Learning self-consistency for deepfake detection. In *ICCV*, 2021.
- [101] Tianfei Zhou, Wenguan Wang, Zhiyuan Liang, and Jianbing Shen. Face forensics in the wild. In *Proceedings of the IEEE/CVF conference on computer vision and pattern recognition*, pages 5778–5788, 2021.

- [102] Mingjian Zhu, Hanting Chen, Qiangyu Yan, Xudong Huang, Guanyu Lin, Wei Li, Zhijun Tu, Hailin Hu, Jie Hu, and Yunhe Wang. Genimage: A million-scale benchmark for detecting ai-generated image. *Advances in Neural Information Processing Systems*, 36, 2024.

Checklist

1. For all authors...
 - (a) Do the main claims made in the abstract and introduction accurately reflect the paper’s contributions and scope? **[Yes]** Our contributions are in Lines 53-59 of the "introduction" section. We claim the scope of deepfake detection in Lines 36-39 of the "introduction" section, and we further clarify our research scope in Lines 105-108 of the "DF40 benchmark" section.
 - (b) Did you describe the limitations of your work? **[Yes]** We describe the limitations in Sec. 7.
 - (c) Did you discuss any potential negative societal impacts of your work? **[No]** Our work is to *detect* those potentially "dangerous" deepfake techniques.
 - (d) Have you read the ethics review guidelines and ensured that your paper conforms to them? **[Yes]**
2. If you are including theoretical results...
 - (a) Did you state the full set of assumptions of all theoretical results? **[No]** We do not provide any theoretical results.
 - (b) Did you include complete proofs of all theoretical results? **[No]** We do not provide any theoretical results.
3. If you ran experiments (e.g. for benchmarks)...
 - (a) Did you include the code, data, and instructions needed to reproduce the main experimental results (either in the supplemental material or as a URL)? **[Yes]** We have written detailed instructions to reproduce the main experimental results in the supplementary.
 - (b) Did you specify all the training details (e.g., data splits, hyperparameters, how they were chosen)? **[Yes]** We have specified all these details in the supplementary.
 - (c) Did you report error bars (e.g., with respect to the random seed after running experiments multiple times)? **[No]** We use the fixed seed that is the same as DeepfakeBench [94] to align the settings and facilitate fair comparison.
 - (d) Did you include the total amount of compute and the type of resources used (e.g., type of GPUs, internal cluster, or cloud provider)? **[Yes]** We have shown these details in the supplementary.
4. If you are using existing assets (e.g., code, data, models) or curating/releasing new assets...
 - (a) If your work uses existing assets, did you cite the creators? **[Yes]** I have cited all the existing software, datasets, and research works.
 - (b) Did you mention the license of the assets? **[Yes]** We provide the license in the supplementary.
 - (c) Did you include any new assets either in the supplemental material or as a URL? **[Yes]** We provide a URL to assess all of our code, dataset, and pre-trained models.
 - (d) Did you discuss whether and how consent was obtained from people whose data you’re using/curating? **[Yes]** All real people in our work are directly cited from the previous/existing works.
 - (e) Did you discuss whether the data you are using/curating contains personally identifiable information or offensive content? **[Yes]** All real people in our work are directly cited from the previous/existing works.
5. If you used crowdsourcing or conducted research with human subjects...
 - (a) Did you include the full text of instructions given to participants and screenshots, if applicable? **[No]**
 - (b) Did you describe any potential participant risks, with links to Institutional Review Board (IRB) approvals, if applicable? **[No]**
 - (c) Did you include the estimated hourly wage paid to participants and the total amount spent on participant compensation? **[No]**

A Appendix

A.1 Dataset Generation Methods & Original Data

A.1.1 Brief Introduction of Generation Methods

Based on previous survey [54], deepfake techniques can be typically classified into four types: face-swapping (FS), face-reenactment (FR), entire face synthesis (EFS), and face editing (FE).

(1) Face-swapping: This paper classifies the face-swapping technique into two domains: *DF-family* and *FS-family*. (i) *DF-family* involves creating a mask around the facial region (some even include the neck [50]) and blending the generated deepfake face back into the background image using that mask. Most existing and famous face forgery datasets, such as FF-DF [67], Celeb-DF [47] and DFDC [20], belong to this line. (ii) *FS-family* methods represent another significant category in face-swapping deepfake generation. These methods typically involve the use of an identity-background encoder. It disentangles a face image’s identity and background information during encoding. Notably, these methods directly generate all content, even the background. Much recent face-swapping research works [90; 13] and popular software (*e.g.*, Roop) are within this line.

(2) Face-reenactment: Generally, this technique can be used to modify source faces, imitating the actions or expressions of another face. Differing from face-swapping, face-reenactment techniques are *rarely* considered in existing datasets. Two commonly used reenactment-based forgeries are Face2Face [77] and NeuralTextures [76]. These two forgeries are implemented in the FF++ dataset. Face2Face employs pairs of original and target faces, using key facial points to generate varied expressions, while NeuralTexture uses rendered images from a 3D face model to migrate expressions. Although these forgeries achieve more realistic visual synthetic results compared to their face-swapping counterparts in FF++, Due to the amazingly rapid development of the AIGC technologies (*e.g.*, Digital Human), these relatively old-fashioned methods cannot represent the modern’ SoTA reenactment methods. Our DF40 implements 13 face-reenactment methods in total, including the classical animation [72; 73], SoTA’s audio-based driven methods [97; 60], image-based driven methods [86; 31; 7]. We also include the well-known best face generation technique, HeyGen, in our dataset for evaluation.

(3) Entire Face Synthesis: This technique can be generally treated as "Face AIGC." With the rapid development of AIGCs, this technique has achieved remarkably notable improvement. The two widely used technologies to generate synthesis faces are GAN (*e.g.*, StarGAN [14]) and Diffusion models (*e.g.*, StableDiffusion [64]).

(4) Face Editing: This technique aims to modify the facial attributes (*e.g.*, age and gender) of the given face images. Most of these works utilize the latent code of StyleGAN [39] to perform editing during GAN inversion.

A.1.2 Details of Implemented Forgery Methods in DF40

We used a total of **40** distinct deepfake generation/synthesis methods (see Tab. 2 of the manuscript for details). We will briefly explain each synthesis method below:

1. FSGAN [57] FSGAN is proposed by Nirkin et al. [57], which is the latest face-swapping method that has become popular recently. The key feature of this method is that it performs reenactment along with the face swap. First, it applies reenactment on the target video based on the source video’s pose, angle, and expression by selecting multiple frames from the source having the most correspondence to the target video. Then, it transfers the missing parts and blends them with the target video. This process makes it much easier to train and does not take much time to generate face-swapped video. We use the code from the official FSGAN GitHub repository [57]. We used the best quality swapping model recommended by the authors of FSGAN to prepare our dataset by fine-tuning the input video pairs and generating better-quality results. We adopt this method because of its efficiency and better quality of the results. It is also used in the DFDC, ForgeryNet, FFIW, and FakeAVCeleb datasets. We use the official code from <https://github.com/NVlabs/imaginaire/> for implementation.

2. FaceSwap [1] FaceSwap is a pure landmark and graphics-based face-swapping method, not employing any neural network. The outcome is relatively poor and considered as the prototype of FS in the FF++ dataset. Despite its limitations, it still provides a basic understanding of face-swapping

techniques. FaceSwap relies on traditional computer vision methods, such as facial landmark detection and image warping, to achieve face-swapping results. Although the quality of the results may not be as high as those produced by more advanced methods, FaceSwap remains an essential reference point in the development of face-swapping technology. Due to its popularity, it was used in FaceForensics++ datasets [67] to generate the face-swapped dataset. We use the official code from <https://github.com/MarekKowalski/FaceSwap/> for implementation.

3. SimSwap [13] SimSwap is one of the state-of-the-art (SOTA) methods for single-frame face swapping. It has not been applied to academic datasets yet. The facefusion software provides a good encapsulation of SimSwap, which can be directly called for use. SimSwap leverages deep learning techniques, such as attention mechanisms and GANs, to achieve high-quality face-swapping results in a single frame. Its ability to produce visually appealing and realistic face swaps has made it a popular choice for both research and practical applications. We use the official code from <https://github.com/neuralchen/SimSwap/> for implementation.

4. InSwapper [33] InSwapper is another SOTA method for single-frame face swapping that is also utilized in Roop [65]. Similar to SimSwap, it has not been widely applied to existing academic deepfake datasets, but many applications in the real world due to its convenience and effectiveness. InSwapper can achieve good single-frame face swap results, but it performs average in terms of frame-to-frame consistency. InSwapper uses advanced deep learning techniques, including GANs and attention mechanisms, to generate realistic face swaps. Its main focus is on preserving the identity of the target face while seamlessly blending the source face’s features. We use the popular code repository from <https://github.com/haofanwang/inswapper/> for implementation.

5. BlendFace [71] BlendFace is the latest SOTA face-swapping method that was published in ICCV 2023. It has a good performance in single-frame face swapping, but the continuous frames in the video tend to jitter noticeably. BlendFace employs advanced deep learning techniques, such as GANs, to generate high-quality face swaps. It also focuses on maintaining the target face’s identity while blending the source face’s features seamlessly. The main challenge faced by BlendFace is to achieve a stable and consistent face swap across video frames, which remains an area for future research. We use the official code from <https://github.com/mapoon/BlendFace/> for implementation.

6. UniFace [90] UniFace is another recent face-swapping technique that was published in ECCV 2022. It leverages disentangled representations to transfer identity and attributes, utilizing Feature Disentanglement to separate identity and attribute embeddings unsupervised. It employs Attribute Transfer and Identity Transfer modules, powered by learned Feature Displacement Fields, to granularly manipulate attributes and model adaptive identity fusion, respectively, with an emphasis on maintaining consistency in reenactment and attribute preservation in swapping. The model is designed to handle challenging conditions like occlusions, extreme lighting, and large poses without reliance on pre-estimated structures. The main drawback of this method is the visible rectangular frame around the swapped face, which affects the overall quality and realism of the face swap. Improving the blending and transition between the source and target faces remains a challenge for UniFace. We use the official code from <https://github.com/xc-csc101/UniFace/> for implementation.

7. MobileFaceSwap [91] MobileFaceSwap reduces the computational load of the model and realizes real-time face swapping on mobile devices. It introduces a new idea of integrating IDs into the network. MobileFaceSwap employs lightweight deep learning architectures, such as MobileNet, to achieve real-time performance on resource-constrained devices. The method focuses on maintaining the quality of the face swap while reducing the computational complexity, making it suitable for mobile applications and other scenarios where computational resources are limited. We use the official code from <https://github.com/Seanseattle/MobileFaceSwap/> for implementation.

8. e4s [50] e4s proposes a framework for explicit disentanglement of shape and texture based on facial components, considering both geometry and texture details. This method aims to create more realistic face swaps by separating and recombining facial features more accurately. By focusing on the individual components of the face, e4s can better preserve the identity of the target face while seamlessly blending the source face’s features. This approach has the potential to improve the overall quality and realism of face swaps in various applications. The primary drawback of e4s is its

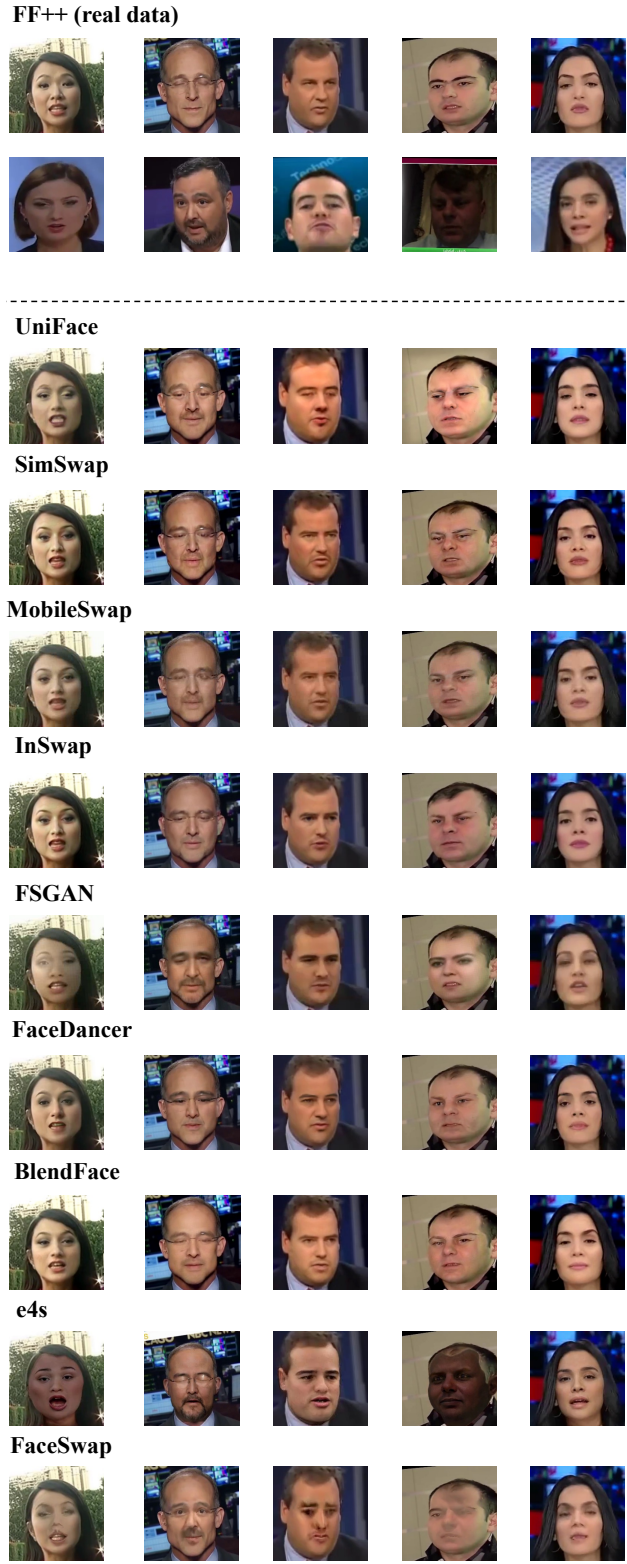


Figure 12: Illustration of visual examples for all FS (face-swapping) generated data on the FF domain.

noticeable temporal inconsistency, which makes it easy to detect using temporal models. We use the official code from <https://github.com/e4s2022/e4s/> for implementation.

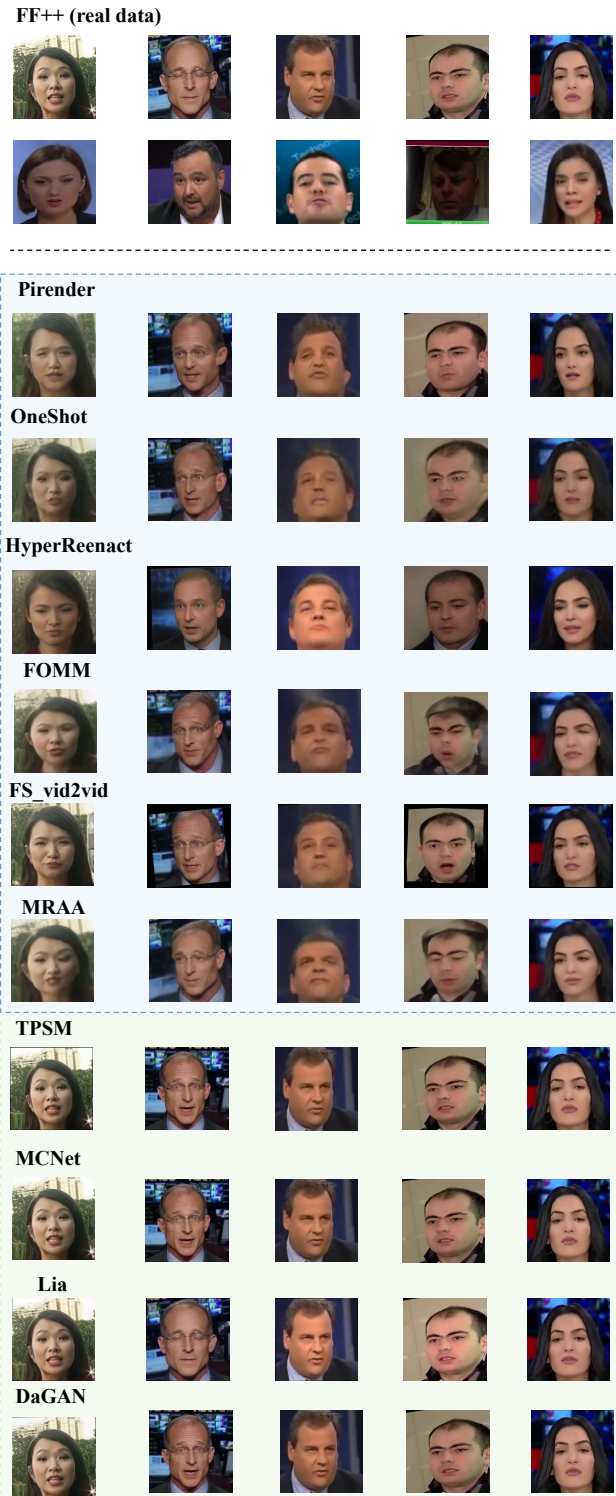


Figure 13: Illustration of visual examples for all FR (face-reenactment) generated data on the FF domain.

9. FaceDancer [66] FaceDancer is a very recent work that was published in CVPR 2023, which proposes a single-stage, identity-based method for face swapping of unknown identities. This method aims to create high-quality face swaps even when the source and target faces have not been previously

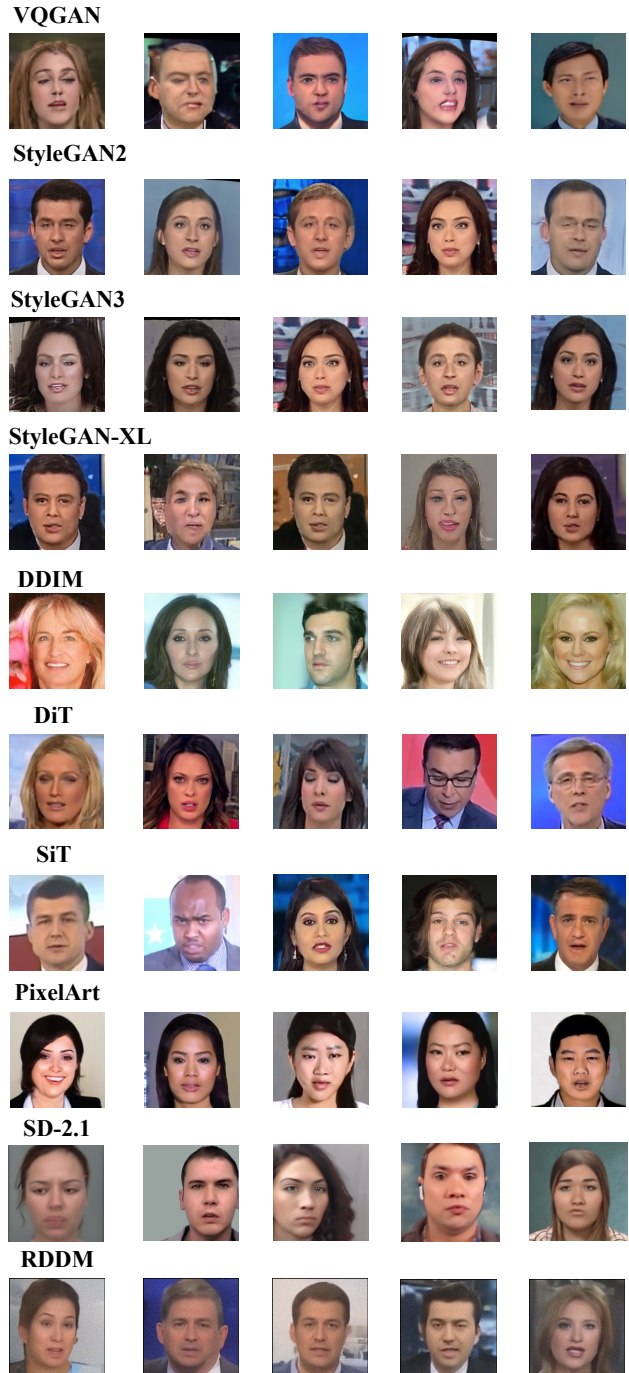


Figure 14: Illustration of visual examples for all EFS (entire face synthesis) generated data on the FF domain.

encountered during training. FaceDancer employs advanced deep learning techniques, such as GANs and attention mechanisms, to achieve realistic results while maintaining the identity of the target face. This method has the potential to broaden the applicability of face-swapping technology to a wider range of scenarios and use cases. This technology provides highly realistic visual results at both spatial and temporal levels. We use the official code from <https://github.com/felixrosberg/FaceDancer/> for implementation.

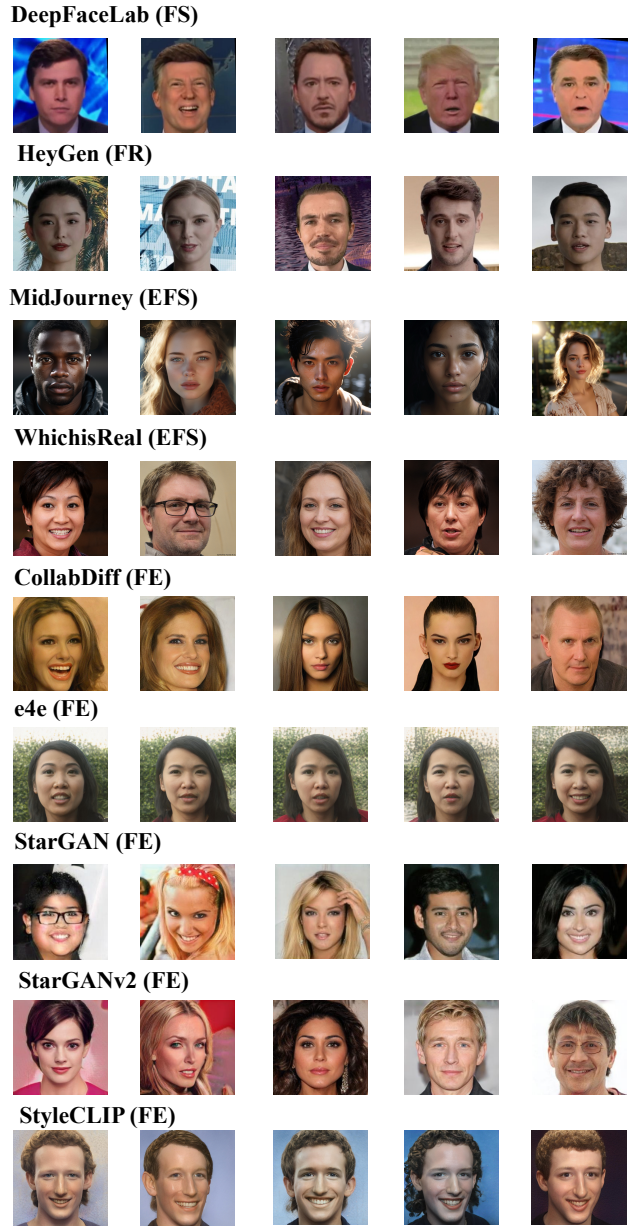


Figure 15: Illustration of visual examples for all unknown forgery data, including all types like FS, FR, EFS, and FE, simulating the real-world SoTA deepfakes.

10. DeepFaceLab [18] DeepFaceLab [18] is a leading deepfake generation method. According to them, the majority of deepfake videos are generated by DeepFaceLab or other similar techniques (auto-encoder-based DF-family face-swapping techniques) such as DeepFake [19] used in FF++ and face-swap GAN [69]. They provide a complete, easy-to-use pipeline and provide end-to-end code with a windows software tool as well. They have also shared some synthesis models that can be used to generate deepfakes based on our requirements. Their method is a modification of the original Faceswap model in which they added an intervening network between the encoder and decoders. It helps the network to extract common features between source and target videos. Moreover, their loss function includes a mean squared error along with a structural dissimilarity index. We used this deepfake generation method in our paper to include the most recent and widely used method in our DF40. We use its official code repository from <https://github.com/iperov/DeepFaceLab/> to create fake videos one by one.

11. FOMM [72] FOMM is a highly classic method of image animation and face reenactment, previously used in the ForgeryNet dataset [27]. It employs deep learning techniques, such as GANs and attention mechanisms, to generate high-quality image animations and face reenactment results. FOMM has been widely used in various applications, including video editing, virtual reality, and digital content creation. Its ability to produce visually appealing and realistic animations has made it a popular choice for both research and practical applications. Thus, we propose to implement this classical synthesis method in our benchmark. We use the official code from <https://github.com/AliaksandrSiarohin/first-order-model/> for implementation.

12. FS_Vid2vid [84] FS_Vid2vid is another popular and classical synthesis method proposed by NVIDIA. It can generate unseen domain videos. However, when the test domain is significantly different from the training domain or the keypoint estimation is inaccurate, the effect is poor. FS_Vid2vid employs advanced deep learning techniques, such as GANs and attention mechanisms, to generate high-quality face swaps across different domains. The main challenge faced by this method is to achieve stable and consistent face swaps when dealing with significant domain differences or inaccurate keypoint estimation. Improving the robustness and generalizability of FS_Vid2vid remains an area for future research. We use the official code from <https://github.com/NVlabs/few-shot-vid2vid/> for implementation.

13. Wav2Lip [60] Recently, audio-based facial reenactment techniques along with lip-syncing have been proposed by researchers. In lip-sync, the source person controls the mouth movement, and in face reenactment, facial features are manipulated in the target video. One of the most recent audio-driven facial reenactment methods is Wav2Lip, which aims to lip-sync the video with respect to any desired speech signal by reenacting the face. Wav2Lip has been widely used in various applications, including video editing, virtual reality, and digital content creation. Its ability to produce visually appealing and realistic lip-sync animations has made it a popular choice for both research and practical applications. We used this facial reenactment method because of the efficiency of its synthesis process for generating lip-synced video. We use the official code from <https://github.com/Rudrabha/Wav2Lip/> for implementation. Also, the audio and text data to be used for driving is randomly sampled from LRS3 [3].

14. MRAA [73] MRAA is also a highly classic image animation method, but there seems to be no existing deepfake dataset applied to this dataset so far. It identifies object parts, tracks them in driving videos, and estimates motion using principal axes within regions, leading to more stable and semantically meaningful representations. It also models non-object motion with an affine transformation to decouple foreground from background and disentangle shape and pose in the region space for improved animation fidelity. The framework is self-supervised, label-free, and optimized by reconstruction losses. MRAA has the potential to improve the overall quality and realism of image animations in various applications. We use the official code from <https://github.com/snap-research/articulated-animation/> for implementation.

15. OneShotFree [85] OneShotFree presents a reenactment-based approach for animating articulated objects with distinct parts, addressing the limitations of previous unsupervised methods that struggle with motion representation and articulation. It identifies object parts, tracks them in driving videos, and estimates motion using principal axes within regions, leading to more stable and semantically meaningful representations. It also models non-object motion with an affine transformation to decouple foreground from background and disentangle shape and pose in the region space for improved animation fidelity. The framework is self-supervised, label-free, optimized by reconstruction losses, and surpasses SoTA benchmarks, particularly for articulated objects like human bodies. We use the official code from <https://github.com/zhanglonghao1992/One-Shot-Free-View-Neural-Talking-Head-Synthesis/> for implementation.

16. PIRender [63] PInder is a neural rendering system for generating controllable portrait images by manipulating the motion of existing faces through intuitive and semantically meaningful parameters. It leverages 3D Morphable Models (3DMM) parameters for facial control, enabling precise adjustments to expressions and poses. Unlike many existing techniques that offer limited or indirect editing capabilities, PInder provides direct, fine-grained control for intuitive image editing, allowing realistic modifications to facial aspects like posture and expressions without the need for specialized software skills. Additionally, it's extended to address the audio-driven facial reenactment,

synthesizing coherent videos from a single reference image and audio stream, showcasing the potential for intuitive controls in portrait manipulation and synthesis. We use the official code from <https://github.com/RenYurui/PIRender/> for implementation.

17. TPSM [99] TPSM (or called TPSMM) presents a thin-plate spline motion model for image animation, an unsupervised method aimed at addressing the challenge of animating objects with large pose discrepancies between source and driving images. It introduces a new framework, starting with thin-plate splines to estimate more flexible optical flow, enabling smoother warping of feature maps from source to drive image domain. Multi-resolution occlusion masks are employed to enhance feature fusion to improve occluded region restoration. Additionally, dedicated auxiliary losses are designed to ensure a clear division of labor among network modules, promoting high-quality image generation. The method is demonstrated to animate various objects, including faces, bodies, and animations, showing improved performance on benchmarks and highlighting its potential for handling unseen manipulations. We use the official code from <https://github.com/yoyo-nb/Thin-Plate-Spline-Motion-Model/> for implementation.

18. LIA [86] LIA is a recent SoTA face reenactment that was published in ICLR 2022, which edits the Latent code by learning linear changes in the Latent space, *i.e.*, learning a set of orthogonal Motion directions. This method aims to create more realistic face reenactments and animations by editing the Latent code directly. LIA is evaluated on real-world videos, demonstrating the capability to animate still images without bias, eliminating the need for structure. This approach has the potential to improve the overall quality and realism of face swaps and animations in various applications. We use the official code from <https://github.com/wyhsirius/LIA/> for implementation.

19. DaGAN [31] This method is a depth-aware generative adversarial network (DaGAN) for talking head generation, aiming to create realistic synthetic videos that encapsulate the identity of a person from a source image and the pose from a driving video. It uniquely incorporates unsupervised depth recovery to learn dense facial geometry (depth) from videos, which is vital for accurate face synthesis and distinguishing facial structures amidst cluttered backgrounds without requiring expensive annotations. Depth maps facilitate the estimation of sparse key points capturing essential head movements and guide the generation of motion fields for warping source representations via depth-aware attention. Comprehensive experiments validate the model’s capacity to generate high-quality videos, achieving significant advancements in unseen faces and showcasing the effectiveness of depth awareness in talking head synthesis. We use the official code from <https://github.com/harlanhong/CVPR2022-DaGAN/> for implementation.

20. SadTalker [97] SadTalker is another recent popular talking head synthesis method that was published in CVPR 2023. The system animates talking heads in videos through audio-driven images using realistic facial expressions and head movements. It decomposes the problem into two stages: audio-motion mapping and 3D motion modeling. The ExpNet learns to extract facial expressions from audio with the aid of an initial identity reference frame’s expression coefficients, ensuring lip synchronization and reducing uncertainty. PoseVAE models head movements in diverse styles, ensuring coherence with the beat alignment to audio. Evaluations show that SadTalker surpasses previous methods in generating higher-quality videos with accurate lip-sync and motion and reduced blurring, especially for challenging tasks like head pose transfer and talking-head videos. The system demonstrates the potential for creating coherent videos with natural-looking animations from audio and reference images, advancing video conferencing and digital media applications. We use the official code from <https://github.com/OpenTalker/SadTalker/> for implementation.

21. MCNet [30] MCNet is another recent SoTA reenactment method that was published in ICCV 2023. This work presents a novel approach for generating high-fidelity talking head videos, aiming to animate a static source image with dynamic poses and expressions derived from a separate driving video while preserving the original person’s identity. This is achieved through the Implicit Identity Representation Conditioned Memory Compensation Network (MCNet), which addresses the issue of ambiguous generation caused by large, complex motions in the driving video. MCNet introduces a unique mechanism that learns a global facial representation space and employs an implicit identity representation conditioned memory bank to provide rich structural and appearance priors. These priors help compensate for insufficient information in occluded regions or subtle expression variations, significantly reducing artifacts and enhancing video quality. The system incorporates a memory

compensation module (MCM) and an implicit identity representation conditioned memory module (IICM) to query and utilize the learned memory effectively. Extensive experimentation affirms its capability to generate realistic talking head videos even under challenging conditions. We use the official code from <https://github.com/harlanhong/ICCV2023-MCNET/> for implementation.

22. HyperReenact [7] HyperReenact is another recent SoTA reenactment method that was published in ICCV 2023. It is a one-shot neural face reenactment method capable of synthesizing realistic talking head sequences of a source individual driven by a target’s facial pose, including 3D head orientation and expression. HyperReenact is designed to handle both self and cross-subject reenactment scenarios, requiring only a single source image. It excels in minimizing visual artifacts, even when there are drastic differences in head pose between the source and target images or when conducting cross-subject reenactment. By leveraging the photorealism and disentangled properties of a pre-trained StyleGAN2 model, HyperReenact first inverts real images into the latent space before refining and retargeting them. The method is compared favorably with several state-of-the-art reenactment techniques, showcasing its proficiency in generating artifact-free details around facial areas such as the mouth and eyes, even under extreme head poses. Additionally, the paper includes extensive quantitative and qualitative evaluations, demonstrating HyperReenact’s efficiency and effectiveness across various metrics and benchmark tests. We use the official code from <https://github.com/StelaBou/HyperReenact/> for implementation.

23. HeyGen [28] HeyGen is an AI-powered video creation platform that simplifies the process of making professional-quality videos. With its user-friendly interface and advanced features, HeyGen has become a popular choice for users looking to create high-quality, engaging content without the need for extensive editing skills and time investment. One of the standout features of HeyGen is its AI-powered text-to-speech functionality, which allows users to effortlessly convert written text into natural-sounding speech. This feature enables users to create engaging voiceovers for their videos without the need for professional voice actors or expensive recording equipment. In addition to its text-to-speech capabilities, HeyGen also offers customizable avatars that can be used to represent speakers in the videos. These avatars can be tailored to match the desired appearance and style of the user, adding a personal touch to the video content. Furthermore, HeyGen’s automated professional video editor streamlines the video creation process by intelligently combining video clips, images, text, and audio to produce polished and visually appealing videos. This feature saves users significant time and effort typically required for manual video editing. HeyGen’s combination of AI-powered features and user-friendly interface makes it an ideal solution for users looking to create professional-quality videos with minimal effort. Its versatility and efficiency have made it popular for various applications, including content creation, digital marketing, e-learning, and social media promotion. We use the software from its official website <https://www.heygen.com/> for creating fake videos.

24. VQGAN [24] VQGAN is a classical entire image synthesis method, which introduces a method that enhances transformers’ capability to synthesize high-resolution images, overcoming their traditional inefficiency for long sequences typical of pixel-dense data. The approach enables efficient modeling and synthesis of high-resolution images by integrating CNN inductive bias for local interactions with transformers’ expressiveness. It involves two stages: initially employing CNNs to learn a rich vocabulary of image components, followed by transformers arranging these components within high-resolution images. This method is adaptable to conditional synthesis tasks, allowing both non-spatial information, like object categories, and spatial data, such as segmentation, to guide image generation. Notably, it presents the first instance of transformers generating semantically-guided megapixel images and attains state-of-the-art performance among autoregressive models for class-conditional ImageNet synthesis. We use the official code from <https://github.com/CompVis/taming-transformers/> for implementation.

25. StyleGAN2 [39] StyleGAN2 is an improved version of StyleGAN proposed by NVIDIA, enhancing the image quality and reducing the artifacts in the generated images. The authors propose architectural and training modifications to the StyleGAN, focusing on normalizing the generator’s mapping network, progressively growing, and introducing regularization for improved conditioning between latent codes and images. Their approach enhances image quality, reduces artifacts, and increases the generator’s invertibility while preserving its expressiveness. By improving upon the original StyleGAN, StyleGAN2 can generate more realistic and high-quality human face images with

specific attributes. We use the official code from <https://github.com/NVlabs/stylegan2/> for implementation.

26. StyleGAN3 [37] StyleGAN3 is an improved version of StyleGAN2 and StyleGAN proposed by NVIDIA, enhancing the image quality and reducing the artifacts in the generated images. StyleGAN3 addresses the issue of StyleGAN’s performance degradation when dealing with unstructured datasets like ImageNet, typically designed for controllable synthesis. The authors find the limitation lies not in the training strategy but rather in the model’s inherent design. They leverage the Projected GAN framework to apply powerful priors and a progressive growth strategy, training StyleGAN3 on ImageNet. The outcome, StyleGAN3, achieves a new state-of-the-art large-scale synthesis, generating 1024-resolution images for the first time. It demonstrates inversion and editing beyond portraits or specific classes, showcasing broad applicability. We use the official code from <https://github.com/NVlabs/stylegan3/> for implementation.

27. StyleGAN-XL [68] StyleGAN-XL is another version of the original StyleGAN that has been improved. It tackles the scalability of StyleGAN to datasets, particularly ImageNet’s vastness and diversity, where it traditionally struggled. The authors refute the notion of StyleGAN’s design being unsuitable for diversity and instead blame the training methodology. Introducing Projected GAN and progressive training, they successfully scale StyleGAN3 to ImageNet, birthing StyleGAN-XL, a new state-of-the-art in large-scale synthesis at 1024x2. StyleGAN-XL’s flexibility inverts and edits images outside narrow domains, validating its robustness. We use the official code from <https://github.com/autonomousvision/stylegan-xl/> for implementation.

28. Stable-Diffusion-2.1 [64] Stable-Diffusion is currently among the most popular methods for generating images from text. In addition to text-to-image, it can also perform image-to-image transformations. Stable-Diffusion employs advanced deep learning techniques, such as GANs and attention mechanisms, to achieve high-quality results. By supporting both text-to-image and image-to-image transformations, Stable-Diffusion can generate more diverse and high-quality images and animations. This method has been widely used in various applications, including content creation, data augmentation, and artistic expression, making it a popular choice for both research and practical applications. We use the official code from <https://github.com/Stability-AI/stablediffusion/> for implementation.

29. DDPM [29] DDPM, or the Denoising Diffusion Probabilistic Model, is a pioneering work in the field of diffusion models. It generates high-quality images by gradually denoising them. DDPM employs advanced deep learning techniques, such as GANs and attention mechanisms, to achieve high-quality results. DDPM can generate visually appealing and realistic images with minimal artifacts by using a step-by-step denoising process. This method has been instrumental in advancing the field of diffusion models and has inspired the development of more advanced techniques, such as Stable-Diffusion and Collaborative-Diffusion. We use the official code from <https://github.com/lucidrains/denoising-diffusion-pytorch/> for implementation.

30. RDDM [49] RDDM, or Residual Denoising Diffusion Model, is a very recent advanced diffusion model that was published in CVPR 2024. It aims to improve the robustness and stability of the image generation process. By separating the conventional single denoising diffusion process into residual and noise diffusion components, RDDM establishes a dual diffusion framework. This framework employs residual diffusion to model directed degradation from a target image to a degraded input, guiding restoration processes, while noise diffusion accounts for stochastic perturbations. RDDM’s innovation lies in its ability to balance certainty (via residuals) and diversity (through noise), thereby unifying tasks with diverse requirements like image generation and restoration within a single, coherent model. We use the official code from <https://github.com/nachifur/RDDM/> for implementation.

31. PixelArt- α [10] PixelArt- α is a very recent image synthesis method that was published in ICLR 2024. This work presents PixelArt- α , a Transformer-based text-to-image synthesis model that achieves competitive image generation quality similar to leading models like Midjourney [53], with a focus on high-resolution outputs up to 1024x1024 pixels, all while maintaining a significantly reduced training cost. To overcome the hurdles of extensive computational expenses associated with advanced text-to-image models, PixelArt- α employs a three-stage training strategy. This strategy separately

optimizes pixel dependencies, aligns text and images, and enhances image aesthetics. Furthermore, a new auto-labeling system enriches the dataset with high-concept-density captions, enhancing text-image alignment efficiency. Experimental results highlight PixelArt- α 's capability to generate images of exceptional quality with remarkable adherence to textual descriptions, affirming its potential as a more environmentally and economically sustainable solution for photorealistic text-to-image synthesis. We use the official code from <https://github.com/PixArt-alpha/PixArt-alpha/> for implementation.

32. DiT [59] DiT is a very popular architecture for realistic image synthesis recently. The work presents a novel class of diffusion models that leverage transformer architectures, termed Diffusion Transformers (DiTs), for image synthesis tasks. These models replace the traditionally used U-Net backbone with transformers operating on latent image patches, demonstrating improved scalability and performance. The study analyzes the scalability of DiTs based on their forward pass complexity, measured in Gflops, revealing that models with higher computational capacity yield consistently lower FID scores, indicative of better image quality. Notably, the largest variants of DiTs, named DiT-XL/2, have surpassed previous diffusion models' performance on class-conditional ImageNet benchmarks at resolutions of 512x512 and 256x256, achieving a SoTA FID score of 2.27 at the latter resolution. The success of DiTs suggests a promising avenue for further scaling and potential integration into text-to-image synthesis pipelines, capitalizing on transformers' strong capabilities in generative modeling. We use the official code from <https://github.com/facebookresearch/DiT/> for implementation. We adopt the DiT-XL/2 version for generation in our benchmark.

33. SiT [5] SiT is another very popular architecture for realistic image synthesis recently. The paper introduces Scalable Interpolant Transformers (SiT), a novel family of generative models that build upon Diffusion Transformers (DiTs), focusing on enhancing diffusion-based image synthesis. SiT employs an interpolant framework, enabling more flexible distribution connections and facilitating a modular exploration of design elements in generative models such as learning dynamics, objectives, interpolant choices, and sampling strategies. By meticulously integrating these components, SiT outperforms DiT models across various sizes on the conditional ImageNet 256x256 benchmark, utilizing the same backbone architecture, parameter count, and computational complexity (GFLOPs). SiT's adaptability in tuning diffusion coefficients independently from the learning process further pushes its performance, achieving an FID-50K score of 2.06. This work underscores the potential of transformer-based architectures in advancing generative models and paves the way for future developments in scalable and efficient image generation. We use the official code from <https://github.com/willisma/SiT/> for implementation.

34. MidJourney [53] MidJourney is a really popular application, software, and image synthesis method that focuses on generating highly realistic content. Midjourney is a generative artificial intelligence program and service created and hosted by the San Francisco-based independent research lab Midjourney, Inc. Midjourney generates images from natural language descriptions, called prompts, similar to OpenAI's DALL-E and Stability AI's Stable Diffusion. By generating intermediate representations, MidJourney can be used for various applications, such as creative content generation. Its ability to produce realistic synthesis images makes it a popular choice for both research and practical applications. We use the software from its official website <https://www.midjourney.com/home/> for creating fake images. We adopt the latest version, MidJourney-6, for all generations.

35. WhichFaceIsReal [88] WhichFaceIsReal (or called WhichisReal) is a really popular software to create high realistic GAN-generated images and has been widely used in many academic research such as [82]. This software has been developed by Jevin West and Carl Bergstrom at the University of Washington as part of the Calling Bullshit project. All images are either computer-generated from thispersondoesnotexist.com using the StyleGAN software or real photographs from the FFHQ dataset of Creative Commons and public domain images. We use the software from its official website <https://www.whichfaceisreal.com/> for creating fake images. We create 2,000 fake images using this software in our benchmark to simulate the real-world realistic GAN-generated face content.

36. Collaborative-Diffusion [32] Collaborative-Diffusion (or called CollabDiff) is a very recent face editing method that was published in CVPR 2023. The proposed framework is designed for multi-modal face generation and editing. Unlike traditional diffusion models that primarily operate under single-modality control, this approach enables the simultaneous utilization of various

modalities—such as text descriptions and facial masks—to guide the creation and modification of facial images. By leveraging pre-trained uni-modal diffusion models in conjunction, the system synthesizes high-quality, coherent images that adhere to the specified conditions without necessitating additional training. The implementation relies on Latent Diffusion Models (LDM) balanced for quality and efficiency, working within an autoencoder’s latent space to manage computational demands. A Variational Autoencoder (VAE) is trained on the CelebA-HQ dataset to handle the transformation between image and latent representations. This collaborative synthesis method opens new avenues for creative expression in face manipulation tasks by empowering users to define age, facial features, or other attributes through a mix of textual and visual directives. We use the official code from <https://github.com/ziqihuangg/Collaborative-Diffusion/> for implementation.

37. e4e [78] e4e, similar to pspNet, aims to improve the accuracy of projecting real images into the StyleGAN latent space. It mainly focuses on real-image editing using StyleGAN inversion, introducing an encoder architecture, referred to as e4e, tailored for effective editing post-inversion. The authors delve into the latent space characteristics of StyleGAN, revealing a tradeoff between distortion (reconstruction fidelity) and editability, as well as between distortion and perceptual quality. They outline design principles for encoders to balance these tradeoffs, enabling inversions that are conducive to meaningful manipulation while maintaining visual authenticity. Extensive qualitative and quantitative evaluations, along with a user study, demonstrate that the proposed inversion method followed by common editing techniques produces high-quality edits on real images from various challenging domains like cars and horses, with minimal loss in reconstruction accuracy. The paper further supplements these findings with detailed implementation specifics and additional experimental results in an appendix. We use the official code from <https://github.com/omertov/encoder4editing/> for implementation.

38. StarGAN [14] StarGAN is a very classical face editing method and has been applied in many academic datasets such as ForgeryNet [27]. StarGAN is a unified generative adversarial network model designed for image-to-image translation across multiple domains using a single generator and discriminator network. This innovative approach addresses the limitations of previous methods, which required separate models for each pair of domains, by enabling simultaneous training on diverse datasets within one framework. Consequently, StarGAN achieves enhanced image translation quality and versatility, allowing it to transform input images adaptively into any target domain specified. The system incorporates an auxiliary classifier to ensure images are correctly classified post-translation and employs a reconstruction loss to maintain content consistency between the input and output images. The authors express the hope that StarGAN will facilitate the development of various intriguing image translation applications spanning multiple domains. We use the official code from <https://github.com/yunjey/stargan/> for implementation.

39. StarGANv2 [15] StarGANv2 is an improved version of StarGAN. It is an advanced image-to-image translation model capable of producing diverse images across multiple domains with a single framework. It addresses two pivotal challenges: generating images of varied styles within a target domain and managing translations across numerous domains. StarGAN v2 surpasses preceding models’ ability to synthesize images featuring rich styles across diverse domains, as validated through experiments on CelebA-HQ and a newly introduced animal faces dataset (AFHQ), which exhibits extensive inter- and intra-domain variability. The innovation lies in its style code generation process, style space flexibility, and the effective use of training data from multiple domains, resulting in a model that generalizes well to unseen images. The paper also emphasizes the model’s capability for both latent-guided and reference-guided synthesis. We use the official code from <https://github.com/clovaai/stargan-v2/> for implementation.

40. StyleCLIP [58] StyleCLIP is a popular face editing method that integrates the power of Contrastive Language-Image Pre-training (CLIP) models with StyleGAN to achieve text-driven manipulation of imagery without requiring manual intervention or predefined manipulation paths. StyleCLIP offers three key techniques: text-guided latent optimization using CLIP as a loss function for flexible yet time-consuming edits, a latent mapper trained for specific text prompts to provide local latent space adjustments swiftly, and a method mapping text prompts to global, input-agnostic style space directions within StyleGAN, enabling control over manipulation intensity and disentanglement. The work underscores the synergy of CLIP’s broad visual concept understanding and StyleGAN’s generative capabilities, opening up new possibilities for intuitive and creative image ma-

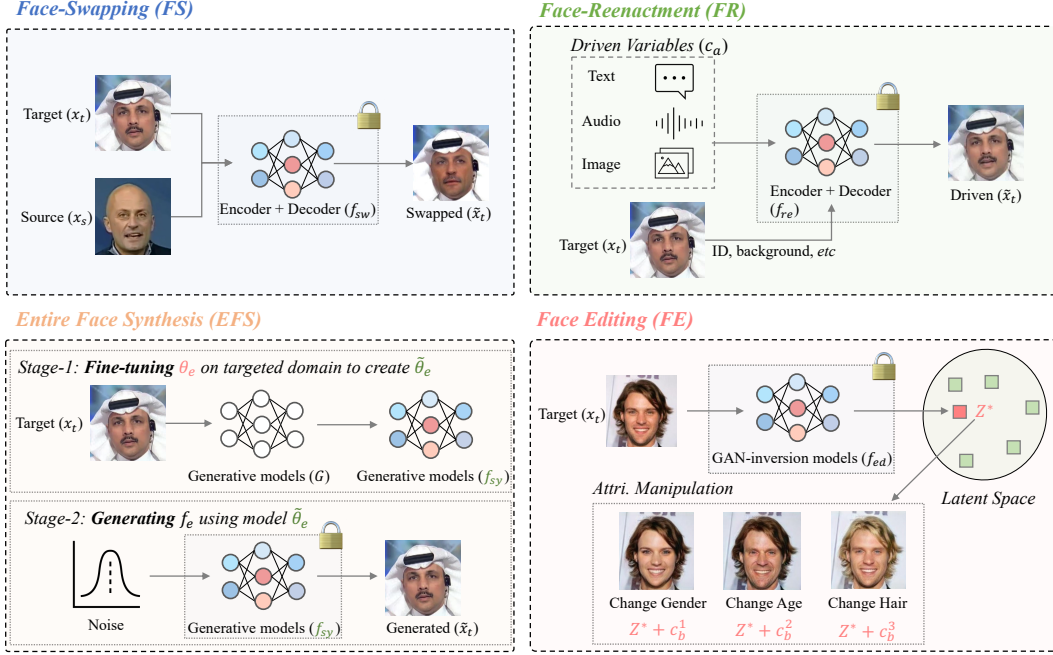


Figure 16: The general fake data generation pipeline of the proposed *DF40* dataset.

manipulation tasks. We use the official code from <https://github.com/orpatashnik/StyleCLIP/> for implementation.

A.1.3 Formulation of Manipulation Methods

To guarantee the *diversity* of deepfake approaches in the proposed DF40, we introduce and implement **40** distinct deepfake techniques, which are listed in Tab. 2. A detailed description of each deepfake method is provided in the supplementary. They are selected according to perspectives of modeling types, conditional sources, forgery effects, and functions. Formally, we denote $x_t(i_t, a_t, b_t)$ as the *target* subject to be manipulated, which possesses attributes (i : person identity, a : identity-agnostic content, b : external attributes) that can uniquely determine itself, while the *source* $x_s(i_s, a_s, b_s)$ is regarded as the *conditional media* (c), driving the *target* to change either identity or attributes or even both. We use $f_{sw}, f_{re}, f_{sy}, f_{ed}$ to represent four types of deepfakes in our work: *FS*, *FR*, *EFS*, and *FE*, respectively. Fig. 1 provides some visual examples for each category in DF40, and Fig. 16 generally illustrates them from the method perspective. (i) *FS Approach*: From Fig. 16(a), FS aims to replace the content of x_t with that of x_s preserving the identity i_s . Formally, $\tilde{x}_t(\tilde{i}_s, a_t, b_t)$ only swaps identity i from the source x_s to the target x_t , and the identity-agnostic content a are preserved. The swapping process can be expressed as:

$$f_{sw}(x_t(i_t, a_t, b_t), x_s(i_s, a_s, b_s)|\text{swap}) = \tilde{x}_t(\tilde{i}_s, a_t, b_t) \quad (5)$$

(ii) *FR Approach*: From Fig. 16(b), FR on $x_t(i_t, a_t, b_t)$ preserves its identity i_t but has its *intrinsic* attributes a_t , e.g., pose, mouth and expression manipulated by a driven variable c_a and forms $\tilde{x}_t(i_t, \tilde{a}_s, b_t)$. Mathematically, we can drive the following equation:

$$f_{re}(x_t(i_t, a_t, b_t)|c_a) = \tilde{x}_t(i_t, \tilde{a}_s, b_t). \quad (6)$$

(iii) *EFS Approach*: EFS generates a completely synthesis face $\tilde{x}_t(\tilde{i}_t, \tilde{a}_t, \tilde{b}_t)$. In order to bridge the personal identity gap between generative models and other deepfake methods, we fine-tune the generative model G with the same real data as other forgery methods (e.g., e4s [50]) and obtain a face-synthesis model f_{sy} . After that, we can synthesize new synthesis faces from noise n as follows:

$$f_{sy}(n) = \tilde{x}_t(\tilde{i}_t, \tilde{a}_t, \tilde{b}_t). \quad (7)$$

The general generation process can be seen in Fig. 16(c). (iv) *FE Approach*: From Fig. 16(d), FE on $x_t(i_t, a_t, b_t)$ has its *external* attributes b_t altered, such as facial hair, age, gender, and ethnicity,

Algorithm 1 FS Method

Input: Target face $x_t(i_t, a_t, b_t)$, Source face $x_s(i_s, a_s, b_s)$

Output: Manipulated face \tilde{x}_t

- 1: Define x_t as the target face with attributes i_t, a_t, b_t
 - 2: Define x_s as the source face with attributes i_s, a_s, b_s
 - 3: Apply FS method to swap identity i from the source x_s to the target x_t , preserving the identity-agnostic content a
 - 4: $\tilde{x}_t(i_s, a_t, b_t) \leftarrow f_{sw}(x_t(i_t, a_t, b_t), x_s(i_s, a_s, b_s)|\text{swap})$
 - 5: **return** \tilde{x}_t
-

Algorithm 2 FR Method

Input: Target face $x_t(i_t, a_t, b_t)$, Conditional source c_a

Output: Manipulated face \tilde{x}_t

- 1: Define x_t as the target face with attributes i_t, a_t, b_t
 - 2: Define c_a as the conditional source to manipulate the intrinsic attributes a_t
 - 3: Apply FR method to manipulate the intrinsic attributes a_t of the target face x_t , preserving its identity i_t
 - 4: $\tilde{x}_t(i_t, \tilde{a}_s, b_t) \leftarrow f_{re}(x_t(i_t, a_t, b_t)|c_a)$
 - 5: **return** \tilde{x}_t
-

controlled by conditional source c_b , to obtain $\tilde{x}_t(i_t, a_t, \tilde{b}_s)$. We also include multiple attribute manipulation with two editing approaches, *e.g.*, both hair and eyebrows are manipulated. We can formulate the transformation as follows:

$$f_{ed}(x_t(i_t, a_t, b_t)|c_b) = \tilde{x}_t(i_t, a_t, \tilde{b}_s), \quad (8)$$

where $\tilde{\cdot}$ means that the element is manipulated by forgery algorithms.

A.1.4 Details of Original Datasets

In this study, we utilize several existing datasets to generate synthetic data for research purposes. The face data in these datasets mainly come from existing academic datasets, as shown in Table 2. In the following, we will introduce the leading institutions, dataset links, and official copyright issues for each dataset:

FF++ Dataset [67] The FaceForensics++ (FF++) dataset is designed for the detection and analysis of manipulated facial images and videos, specifically focusing on deepfake techniques. It contains over 1000 original videos and their manipulated versions generated using four different manipulation methods, namely Deepfakes [19], Face2Face [77], FaceSwap [25], and NeuralTextures [76]. The dataset is widely used for developing and benchmarking deepfake detection algorithms. Note some research works treat FaceShifter as another forgery method of the FF++, such as [23]. However, here we only consider the four mentioned methods that are included in the original FF++ paper [67]. Also, there are three versions of FF++ in terms of compression level, *i.e.*, raw, lightly compressed (c23), and heavily compressed (c40). The FF++ dataset is led by the University of Munich in Germany. The dataset can be accessed through the following link: <https://github.com/ondyari/FaceForensics>. The copyright information can be found at <https://github.com/ondyari/FaceForensics/blob/master/LICENSE>. The real human data sources for this dataset are not explicitly mentioned.

Celeb-DF (CDF) Dataset [47] The Celeb-DF dataset is a large-scale dataset containing both real and manipulated celebrity videos, aimed at facilitating the development of deepfake detection algorithms. CDF dataset has two different versions: CDF-v1 and CDF-v2. Mostly, CDF-v2 is the default version of CDF. Here, we also adopt the CDF-v2 version. It consists of more than 5900 videos, with 563 real videos and over 5300 deepfake videos generated using a modified version of the DeepFakes approach. The dataset is designed to evaluate the performance of deepfake detection methods in real-world scenarios. The Celeb-DF dataset is led by the State University of New York at Buffalo. The dataset can be accessed through the following link: <https://github.com/yuezunli/>

Algorithm 3 EFS Method

Input: Noise n , Real Data D , Generative Model G

Output: Manipulated face \tilde{x}_t

- 1: Define n as the noise used to generate a completely synthetic face
 - 2: Fine-tune the generative model G with the real data D to obtain a face-synthesis model f_{sy}
 - 3: Apply EFS method to generate a completely synthetic face from noise n using the fine-tuned model f_{sy}
 - 4: $\tilde{x}_t(\tilde{i}_t, \tilde{a}_t, \tilde{b}_t) \leftarrow f_{sy}(n)$
 - 5: **return** \tilde{x}_t
-

Algorithm 4 FE Method

Input: Target face $x_t(i_t, a_t, b_t)$, Conditional source c_b

Output: Manipulated face \tilde{x}_t

- 1: Define x_t as the target face with attributes i_t, a_t, b_t
 - 2: Define c_b as the conditional source to manipulate the external attributes b_t
 - 3: Apply FE method to alter the external attributes b_t of the target face x_t , preserving its identity i_t and intrinsic attributes a_t
 - 4: $\tilde{x}_t(i_t, a_t, \tilde{b}_s) \leftarrow f_{ed}(x_t(i_t, a_t, b_t)|c_b)$
 - 5: **return** \tilde{x}_t
-

[celeb-deepfakeforensics](https://github.com/celeb-deepfakeforensics). The real human data sources for this dataset are not explicitly mentioned. The copyright information can be found at <https://docs.google.com/forms/d/e/1FAIpQLScoXint8ndZXyJi2Rcy4MvDHkkZLyBFKN43lTeyiG88wrG0rA/viewform?pli=1>.

UADFV Dataset [46] The UADFV dataset is also led by the State University of New York at Buffalo. The dataset can be accessed through the following link: <https://docs.google.com/forms/d/e/1FAIpQLSckPo0v15TIZ9Mn0nGSscIVgKRM9tFW0mj9eHKx57Yp-XcnxA/viewform>. The real human data in this dataset seems to be directly crawled from the internet, as no official website is provided. The copyright information can be found at <https://docs.google.com/forms/d/e/1FAIpQLSckPo0v15TIZ9Mn0nGSscIVgKRM9tFW0mj9eHKx57Yp-XcnxA/viewform>.

CelebA Dataset [51] The CelebA dataset is a large-scale face attributes dataset containing over 200,000 celebrity images, annotated with 40 attribute labels, such as gender, age, and facial expressions. It is primarily used for face attribute recognition tasks, including attribute prediction, face recognition, and face editing. The dataset has been widely adopted by the research community for developing and evaluating various machine learning models, including deep learning approaches. The CelebA dataset is led by the Chinese University of Hong Kong. The dataset can be accessed through the following link: <https://mmlab.ie.cuhk.edu.hk/projects/CelebA.html>. The real human data sources for this dataset are not explicitly mentioned. The complete copyright information for this dataset is not provided.

FFHQ Dataset [38] The Flickr-Faces-HQ (FFHQ) dataset is a high-quality dataset of human faces designed for training generative adversarial networks (GANs) and other machine-learning models to generate realistic human faces. It contains 70,000 high-resolution images (1024x1024 pixels) of diverse human faces collected from Flickr and annotated with age, gender, and ethnicity information. The dataset has been used in various applications, such as style-based GANs, super-resolution, and facial attribute manipulation. The FFHQ dataset is led by NVIDIA. The dataset can be accessed through the following link: <https://github.com/NVlabs/ffhq-dataset>. The real human data sources for this dataset come from Flickr: <https://www.flickr.com/>. The copyright information for this dataset is not explicitly mentioned.

VFHQ Dataset [89] The Varied Faces-HQ (VFHQ) dataset is a high-quality dataset of diverse human faces designed for training and evaluating generative models, such as GANs, in generating realistic and diverse human faces. It consists of 28,000 high-resolution images (1024x1024 pixels) collected from the internet, with a focus on diversity in terms of age, gender, ethnicity, and facial expressions. The dataset is widely used for developing and benchmarking generative models and face-related ap-

plications. The VFHQ dataset is led by the Shenzhen Institutes of Advanced Technology, the Chinese Academy of Sciences, and the ARC Lab of Tencent PCG. The dataset can be accessed through the following link: <https://liangbinxie.github.io/projects/vfhq/>. The copyright information can be found at <https://liangbinxie.github.io/projects/vfhq/license.txt>. The real human data sources for this dataset are not explicitly mentioned.

A.2 Introduction of the Used Detection Models

Detector Implementation Here, we describe the general idea of the 7 detection algorithms used in our evaluation as follows.

- 1) **Xception**[67]: Xception is a deepfake detection method based on the XceptionNet model[16] trained on the FaceForensics++ dataset [67]. It has three variants: Xception-raw, Xception-c23, and Xception-c40, which are trained on raw videos, and H.264 videos with medium (23) and high degrees (40) of compression, respectively. In our work, we use the c23 version by default. Many detection works utilize Xception as their backbone or baseline, making it a popular choice in the field.
- 2) **RECCE** [8]: RECCE is a reconstruction-based detector that constructs a graph over encoder and decoder features in a multi-scale manner. It further utilizes the reconstruction differences as the forgery traces on the graph output as a guide to the final representation, which is fed into a classifier for forgery detection. The model performs end-to-end optimization for reconstruction and classification learning, and uses Xception as the backbone for extracting features from the given image.
- 3) **SPSL**[48]: SPSL is a frequency-based detector that combines spatial image and phase spectrum to capture the up-sampling artifacts of face forgery, improving the transferability (generalization ability) for face forgery detection. The paper provides a theoretical analysis of the validity of utilizing the phase spectrum and highlights the importance of local texture information over high-level semantic information for face forgery detection. This detector utilizes the Xception backbone[16] for feature extraction. The code for this detector is not publicly available, so we use the implementation version in DeepfakeBench [94]. This model uses Xception as the backbone for extracting features from the given image.
- 4) **SRM**[52]: SRM is also a frequency-based detector that extracts high-frequency noise features and fuses two different representations from RGB and frequency domains to improve the generalization ability for face forgery detection. This detector utilizes the Xception backbone[16] for feature extraction, and its code is not publicly available, so we use the implementation version in DeepfakeBench [94]. The code for this detector is not publicly available, so we use the implementation version in DeepfakeBench [94]. This model uses Xception as the backbone for extracting features from the given image.
- 5) **SBI** [70]: introduces a novel approach for deepfake detection using self-blended images (SBIs), which are synthetically created by blending pseudo source and target images derived from single pristine images. This technique reproduces common forgery artifacts like blending boundaries and statistical inconsistencies, thereby generating more generalized and less recognizable fake samples. Unlike conventional methods that often overfit to specific manipulation artifacts seen during training, SBIs encourage classifiers to learn broader, more robust representations that generalize better to unseen manipulations and scenes. Extensive experimentation demonstrates the efficacy of the proposed method, particularly in closing the domain gap between training and test sets, as evidenced by significant performance improvements on the DFDC and DFDCP datasets. To align the settings with other detectors, we use the implementation version in DeepfakeBench [94] (v2 version).
- 6) **RFM** [79]: proposes an attention-based data augmentation framework, Representative Forgery Mining (RFM), which selectively occludes the top-sensitive facial areas, compelling the detector to explore previously overlooked regions for more representative forgery cues. This strategy is designed to refine and expand the detector’s attention, enhancing its capacity to identify manipulated facial images generated by diverse techniques. To align the settings with other detectors, we use the implementation version in DeepfakeBench [94] (v2 version).
- 7) **CLIP** [62]: stands for Contrastive Language-Image Pretraining, is an innovative artificial intelligence model developed by OpenAI. This model is designed to understand and generate a

meaningful connection between images and texts. Unlike traditional models that are trained for one specific task, CLIP is trained on a variety of data from the internet, enabling it to handle a wide range of tasks without requiring task-specific training data. It achieves this by learning to associate images and texts in a similar way to how humans do, making it a significant step forward in the field of AI. CLIP has broad applications, ranging from creating art to assisting in scientific research. To align the settings with other detectors, we use the implementation version in DeepfakeBench [94] (v2 version).

A.3 Experimental Setup and Full Experimental Results

A.3.1 Experimental Setup

Training Details. In the training module, we utilize the Adam optimization algorithm with a learning rate of 0.0002, except for CLIP. The batch size is set to 32 for both training and testing. For CLIP, we use the pre-trained weights from the default CLIP from OpenAI. For other detectors, we initialize the pre-trained weights from ImageNet. We summarize all the configurations used in our experiments (see Tab. 17). All experiments are conducted in a standardized environment using the NVIDIA V100 GPU to ensure fair and consistent evaluation. More software library dependencies can be seen on our website.

Evaluation Metrics. Regarding evaluation, we compute the frame-level Area Under the Curve (AUC) as our primary evaluation metric. We report video-level AUC for the video detector (*i.e.*, I3D). Note we can only perform training and testing I3D on FS and FR due to EFS and FE do not have video-format data. Furthermore, unlike DeepfakeBench, which does not involve using the validation set, we use the validation set to select the best-performing models and apply this checkpoint to detect *all* other testing data.

Training and Testing Data Split. (1) For FF++: We adhere to the *official* data split method, which uses 720 selected videos for training and 140 for testing and validation. When training models using the FF domain, such as FS (FF), we use the 720 corresponding fake videos for training and the original 720 real videos as real samples. **(2) For CDF:** We only use the 518 testing videos for all generations. Specifically, the original CDF testing data consists of 340 fake videos and 178 real videos. We select all video pairs (*e.g.*, ID1_ID2) from the 340 fake videos and create 680 fake videos, including the case of ID2_ID1. Thus, we have 680 fake videos for each method in the CDF domain. **(3) For DeepFaceLab:** We choose the 50 real videos from the original UADFV dataset [46] and then construct 100 pairs (*e.g.*, ID1_ID2 and ID2_ID1) for creating fake videos.

Data Augmentation Our benchmark employs a series of widely used data augmentation methods for image processing, which are described as follows:

1. **Rotation:** Randomly rotates the image within a range of -10 to 10 degrees with a 0.5 probability, introducing diversity in object orientations and enhancing model robustness.
2. **Isotropic Resize:** Resizes the image while maintaining isotropy, preserving the aspect ratio, and accommodating different object sizes and proportions.
3. **Random Brightness and Contrast:** Randomly adjusts brightness and contrast with a 0.5 probability, helping the model generalize better to different lighting conditions.
4. **FancyPCA:** Applies the FancyPCA algorithm with a 0.5 probability, altering the principal components of the image to change the color distribution and create diverse training samples.
5. **Hue Saturation Value (HSV) Adjustment:** Randomly adjusts the hue, saturation, and value of the image, allowing for variations in color representation.
6. **Image Compression:** Applies image compression with a 0.5 probability, introducing artifacts and simulating real-world scenarios with lower-quality images or compression artifacts, improving model robustness in practical applications.

Regarding video methods, it is worth noting that the I3D model does not implement any augmentations. This is a limitation of the current implementation, and future work could explore incorporating video-specific augmentations to enhance the model’s performance and robustness further.

Table 10: Summary of the datasets used for deepfake detection. The table provides information on the number of real and fake videos, the total number of videos, whether rights have been cleared, the number of agreeing subjects, the total number of subjects, the number of synthesis methods, and the number of perturbations.

| Dataset | Real Videos | Fake Videos | Total Videos | Rights Cleared | Total Subjects | Synthesis Methods | Perturbations | Download Link |
|------------------|-------------|-------------|--------------|----------------|----------------|-------------------|---------------|----------------------------|
| FF++ [67] | 1000 | 4000 | 5000 | NO | N/A | 4 | 2 | Hyper-link |
| FaceShifter [44] | 1000 | 1000 | 2000 | NO | N/A | 1 | - | Hyper-link |
| CDF-v2 [47] | 590 | 5639 | 6229 | NO | 59 | 1 | - | Hyper-link |
| DF-1.0 [35] | 50,000 | 10,000 | 60,000 | YES | 100 | 1 | 7 | Hyper-link |

External Testing Datasets Our benchmark currently incorporates a collection of 4 widely recognized and extensively used datasets in the realm of deepfake forensics: FaceForensics++ (FF++/FF) [67], CelebDF-v2 (CDF-v2/CDF) [47], FaceShifter (Fsh) [44], and DeeperForensics-1.0 (DF-1.0) [35]. The detailed descriptions of each dataset are presented in Tab. 10.

Specifically, FF++ [67] is a large-scale database comprising over 1.8 million forged images from 1000 pristine videos. Forged images are generated by four face manipulation algorithms using the same set of pristine videos, *i.e.*, DeepFakes (FF-DF) [19], Face2Face (FF-F2F) [77], FaceSwap (FF-FS) [25], and NeuralTexture (FF-NT) [76]. Note that there are three versions of FF++ in terms of compression level, *i.e.*, raw, lightly compressed (c23), and heavily compressed (c40). Following previous works [94], we adopt the c23 version for our experiments. CDF is another popular face-swapping dataset that includes 5,639 synthetic videos and 890 real videos downloaded from YouTube. In our experiments, 518 testing videos are used for evaluation. Fsh and DF-1.0 generate high-fidelity face-swapping videos based on real videos from FF++.

In addition to these face forgery detection datasets, we also consider evaluating models trained on our DF40 into other *non-face* domain datasets (see results in Tab. 7 of the manuscript). Here, we select the recent representative dataset GenImage [102]. This dataset comprises over a million pairs of images, including both AI-synthesized fake images and genuine collected images, covering diverse content categories. It leverages SoTA generative techniques, including both diffusion models and GANs.

A.3.2 Full Experimental Results and Discussion

In the main paper, we conduct evaluations under four standard protocols: Cross-forgery evaluation (**Protocol-1**), Cross-domain evaluation (**Protocol-2**), Toward unknown forgery and domain evaluation (**Protocol-3**), and One-Verse-All (OvA) evaluation (**Protocol-4**). For the OvA, we only show the heatmap to give an intuitive understanding of the performance. Here, we present the full results of OvA, including $2*31*31$ evaluations. The results can be seen in Tab. 11 (testing on FS, FF domain), Tab. 12 (testing on FR, FF domain), Tab. 13 (testing on EFS, FF domain), Tab. 14 (testing on FS, CDF domain), Tab. 15 (testing on FR, CDF domain), Tab. 16 (testing on EFS, CDF domain).

Further Discussion of Protocol-4: Training on DF40 (FF) and Testing on FS (FF). The key observation and finding in Tab. 11 is as follow:

- (1) UniFace, BlendFace, and MobileSwap detection methods show high AUC values when detecting SimSwap deepfakes, indicating that these methods are particularly effective at detecting SimSwap-generated deepfakes. Conversely, FaceSwap deepfakes are most effectively detected by their own detection method (FaceSwap), with an AUC of 0.992.
- (2) Among face-reenactment deepfake detection methods, Wav2Lip shows high AUC values in detecting UniFace, BlendFace, MobileSwap, and SimSwap deepfakes. This suggests that the Wav2Lip detection method is more versatile and effective in detecting various face-swapping deepfakes. However, it performs poorly in detecting FaceSwap deepfakes, with an AUC of 0.380.
- (3) In the entire face synthesis category, DiT and SiT detection methods exhibit higher AUC values when detecting UniFace, BlendFace, and MobileSwap deepfakes, compared to other entire face synthesis detection methods. This suggests that these two methods are more effective in detecting face-swapping deepfakes, while other methods like StyleGAN2, StyleGAN3, and StyleGAN-XL have lower AUC values, making them less effective.

(4) The detection methods generally show a decline in performance when tested on face editing deepfakes, as indicated by lower AUC values in the last few rows of the table. This suggests that face editing deepfakes are more challenging to detect, possibly due to their subtler manipulations and greater diversity in editing techniques.

(5) The AUC values tend to be lower when detection methods are tested on deepfakes from different data domains (FF and CDF). This underlines the importance of incorporating cross-data-domain evaluations in the development and assessment of deepfake detection methods. It also highlights the need to improve the generalization capabilities of these methods to handle diverse deepfake techniques and data domains effectively.

In summary, the table reveals the varying effectiveness of detection methods across different deepfake types and data domains. It emphasizes the need for more robust detection methods that can generalize well across diverse deepfake techniques and data sources, as well as the importance of cross-data-domain evaluations in assessing detection performance.

Further Discussion of Protocol-4: Training on DF40 (FF) and Testing on FR (FF). The key observation and finding in Tab. 12 is as follow:

(1) FSGAN detection method consistently achieves high AUC values across most of the face-reenactment deepfakes, indicating that it is particularly effective in detecting these deepfakes. On the other hand, the Hyperreenact detection method demonstrates a varying performance, with high AUC values for detecting MobileSwap and FOMM deepfakes but lower AUC values for detecting FaceSwap and Sadtalker deepfakes.

(2) Among the face-swapping deepfake detection methods, UniFace, BlendFace, and MobileSwap show relatively high AUC values when detecting FSGAN deepfakes. This suggests that these methods are more effective at detecting FSGAN-generated deepfakes compared to other face-swapping deepfakes.

(3) The Wav2Lip detection method, which belongs to the face-reenactment category, exhibits high AUC values when detecting SimSwap deepfakes, indicating its effectiveness in detecting this specific face-swapping deepfake. However, its performance is inconsistent across other face-swapping deepfakes, with lower AUC values for detecting FaceSwap and e4s deepfakes.

(4) The detection methods trained on DF40 (FF) generally show a decline in performance when tested on face editing deepfakes, as indicated by lower AUC values in the last few rows of the table. This suggests that face-editing deepfakes are more challenging to detect, possibly due to their subtler manipulations and greater diversity in editing techniques.

(5) The AUC values tend to be lower when detection methods are tested on deepfakes from different data domains (FF and CDF). This underlines the importance of incorporating cross-data-domain evaluations in the development and assessment of deepfake detection methods. It also highlights the need to improve the generalization capabilities of these methods to handle diverse deepfake techniques and data domains effectively.

In summary, the table reveals the varying effectiveness of detection methods across different deepfake types and data domains when trained on DF40 (FF) and tested on FR (FF). It emphasizes the need for more robust detection methods that can generalize well across diverse deepfake techniques and data sources, as well as the importance of cross-data-domain evaluations in assessing detection performance.

Further Discussion of Protocol-4: Training on DF40 (FF) and Testing on EFS (FF). The key observation and finding in Tab. 13 is as follow:

(1) The LIA detection method consistently achieves high AUC values across most of the entire face synthesis (EFS) deepfakes, indicating that it is particularly effective in detecting these deepfakes. On the other hand, the Sadtalker detection method demonstrates a varying performance, with high AUC values for detecting StyleGAN2 and StyleGAN3 deepfakes but lower AUC values for detecting StyleGAN-XL and RDDM deepfakes.

(2) Among the face-swapping deepfake detection methods, UniFace and BlendFace show relatively high AUC values when detecting StyleGAN2 and StyleGAN3 deepfakes. This suggests that these

Table 11: Part of quantitative results of OvA (Protocol-4): **Testing on FS (FF)** and Training on DF40 (FF). FS (FF) denotes all FS data within the FF domain, and DF40 (FF) denotes the combination results of FS (FF), FR (FF), and EFS (FF).

| | UniFace | BlendFace | MobileSwap | FaceSwap | e4s | FaceDancer | FSGAN | InSwap | SimSwap |
|--------------|---------|-----------|------------|----------|-------|------------|-------|--------|---------|
| UniFace | 0.999 | 0.953 | 0.842 | 0.553 | 0.829 | 0.598 | 0.784 | 0.725 | 0.946 |
| BlendFace | 0.982 | 0.996 | 0.984 | 0.571 | 0.711 | 0.611 | 0.845 | 0.838 | 0.955 |
| MobileSwap | 0.864 | 0.963 | 1.000 | 0.531 | 0.720 | 0.659 | 0.856 | 0.800 | 0.916 |
| FaceSwap | 0.614 | 0.681 | 0.725 | 0.992 | 0.634 | 0.518 | 0.78 | 0.591 | 0.576 |
| e4s | 0.829 | 0.736 | 0.688 | 0.531 | 1.000 | 0.637 | 0.763 | 0.668 | 0.610 |
| FaceDancer | 0.851 | 0.803 | 0.801 | 0.463 | 0.791 | 0.992 | 0.841 | 0.737 | 0.810 |
| FSGAN | 0.891 | 0.926 | 0.952 | 0.461 | 0.757 | 0.749 | 0.969 | 0.824 | 0.851 |
| InSwap | 0.905 | 0.930 | 0.925 | 0.516 | 0.623 | 0.662 | 0.866 | 0.999 | 0.963 |
| SimSwap | 0.984 | 0.984 | 0.982 | 0.417 | 0.668 | 0.684 | 0.833 | 0.840 | 1.000 |
| DaGAN | 0.667 | 0.756 | 0.894 | 0.430 | 0.744 | 0.644 | 0.726 | 0.705 | 0.703 |
| FOMM | 0.519 | 0.671 | 0.765 | 0.491 | 0.711 | 0.643 | 0.738 | 0.724 | 0.560 |
| Hyperreanact | 0.638 | 0.612 | 0.643 | 0.517 | 0.600 | 0.510 | 0.614 | 0.522 | 0.546 |
| TPSM | 0.693 | 0.750 | 0.890 | 0.468 | 0.763 | 0.645 | 0.740 | 0.714 | 0.671 |
| FS_vid2vid | 0.557 | 0.591 | 0.621 | 0.498 | 0.624 | 0.607 | 0.696 | 0.647 | 0.536 |
| MCNet | 0.700 | 0.768 | 0.862 | 0.482 | 0.709 | 0.675 | 0.783 | 0.767 | 0.673 |
| LIA | 0.860 | 0.852 | 0.835 | 0.525 | 0.858 | 0.759 | 0.899 | 0.840 | 0.650 |
| Wav2Lip | 0.936 | 0.944 | 0.746 | 0.380 | 0.620 | 0.611 | 0.723 | 0.698 | 0.939 |
| MRAA | 0.575 | 0.656 | 0.686 | 0.531 | 0.718 | 0.666 | 0.805 | 0.700 | 0.483 |
| OneShot | 0.515 | 0.638 | 0.789 | 0.527 | 0.760 | 0.672 | 0.681 | 0.681 | 0.543 |
| Pirender | 0.578 | 0.643 | 0.788 | 0.483 | 0.794 | 0.658 | 0.693 | 0.646 | 0.554 |
| Sadtalker | 0.78 | 0.847 | 0.985 | 0.371 | 0.699 | 0.738 | 0.754 | 0.865 | 0.804 |
| StyleGAN2 | 0.466 | 0.507 | 0.47 | 0.536 | 0.479 | 0.455 | 0.578 | 0.469 | 0.476 |
| StyleGAN3 | 0.465 | 0.507 | 0.472 | 0.536 | 0.479 | 0.454 | 0.578 | 0.470 | 0.476 |
| StyleGAN-XL | 0.525 | 0.572 | 0.575 | 0.567 | 0.533 | 0.462 | 0.504 | 0.572 | 0.551 |
| DDIM | 0.677 | 0.589 | 0.601 | 0.503 | 0.758 | 0.644 | 0.605 | 0.598 | 0.634 |
| DiT | 0.935 | 0.670 | 0.316 | 0.519 | 0.777 | 0.659 | 0.707 | 0.636 | 0.717 |
| pixart | 0.628 | 0.525 | 0.397 | 0.515 | 0.577 | 0.549 | 0.584 | 0.542 | 0.583 |
| SiT | 0.905 | 0.693 | 0.551 | 0.577 | 0.797 | 0.694 | 0.778 | 0.700 | 0.679 |
| SD2.1 | 0.607 | 0.526 | 0.470 | 0.477 | 0.597 | 0.555 | 0.554 | 0.532 | 0.465 |
| VQGAN | 0.668 | 0.718 | 0.635 | 0.460 | 0.650 | 0.521 | 0.655 | 0.618 | 0.591 |
| RDDM | 0.535 | 0.520 | 0.494 | 0.485 | 0.482 | 0.580 | 0.547 | 0.472 | 0.495 |

methods are more effective at detecting these specific entire face synthesis deepfakes compared to other face-swapping deepfakes.

(3) The Wav2Lip detection method, which belongs to the face-reenactment category, exhibits high AUC values when detecting DDIM deepfakes, indicating its effectiveness in detecting this specific entire face synthesis deepfake. However, its performance is inconsistent across other entire face synthesis deepfakes, with lower AUC values for detecting StyleGAN2 and StyleGAN3 deepfakes.

(4) The detection methods trained on DF40 (FF) generally show a decline in performance when tested on face editing deepfakes, as indicated by lower AUC values in the last few rows of the table. This suggests that face editing deepfakes are more challenging to detect, possibly due to their subtler manipulations and greater diversity in editing techniques.

(5) The AUC values tend to be lower when detection methods are tested on deepfakes from different data domains (FF and CDF). This underlines the importance of incorporating cross-data-domain evaluations in the development and assessment of deepfake detection methods. It also highlights the need to improve the generalization capabilities of these methods to handle diverse deepfake techniques and data domains effectively.

In summary, the table reveals the varying effectiveness of detection methods across different deepfake types and data domains when trained on DF40 (FF) and tested on EFS (FF). It emphasizes the need for more robust detection methods that can generalize well across diverse deepfake techniques and data sources, as well as the importance of cross-data-domain evaluations in assessing detection performance.

A.3.3 Further Analysis Results

Deeper Analysis of the Influence of Data Domains and Forgery Methods We analyze logits and confidence distributions for real and fake classes using Xception and SBI models, visualized in Fig. 6. (1) **For Xception:** (i) *Same Domain and Method:* Real and fake class distributions have small variance and high mean, with minimal ambiguity in confidence. (ii) *Cross Method, Same Domain:* Fake class distribution has increased variance and lower mean, while real class remains relatively

Table 12: Part of quantitative results of OvA (Protocol-4): **Testing on FR (FF)** and Training on DF40 (FF). FR (FF) denotes all FR data within the FF domain, and DF40 (FF) denotes the combination results of FS (FF), FR (FF), and EFS (FF).

| | DaGAN | FOMM | Hyperreenact | TPSM | FS_vid2vid | MCNet | LIA | Wav2Lip | MRAA | OneShot | Pirender | Sadtalker |
|--------------|-------|-------|--------------|-------|------------|-------|-------|---------|-------|---------|----------|-----------|
| UniFace | 0.659 | 0.644 | 0.907 | 0.695 | 0.692 | 0.724 | 0.779 | 0.711 | 0.579 | 0.574 | 0.544 | 0.593 |
| BlendFace | 0.758 | 0.807 | 0.914 | 0.773 | 0.813 | 0.812 | 0.793 | 0.797 | 0.774 | 0.749 | 0.771 | 0.658 |
| MobileSwap | 0.844 | 0.938 | 0.954 | 0.862 | 0.912 | 0.892 | 0.675 | 0.646 | 0.803 | 0.948 | 0.927 | 0.787 |
| faceswap | 0.530 | 0.714 | 0.321 | 0.524 | 0.574 | 0.583 | 0.632 | 0.443 | 0.691 | 0.690 | 0.682 | 0.471 |
| e4s | 0.819 | 0.840 | 0.822 | 0.829 | 0.894 | 0.849 | 0.783 | 0.596 | 0.827 | 0.827 | 0.799 | 0.641 |
| facedancer | 0.654 | 0.746 | 0.738 | 0.677 | 0.723 | 0.703 | 0.709 | 0.611 | 0.806 | 0.766 | 0.705 | 0.609 |
| fsgan | 0.931 | 0.982 | 0.999 | 0.934 | 0.937 | 0.944 | 0.867 | 0.779 | 0.920 | 0.956 | 0.967 | 0.857 |
| InSwap | 0.818 | 0.888 | 0.723 | 0.839 | 0.895 | 0.871 | 0.796 | 0.669 | 0.848 | 0.881 | 0.780 | 0.711 |
| SimSwap | 0.706 | 0.692 | 0.862 | 0.712 | 0.715 | 0.745 | 0.607 | 0.807 | 0.512 | 0.704 | 0.623 | 0.677 |
| DaGAN | 0.999 | 0.999 | 0.999 | 0.999 | 0.999 | 0.999 | 0.999 | 0.696 | 0.987 | 0.998 | 0.998 | 0.907 |
| FOMM | 0.985 | 0.999 | 0.999 | 0.985 | 0.999 | 0.989 | 0.926 | 0.522 | 0.999 | 0.999 | 0.999 | 0.829 |
| Hyperreenact | 0.629 | 0.786 | 0.999 | 0.695 | 0.745 | 0.755 | 0.653 | 0.528 | 0.686 | 0.658 | 0.743 | 0.453 |
| TPSM | 0.999 | 0.999 | 0.999 | 0.999 | 0.999 | 0.999 | 0.999 | 0.694 | 0.990 | 0.999 | 0.999 | 0.897 |
| FS_vid2vid | 0.984 | 0.986 | 0.989 | 0.985 | 0.999 | 0.988 | 0.976 | 0.518 | 0.984 | 0.989 | 0.984 | 0.696 |
| MCNet | 0.999 | 0.999 | 0.999 | 0.999 | 0.999 | 0.999 | 0.999 | 0.684 | 0.996 | 0.999 | 0.999 | 0.908 |
| LIA | 0.999 | 0.982 | 0.990 | 0.999 | 0.999 | 0.999 | 0.999 | 0.704 | 0.998 | 0.955 | 0.975 | 0.778 |
| Wav2Lip | 0.633 | 0.785 | 0.817 | 0.818 | 0.758 | 0.808 | 0.786 | 0.994 | 0.532 | 0.563 | 0.623 | 0.702 |
| MRAA | 0.924 | 0.998 | 0.978 | 0.936 | 0.986 | 0.955 | 0.935 | 0.520 | 0.999 | 0.987 | 0.988 | 0.677 |
| OneShot | 0.983 | 0.999 | 0.996 | 0.983 | 0.999 | 0.986 | 0.899 | 0.497 | 0.996 | 0.999 | 0.999 | 0.822 |
| Pirender | 0.989 | 0.999 | 0.999 | 0.992 | 0.999 | 0.994 | 0.954 | 0.524 | 0.999 | 0.999 | 0.999 | 0.820 |
| Sadtalker | 0.995 | 0.999 | 0.999 | 0.997 | 0.999 | 0.998 | 0.810 | 0.735 | 0.966 | 0.999 | 0.999 | 0.994 |
| StyleGAN2 | 0.491 | 0.498 | 0.495 | 0.459 | 0.445 | 0.530 | 0.520 | 0.493 | 0.501 | 0.494 | 0.489 | 0.440 |
| StyleGAN3 | 0.492 | 0.499 | 0.495 | 0.459 | 0.446 | 0.531 | 0.520 | 0.493 | 0.502 | 0.497 | 0.492 | 0.441 |
| StyleGAN-XL | 0.567 | 0.634 | 0.750 | 0.542 | 0.540 | 0.590 | 0.538 | 0.505 | 0.595 | 0.591 | 0.553 | 0.507 |
| DDIM | 0.586 | 0.791 | 0.792 | 0.597 | 0.542 | 0.659 | 0.659 | 0.523 | 0.781 | 0.772 | 0.754 | 0.543 |
| DiT | 0.584 | 0.703 | 0.710 | 0.585 | 0.632 | 0.592 | 0.692 | 0.666 | 0.702 | 0.709 | 0.631 | 0.462 |
| Pixart | 0.516 | 0.567 | 0.532 | 0.532 | 0.435 | 0.552 | 0.618 | 0.587 | 0.627 | 0.552 | 0.542 | 0.592 |
| SiT | 0.661 | 0.921 | 0.926 | 0.684 | 0.733 | 0.710 | 0.786 | 0.597 | 0.936 | 0.866 | 0.840 | 0.523 |
| SD2.1 | 0.616 | 0.577 | 0.684 | 0.592 | 0.461 | 0.656 | 0.808 | 0.543 | 0.643 | 0.481 | 0.414 | 0.469 |
| VQGAN | 0.580 | 0.699 | 0.747 | 0.625 | 0.661 | 0.656 | 0.679 | 0.623 | 0.702 | 0.695 | 0.691 | 0.523 |
| RDDM | 0.520 | 0.467 | 0.562 | 0.524 | 0.441 | 0.556 | 0.572 | 0.555 | 0.451 | 0.407 | 0.404 | 0.500 |

Table 13: Part of quantitative results of OvA (Protocol-4): **Testing on EFS (FF)** and Training on DF40 (FF). EFS (FF) denotes all EFS data within the FF domain, and DF40 (FF) denotes the combination results of FS (FF), FR (FF), and EFS (FF).

| | StyleGAN2 | StyleGAN3 | StyleGAN-XL | ddim | DiT | Pixart | SiT | SD2.1 | VQGAN | RDDM |
|--------------|-----------|-----------|-------------|-------|-------|--------|-------|-------|-------|-------|
| UniFace | 0.844 | 0.844 | 0.549 | 0.897 | 0.547 | 0.794 | 0.558 | 0.913 | 0.820 | 0.998 |
| BlendFace | 0.307 | 0.307 | 0.228 | 0.736 | 0.554 | 0.532 | 0.597 | 0.838 | 0.948 | 0.999 |
| MobileSwap | 0.671 | 0.671 | 0.806 | 0.911 | 0.571 | 0.241 | 0.587 | 0.627 | 0.828 | 0.989 |
| faceswap | 0.618 | 0.618 | 0.508 | 0.733 | 0.562 | 0.504 | 0.622 | 0.559 | 0.681 | 0.880 |
| e4s | 0.367 | 0.367 | 0.523 | 0.778 | 0.560 | 0.531 | 0.578 | 0.890 | 0.880 | 0.950 |
| facedancer | 0.858 | 0.858 | 0.770 | 0.868 | 0.584 | 0.467 | 0.619 | 0.881 | 0.812 | 0.870 |
| fsgan | 0.577 | 0.577 | 0.431 | 0.948 | 0.604 | 0.628 | 0.623 | 0.974 | 0.876 | 0.945 |
| InSwap | 0.263 | 0.263 | 0.576 | 0.658 | 0.478 | 0.441 | 0.532 | 0.629 | 0.665 | 0.940 |
| SimSwap | 0.805 | 0.805 | 0.706 | 0.849 | 0.497 | 0.570 | 0.496 | 0.648 | 0.842 | 0.967 |
| DaGAN | 0.807 | 0.807 | 0.907 | 0.789 | 0.614 | 0.572 | 0.627 | 0.889 | 0.582 | 0.999 |
| FOMM | 0.464 | 0.464 | 0.716 | 0.723 | 0.550 | 0.408 | 0.632 | 0.785 | 0.545 | 0.999 |
| Hyperreenact | 0.448 | 0.448 | 0.598 | 0.705 | 0.502 | 0.665 | 0.543 | 0.874 | 0.855 | 0.990 |
| TPSM | 0.828 | 0.828 | 0.921 | 0.839 | 0.569 | 0.520 | 0.600 | 0.877 | 0.581 | 0.999 |
| FS_vid2vid | 0.635 | 0.635 | 0.782 | 0.763 | 0.573 | 0.520 | 0.600 | 0.844 | 0.582 | 0.999 |
| MCNet | 0.695 | 0.695 | 0.778 | 0.806 | 0.533 | 0.524 | 0.590 | 0.853 | 0.386 | 0.999 |
| LIA | 0.999 | 0.999 | 0.758 | 0.775 | 0.512 | 0.729 | 0.634 | 0.998 | 0.590 | 0.999 |
| Wav2Lip | 0.302 | 0.302 | 0.246 | 0.703 | 0.614 | 0.693 | 0.577 | 0.771 | 0.925 | 0.994 |
| MRAA | 0.517 | 0.517 | 0.609 | 0.664 | 0.585 | 0.567 | 0.650 | 0.902 | 0.566 | 0.997 |
| OneShot | 0.682 | 0.682 | 0.875 | 0.772 | 0.600 | 0.337 | 0.625 | 0.701 | 0.754 | 0.994 |
| Pirender | 0.775 | 0.775 | 0.826 | 0.801 | 0.621 | 0.538 | 0.649 | 0.793 | 0.782 | 0.996 |
| Sadtalker | 0.901 | 0.901 | 0.990 | 0.828 | 0.600 | 0.476 | 0.664 | 0.653 | 0.494 | 0.918 |
| StyleGAN2 | 0.999 | 0.999 | 0.473 | 0.671 | 0.506 | 0.395 | 0.486 | 0.609 | 0.602 | 0.464 |
| StyleGAN3 | 0.999 | 0.999 | 0.474 | 0.669 | 0.506 | 0.395 | 0.487 | 0.608 | 0.602 | 0.465 |
| StyleGAN-XL | 0.209 | 0.209 | 0.999 | 0.601 | 0.546 | 0.490 | 0.552 | 0.603 | 0.676 | 0.294 |
| DDIM | 0.819 | 0.819 | 0.363 | 0.999 | 0.550 | 0.633 | 0.589 | 0.939 | 0.877 | 0.964 |
| DiT | 0.795 | 0.795 | 0.341 | 0.891 | 0.995 | 0.773 | 0.994 | 0.855 | 0.976 | 0.979 |
| Pixart | 0.934 | 0.934 | 0.655 | 0.646 | 0.524 | 0.999 | 0.532 | 0.994 | 0.570 | 0.587 |
| SiT | 0.940 | 0.940 | 0.577 | 0.958 | 0.985 | 0.853 | 0.995 | 0.957 | 0.942 | 0.982 |
| SD2.1 | 0.823 | 0.823 | 0.687 | 0.929 | 0.492 | 0.878 | 0.539 | 0.999 | 0.811 | 0.998 |
| VQGAN | 0.356 | 0.356 | 0.787 | 0.709 | 0.579 | 0.506 | 0.595 | 0.835 | 0.999 | 0.999 |
| RDDM | 0.289 | 0.288 | 0.508 | 0.560 | 0.480 | 0.527 | 0.492 | 0.736 | 0.599 | 0.999 |

Table 14: Part of quantitative results of OvA (Protocol-4): **Testing on FS (CDF)** and Training on DF40 (FF). FS (FF) denotes all FS data within the FF domain, and DF40 (FF) denotes the combination results of FS (CDF), FR (CDF), and EFS (CDF).

| | UniFace | BlendFace | MobileSwap | FaceSwap | e4s | FaceDancer | FSGAN | InSwap | SimSwap |
|---------------|---------|-----------|------------|----------|-------|------------|-------|--------|---------|
| UniFace | 0.994 | 0.887 | 0.703 | 0.426 | 0.867 | 0.599 | 0.639 | 0.556 | 0.877 |
| BlendFace | 0.908 | 0.995 | 0.854 | 0.429 | 0.571 | 0.408 | 0.785 | 0.621 | 0.798 |
| MobileSwap | 0.467 | 0.843 | 0.999 | 0.525 | 0.431 | 0.340 | 0.764 | 0.542 | 0.686 |
| faceswap | 0.524 | 0.628 | 0.664 | 0.999 | 0.562 | 0.476 | 0.787 | 0.565 | 0.524 |
| e4s | 0.680 | 0.588 | 0.566 | 0.520 | 0.999 | 0.674 | 0.561 | 0.558 | 0.462 |
| facedancer | 0.694 | 0.651 | 0.571 | 0.254 | 0.739 | 0.997 | 0.602 | 0.551 | 0.535 |
| fsgan | 0.445 | 0.694 | 0.696 | 0.498 | 0.453 | 0.374 | 0.973 | 0.299 | 0.375 |
| InSwap | 0.684 | 0.827 | 0.835 | 0.486 | 0.396 | 0.400 | 0.670 | 0.967 | 0.902 |
| SimSwap | 0.879 | 0.865 | 0.781 | 0.466 | 0.505 | 0.409 | 0.416 | 0.553 | 0.997 |
| DaGAN | 0.227 | 0.368 | 0.602 | 0.549 | 0.496 | 0.699 | 0.706 | 0.328 | 0.298 |
| FOMM | 0.298 | 0.438 | 0.683 | 0.571 | 0.530 | 0.560 | 0.690 | 0.491 | 0.374 |
| HypterReenact | 0.532 | 0.657 | 0.662 | 0.380 | 0.682 | 0.611 | 0.680 | 0.489 | 0.502 |
| TPSM | 0.298 | 0.396 | 0.602 | 0.470 | 0.461 | 0.623 | 0.691 | 0.372 | 0.303 |
| FS_vid2vid | 0.463 | 0.520 | 0.571 | 0.536 | 0.613 | 0.746 | 0.616 | 0.587 | 0.468 |
| MCNet | 0.334 | 0.402 | 0.585 | 0.462 | 0.472 | 0.650 | 0.635 | 0.416 | 0.309 |
| LIA | 0.636 | 0.650 | 0.561 | 0.321 | 0.666 | 0.745 | 0.771 | 0.591 | 0.355 |
| Wav2Lip | 0.877 | 0.841 | 0.437 | 0.416 | 0.558 | 0.642 | 0.616 | 0.506 | 0.828 |
| MRAA | 0.457 | 0.546 | 0.644 | 0.562 | 0.617 | 0.562 | 0.714 | 0.617 | 0.383 |
| OneShot | 0.282 | 0.415 | 0.689 | 0.575 | 0.600 | 0.599 | 0.618 | 0.524 | 0.389 |
| Pirender | 0.297 | 0.399 | 0.620 | 0.396 | 0.612 | 0.560 | 0.614 | 0.410 | 0.304 |
| Sadtalker | 0.134 | 0.225 | 0.620 | 0.365 | 0.311 | 0.413 | 0.551 | 0.306 | 0.188 |
| StyleGAN2 | 0.552 | 0.629 | 0.622 | 0.699 | 0.488 | 0.500 | 0.612 | 0.567 | 0.607 |
| StyleGAN3 | 0.552 | 0.628 | 0.623 | 0.699 | 0.486 | 0.499 | 0.610 | 0.566 | 0.606 |
| StyleGAN-XL | 0.452 | 0.515 | 0.580 | 0.549 | 0.444 | 0.385 | 0.429 | 0.484 | 0.486 |
| DDIM | 0.561 | 0.530 | 0.570 | 0.549 | 0.813 | 0.588 | 0.446 | 0.513 | 0.529 |
| DiT | 0.939 | 0.691 | 0.500 | 0.517 | 0.807 | 0.828 | 0.526 | 0.669 | 0.661 |
| Pixart | 0.558 | 0.478 | 0.378 | 0.451 | 0.544 | 0.535 | 0.455 | 0.462 | 0.497 |
| SiT | 0.874 | 0.651 | 0.600 | 0.587 | 0.816 | 0.782 | 0.650 | 0.654 | 0.564 |
| SD2.1 | 0.546 | 0.522 | 0.478 | 0.363 | 0.616 | 0.593 | 0.488 | 0.482 | 0.454 |
| VQGAN | 0.557 | 0.731 | 0.525 | 0.391 | 0.587 | 0.472 | 0.498 | 0.582 | 0.489 |
| RDDM | 0.482 | 0.547 | 0.527 | 0.579 | 0.410 | 0.496 | 0.525 | 0.496 | 0.484 |

Table 15: Part of quantitative results of OvA (Protocol-4): **Testing on FR (CDF)** and Training on DF40 (FF). FR (FF) denotes all FR data within the FF domain, and DF40 (FF) denotes the combination results of FS (CDF), FR (CDF), and EFS (CDF).

| | DaGAN | FOMM | Hyperreenact | TPSM | FS_vid2vid | MCNet | LIA | Wav2Lip | MRAA | OneShot | Pirender | Sadtalker |
|---------------|-------|-------|--------------|-------|------------|-------|-------|---------|-------|---------|----------|-----------|
| UniFace | 0.604 | 0.615 | 0.762 | 0.518 | 0.668 | 0.667 | 0.578 | 0.6522 | 0.474 | 0.573 | 0.489 | 0.447 |
| BlendFace | 0.585 | 0.626 | 0.737 | 0.457 | 0.671 | 0.636 | 0.683 | 0.670 | 0.547 | 0.625 | 0.579 | 0.386 |
| MobileSwap | 0.677 | 0.877 | 0.694 | 0.464 | 0.762 | 0.715 | 0.532 | 0.317 | 0.527 | 0.902 | 0.737 | 0.481 |
| faceswap | 0.621 | 0.716 | 0.312 | 0.436 | 0.615 | 0.631 | 0.668 | 0.498 | 0.673 | 0.746 | 0.733 | 0.448 |
| e4s | 0.743 | 0.837 | 0.429 | 0.589 | 0.793 | 0.769 | 0.558 | 0.414 | 0.671 | 0.84 | 0.735 | 0.492 |
| facedancer | 0.503 | 0.628 | 0.459 | 0.390 | 0.575 | 0.553 | 0.601 | 0.478 | 0.647 | 0.64 | 0.580 | 0.393 |
| fsgan | 0.584 | 0.727 | 0.959 | 0.491 | 0.619 | 0.660 | 0.602 | 0.415 | 0.508 | 0.601 | 0.665 | 0.444 |
| InSwap | 0.616 | 0.774 | 0.441 | 0.547 | 0.744 | 0.651 | 0.647 | 0.503 | 0.679 | 0.786 | 0.555 | 0.512 |
| SimSwap | 0.468 | 0.497 | 0.539 | 0.365 | 0.467 | 0.497 | 0.332 | 0.547 | 0.245 | 0.565 | 0.411 | 0.345 |
| DaGAN | 0.997 | 0.981 | 0.976 | 0.939 | 0.999 | 0.997 | 0.692 | 0.325 | 0.811 | 0.962 | 0.950 | 0.716 |
| FOMM | 0.936 | 0.999 | 0.971 | 0.793 | 0.991 | 0.949 | 0.757 | 0.350 | 0.976 | 0.994 | 0.989 | 0.678 |
| HypterReenact | 0.699 | 0.827 | 0.999 | 0.527 | 0.845 | 0.756 | 0.639 | 0.435 | 0.714 | 0.791 | 0.792 | 0.431 |
| TPSM | 0.989 | 0.989 | 0.966 | 0.916 | 0.985 | 0.991 | 0.687 | 0.339 | 0.874 | 0.981 | 0.971 | 0.739 |
| FS_vid2vid | 0.963 | 0.970 | 0.982 | 0.909 | 0.998 | 0.967 | 0.812 | 0.472 | 0.958 | 0.975 | 0.972 | 0.630 |
| MCNet | 0.990 | 0.973 | 0.972 | 0.918 | 0.997 | 0.992 | 0.747 | 0.355 | 0.894 | 0.958 | 0.951 | 0.686 |
| LIA | 0.990 | 0.923 | 0.964 | 0.913 | 0.997 | 0.994 | 0.989 | 0.530 | 0.984 | 0.878 | 0.886 | 0.469 |
| Wav2Lip | 0.628 | 0.406 | 0.649 | 0.601 | 0.616 | 0.666 | 0.592 | 0.962 | 0.272 | 0.341 | 0.381 | 0.462 |
| MRAA | 0.901 | 0.995 | 0.932 | 0.760 | 0.985 | 0.933 | 0.889 | 0.417 | 0.995 | 0.988 | 0.977 | 0.632 |
| OneShot | 0.933 | 0.998 | 0.949 | 0.816 | 0.996 | 0.941 | 0.692 | 0.358 | 0.961 | 0.998 | 0.995 | 0.725 |
| Pirender | 0.946 | 0.995 | 0.980 | 0.788 | 0.994 | 0.962 | 0.733 | 0.330 | 0.963 | 0.996 | 0.999 | 0.654 |
| Sadtalker | 0.792 | 0.916 | 0.691 | 0.756 | 0.923 | 0.791 | 0.185 | 0.228 | 0.381 | 0.915 | 0.876 | 0.863 |
| StyleGAN2 | 0.689 | 0.723 | 0.590 | 0.556 | 0.719 | 0.701 | 0.618 | 0.572 | 0.630 | 0.718 | 0.691 | 0.537 |
| StyleGAN3 | 0.689 | 0.723 | 0.592 | 0.555 | 0.719 | 0.701 | 0.619 | 0.571 | 0.630 | 0.720 | 0.692 | 0.538 |
| StyleGAN-XL | 0.549 | 0.564 | 0.456 | 0.485 | 0.545 | 0.561 | 0.520 | 0.463 | 0.506 | 0.567 | 0.496 | 0.410 |
| DDIM | 0.494 | 0.691 | 0.502 | 0.345 | 0.480 | 0.540 | 0.571 | 0.397 | 0.591 | 0.705 | 0.695 | 0.380 |
| DiT | 0.707 | 0.748 | 0.549 | 0.592 | 0.716 | 0.699 | 0.693 | 0.625 | 0.687 | 0.751 | 0.664 | 0.417 |
| Pixart | 0.506 | 0.570 | 0.717 | 0.478 | 0.489 | 0.522 | 0.493 | 0.506 | 0.596 | 0.598 | 0.524 | 0.489 |
| SiT | 0.689 | 0.893 | 0.771 | 0.532 | 0.742 | 0.716 | 0.801 | 0.518 | 0.881 | 0.871 | 0.790 | 0.405 |
| SD2.1 | 0.580 | 0.624 | 0.519 | 0.399 | 0.583 | 0.609 | 0.688 | 0.479 | 0.570 | 0.598 | 0.440 | 0.334 |
| VQGAN | 0.580 | 0.694 | 0.404 | 0.460 | 0.618 | 0.615 | 0.648 | 0.545 | 0.575 | 0.733 | 0.669 | 0.421 |
| RDDM | 0.632 | 0.633 | 0.469 | 0.530 | 0.728 | 0.650 | 0.545 | 0.517 | 0.513 | 0.622 | 0.430 | 0.482 |

Table 16: Part of quantitative results of OvA (Protocol-4): **Testing on EFS (CDF)** and Training on DF40 (FF). EFS (FF) denotes all EFS data within the FF domain, and DF40 (FF) denotes the combination results of FS (CDF), FR (CDF), and EFS (CDF).

| | StyleGAN2 | StyleGAN3 | StyleGAN-XL | ddim | DiT | Pixart | SiT | SD2.1 | VQGAN | RDDM |
|----------------|-----------|-----------|-------------|-------|-------|--------|-------|-------|-------|-------|
| UniFace | 0.697 | 0.639 | 0.592 | 0.784 | 0.544 | 0.709 | 0.568 | 0.882 | 0.703 | 0.999 |
| BlendFace | 0.498 | 0.309 | 0.326 | 0.457 | 0.585 | 0.360 | 0.602 | 0.747 | 0.895 | 0.984 |
| MobileSwap | 0.578 | 0.550 | 0.498 | 0.598 | 0.495 | 0.175 | 0.511 | 0.444 | 0.570 | 0.997 |
| faceswap | 0.538 | 0.480 | 0.334 | 0.540 | 0.470 | 0.428 | 0.539 | 0.476 | 0.570 | 0.997 |
| e4s | 0.345 | 0.298 | 0.469 | 0.638 | 0.494 | 0.336 | 0.488 | 0.808 | 0.754 | 0.997 |
| facedancer | 0.487 | 0.601 | 0.492 | 0.711 | 0.469 | 0.387 | 0.544 | 0.716 | 0.551 | 0.956 |
| fsgan | 0.551 | 0.330 | 0.789 | 0.536 | 0.417 | 0.479 | 0.408 | 0.879 | 0.372 | 0.933 |
| InSwap | 0.441 | 0.342 | 0.487 | 0.393 | 0.514 | 0.258 | 0.549 | 0.449 | 0.584 | 0.993 |
| SimSwap | 0.522 | 0.406 | 0.507 | 0.552 | 0.456 | 0.237 | 0.422 | 0.340 | 0.567 | 0.990 |
| DaGAN | 0.408 | 0.304 | 0.675 | 0.206 | 0.466 | 0.320 | 0.424 | 0.625 | 0.207 | 0.985 |
| FOMM | 0.477 | 0.431 | 0.610 | 0.240 | 0.631 | 0.223 | 0.630 | 0.615 | 0.547 | 0.865 |
| HypsterReenact | 0.588 | 0.469 | 0.795 | 0.515 | 0.490 | 0.506 | 0.436 | 0.648 | 0.681 | 0.853 |
| TPSM | 0.370 | 0.379 | 0.744 | 0.199 | 0.517 | 0.289 | 0.507 | 0.580 | 0.342 | 0.973 |
| FS_vid2vid | 0.550 | 0.581 | 0.723 | 0.346 | 0.662 | 0.436 | 0.662 | 0.746 | 0.629 | 0.996 |
| MCNet | 0.312 | 0.389 | 0.653 | 0.215 | 0.470 | 0.405 | 0.467 | 0.627 | 0.294 | 0.974 |
| LIA | 0.739 | 0.905 | 0.575 | 0.398 | 0.370 | 0.671 | 0.439 | 0.992 | 0.352 | 0.999 |
| Wav2Lip | 0.206 | 0.182 | 0.305 | 0.534 | 0.597 | 0.445 | 0.563 | 0.680 | 0.868 | 0.995 |
| MRAA | 0.607 | 0.608 | 0.616 | 0.409 | 0.683 | 0.468 | 0.714 | 0.853 | 0.632 | 0.902 |
| OneShot | 0.556 | 0.507 | 0.754 | 0.305 | 0.654 | 0.157 | 0.637 | 0.363 | 0.703 | 0.870 |
| Pirender | 0.499 | 0.631 | 0.696 | 0.344 | 0.622 | 0.242 | 0.612 | 0.471 | 0.787 | 0.912 |
| Sadtalker | 0.430 | 0.683 | 0.828 | 0.168 | 0.379 | 0.176 | 0.369 | 0.257 | 0.081 | 0.162 |
| StyleGAN2 | 0.590 | 0.994 | 0.517 | 0.551 | 0.491 | 0.425 | 0.505 | 0.558 | 0.599 | 0.811 |
| StyleGAN3 | 0.590 | 0.994 | 0.518 | 0.550 | 0.491 | 0.424 | 0.504 | 0.558 | 0.598 | 0.810 |
| StyleGAN-XL | 0.384 | 0.211 | 0.810 | 0.467 | 0.486 | 0.405 | 0.541 | 0.504 | 0.676 | 0.833 |
| DDIM | 0.588 | 0.554 | 0.318 | 0.999 | 0.481 | 0.474 | 0.539 | 0.737 | 0.673 | 0.944 |
| DiT | 0.824 | 0.744 | 0.315 | 0.922 | 0.986 | 0.862 | 0.992 | 0.858 | 0.912 | 0.999 |
| Pixart | 0.528 | 0.730 | 0.571 | 0.684 | 0.584 | 0.999 | 0.572 | 0.971 | 0.554 | 0.934 |
| SiT | 0.986 | 0.954 | 0.400 | 0.973 | 0.969 | 0.935 | 0.991 | 0.973 | 0.858 | 0.978 |
| SD2.1 | 0.456 | 0.441 | 0.551 | 0.650 | 0.477 | 0.869 | 0.506 | 0.999 | 0.543 | 0.999 |
| VQGAN | 0.254 | 0.257 | 0.434 | 0.578 | 0.531 | 0.408 | 0.520 | 0.522 | 0.999 | 0.999 |
| RDDM | 0.354 | 0.345 | 0.429 | 0.589 | 0.558 | 0.546 | 0.542 | 0.787 | 0.693 | 0.999 |

unchanged. (iii) *Cross Domain, Same Method*: Real class distribution has increased variance and lower mean, while fake class remains relatively unchanged, causing a slight performance decrease. (iv) *Cross Method and Domain*: Both real and fake class distributions have significantly increased variance and lower means, decreasing overall performance. This verifies **Finding-6. (2) For SBI**: It shows a different behavior than Xception. The real class distribution consistently has a small variance and high mean, while the fake class distribution has a larger variance and lower mean. This suggests that SBI learns a robust distribution for real classes, generalizing well in the FF domain using the FS method (0.81 AUC). However, when the real class distribution changes (*e.g.*, in the CDF domain), performance drops significantly (to 0.679 AUC). This indicates that SBI might operate like an "anomaly detection method" based on deviations from the learned real class distribution.

A.4 Dataset Publication

A.4.1 Links

We provide a private direct link to the dataset is shared with the reviewers at https://anonymous.4open.science/r/DF40_6E0E/ to keep the *single-blind review*, where we give the *OneDrive download link*, *associated codes*, and *visual examples* for illustrating partial forgery images/videos of DF40. We will provide the *official website*, *download links*, and *license* for the dataset after publication. Our dataset with documentation and associated codes (for reproduction of our experimental results) is maintained under the following license: <https://creativecommons.org/licenses/by-nc/4.0/>.

A.4.2 Hosting Platform & Access to Dataset

In the review process, we host our dataset on the OneDrive account, where reviewers and AC can access the fake videos and images of our dataset. After publication, we will host our dataset on an official website with detailed instructions and official download links. Also, after publication, a dataset *request form* (Google form) to monitor and restrict the free use of our deepfake dataset. In this manner, everyone has to fill out the dataset request form, which we will manually screen to limit misuse.

Table 17: The results of our experiments are generated using the following settings.

| Training Config | CLIP | Other Detectors |
|------------------------|-------------------|----------------------|
| Image Size | 224, 224 | 256, 256 |
| Weight Initialization | CLIP Pre-trained | ImageNet Pre-trained |
| Optimizer | Adam | Adam |
| Base Learning Rate | 1e-5 | 2e-4 |
| Weight Decay | 5e-4 | 5e-4 |
| Optimizer Momentum | B1, B2=0.9, 0.999 | B1, B2=0.9, 0.999 |
| Batch Size | 32 | 32 |
| Training Epochs | 15 | 15 |
| Learning Rate Schedule | None, Constant | None, Constant |
| Flip Probability | 0.5 | 0.5 |
| Rotate Probability | 0.5 | 0.5 |
| Rotate Limit | [-10, 10] | [-10, 10] |
| Blur Probability | 0.5 | 0.5 |
| Blur Limit | [3, 7] | [3, 7] |
| Brightness Probability | 0.5 | 0.5 |
| Brightness Limit | [-0.1, 0.1] | [-0.1, 0.1] |
| Contrast Limit | [-0.1, 0.1] | [-0.1, 0.1] |
| Quality Lower | 40 | 40 |
| Quality Upper | 100 | 100 |

A.4.3 Licensing

Our DF40 dataset is available under the Creative Commons NonCommercial license (CC BY-NC). More details can be seen in <https://creativecommons.org/licenses/by-nc/4.0/>.

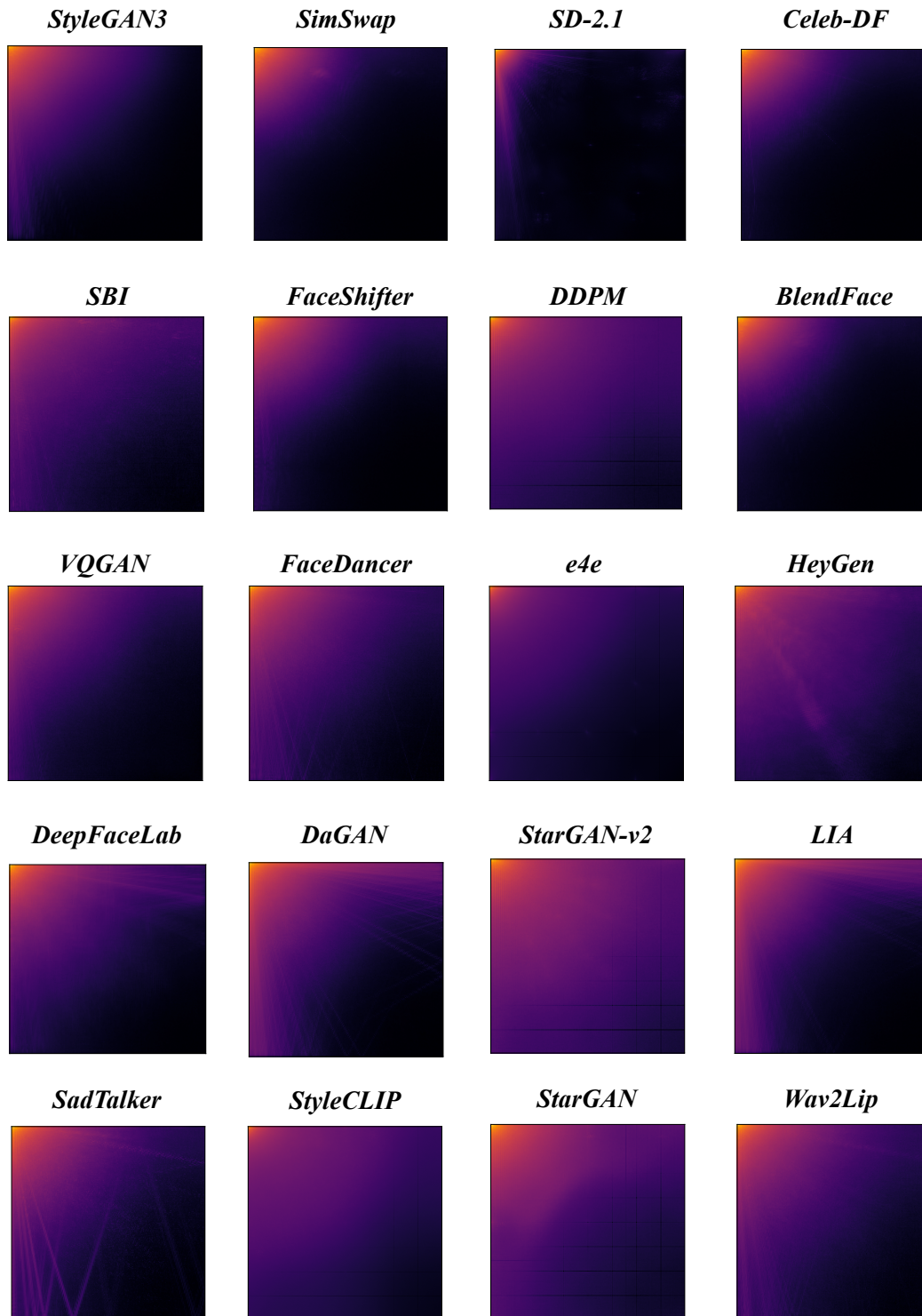


Figure 17: Std of the frequency analysis for visualizing different deepfake methods from the frequency domain.